INNOVATIVE DESIGN OF COMPOSITE STRUCTURES: THE USE OF CURVILINEAR FIBER FORMAT IN STRUCTURAL DESIGN OF COMPOSITES[1]

R. F. Charette[2]
M. W. Hyer[3]
Department of Mechanical Engineering
University of Maryland
College Park, MD 20742
Technical Report 90-1
March 1990

NAG1-665

FINAL REPORT

(1) Work supported by Grant NAG-1-665 from the Structural Mechanics Branch of Langley Research Center. Grant Monitor: Dr. Michael P. Nemeth

(2) Currently, David Taylor Research Center
Code 1720
Bethesda, MD 20084

(3) Current, Professor, Department of Engineering Science and Mechanics, Virginia Polytechnic Institute and State University, Blacksburg, VA 24061-0219

ABSTRACT

This study investigates the influence of a curvilinear fiber format on load carrying capacity of a layered fiber-reinforced plate with a centrally located hole. A curvilinear fiber format is descriptive of layers in a laminate having fibers which are aligned with the principal stress directions in those layers. Laminates of five curvilinear fiber format designs and four straightline fiber format designs are considered. A quasi-isotropic laminate having a straightline fiber format is used to define a baseline design for comparison with the other laminate designs. Four different plate geometries are considered and differentiated by two values of hole diameter/plate width equal to 1/6 and 1/3, and two values of plate length/plate width equal to 2 and 1. With the plates under uniaxial tensile loading on two opposing edges, alignment of fibers in the curvilinear layers with the principal stress directions is determined analytically by an iteration procedure. In-plane tensile load capacity is computed for all of the laminate designs using a finite element analysis method. A maximum strain failure criterion and the Tsai-Wu failure criterion are applied to determine failure loads and failure modes. Resistance to buckling of the laminate designs to uniaxial compressive loading is analyzed using the commercial code Engineering Analysis Language. Results indicate that the curvilinear fiber format laminates have higher in-plane tensile load capacity and comparable buckling resistance relative to the straightline fiber format laminates.

Preface

This report constitutes the thesis of Robert F. Charette submitted for the partial fulfillment of a Master of Science in Mechanical Engineering at the University of Maryland, College Park.

Acknowledgements

The work reported on herein was conducted under the support of Grant NAG-1-665 from the Structural Mechanics Branch of the Langley Research Center to the University of Maryland. A portion of the study was conducted while the authors were in residence at the Center. The use of the facilities of the Langley Research Center are appreciated, as is the financial support of the Grant. The advice from the interaction with the Grant Monitor, Dr. Michael P. Nemeth, are also appreciated.

TABLE OF CONTENTS

LIST OF FIGURES

LIST OF TABLES

List Of Symbols

L, W, H	Length, Width, Thickness of plate (laminate)
h	Thickness of one layer (lamina)
D	Diameter of hole in plate
N	Layer (lamina) number
x, y, z	Global coordinate system (laminate axes)
1, 2, 3	Cartesian coordinate system (lamina axes) 1-axis : fiber direction 2-axis : transverse to fiber direction 3-axis : z-axis direction
n, s	Normal and tangential coordinates
r, s	Natural coordinates
Φ_i	Interpolation (shape) function, eight-node isoparametric element, i = 1,...,8
u^0, v^0, w^0	Displacement of plate middle surface
u, v, w	Displacement in the x, y, z directions
ϵ_x^0, ϵ_y^0, ϵ_z^0	Normal strain components (middle surface)
Γ_x^0 , Γ_y^0 , Γ_{xy}^0	Shear strain components (middle surface)
K_x^0 , K_y^0 , K_z^0	Curvatures of the plate (middle surface)
ϵ_x, ϵ_y, ϵ_z	Normal strain components
Γ_{xy}, Γ_{yz}, Γ_{zx}	Shear strain components
σ_x, σ_y, σ_z	Normal stress components
τ_{xy}, τ_{yz}, τ_{zx}	Shear stress components
ϵ_1, ϵ_2, ϵ_3	Normal strain components (lamina axes)
Γ_{23}, Γ_{31}, Γ_{12}	Shear strain components (lamina axes)
σ_1, σ_2, σ_3	Normal stress components (lamina axes)
τ_{23}, τ_{31}, τ_{12}	Shear stress components (lamina axes)
θ	Transformation angle, x-axis to 1-axis

ϕ	Transformation angle, $\phi = \pi/2 - \theta$
C_{ij}	Stiffness coefficients : i,j = 1,2,3,4,5,6
Q_{ij}	Reduced stiffness coefficient, lamina axes i,j = 1,2,6
$\bar{Q}_{ij}$	Reduced stiffness coefficient, laminate axes i,j = 1,2,6
T	Transformation matrix
E_i	Modulus of elasticity in tension and compression, i = 1,2
G_{ij}	Modulus of elasticity in shear, i,j = 1,2
μ_{ij}	Poisson's Ratio, i,j = 1,2
E_1	Modulus of elasticity, fiber direction
E_2	Modulus of elasticity, transverse to fibers
G_{12}	In-plane shear modulus
μ_{12}, μ_{21}	Poisson's ratio, lamina axes
N_x, N_y, N_{xy}	Force resultant
M_x, M_y, M_{xy}	Moment resultant
Q_x, Q_y, Q_n	Shear force resultant
M_n, M_{ns}	Moment resultant
N_n, N_{ns}	Force resultant
$\bar{N}_n$, $\bar{N}_{ns}$	Prescribed force resultant
a_{nx}, a_{ny}	Cosine of angle between n axis and x, y axes
a_{sx}, a_{sy}	Cosine of angle between s axis and x, y axes
A_{ij}	Laminate extensional stiffness coefficient, i,j = 1,2,6
B_{ij}	Laminate bending/extensional stiffness coefficient, i,j = 1,2,6
D_{ij}	Laminate bending stiffness coefficient, i,j = 1,2,6

Ω	Interior region of plate
Γ_1	Boundary of hole in plate
Γ_2	Outer boundary of plate
π	Total potential energy
U	Total strain energy
V	Potential energy of applied forces
$\underline{u}$	Strain energy per unit volume
$\underline{V}$	Volume
C_{ijkl}	Material stiffness coefficient (4th order tensor), i,j,k,l = 1,2,3
ϵ_{ij}	Strain component (2nd order tensor) i,j = 1,2,3
τ_{ij}	Stress component (2nd order tensor) i,j = 1,2,3
u_n^0 , u_s^0	Displacement (middle surface)
τ_{nn}, τ_{ns}	Stress components: n,s coordinate system
$q(x,y)$	Normal load distribution on region Ω
$\delta^{(1)}(\ldots)$	Delta operator, first variation
$(\alpha)_{,\beta}$	Notational convention, differentiation of a variable α with respect to a variable β

CHAPTER I

INTRODUCTION

Advanced fiber-reinforced composite materials were introduced roughly two decades ago as a high performance structural material with enormous possibilities for increasing structural efficiency. Initial research on composite materials centered on producing the material at a reasonable cost and fabricating simple structural shapes from the materials. Additional research was also conducted with regard to analyzing and predicting how those simple structural shapes would respond to loads.

The next area of research focused on the complex and sometimes unpredictable failure mechanisms of composite materials. Many variables affect the structural response of composite materials, and since the behavior of metals had been well studied, many fiber-reinforced components were designed to behave somewhat like metals. This approach was acceptable because fabrication of the components was of major concern. The metal-like construction of composites was accepted because the lower density of composite materials produced a weight savings in the components. However, use of composite materials in this manner did not take advantage of the major attributes of composite materials which allow for tailoring the composite material to fit the application. The strength and stiffness of a composite material can be aligned in directions which correspond to the loads

applied to a structural component.

Military aircraft and both military and civilian spacecraft have been designed and used successfully with advanced fiber-reinforced composite materials as part of the overall design. Fiber-reinforced composite materials are now being studied for use in business aircraft, and to some extent, commercial aircraft. Even though composite materials have seen increased usage, the potential advantages of advanced fiber-reinforced composite materials have not been fully realized, or even investigated. The development and use of composite materials in structures has followed a conservative approach. This conservative approach has resulted in some of the detrimental characteristics of composites eroding some of its advantages. As a result, in many cases only a marginal gain in efficiency is realized when a composite material is used instead of a metal. For example, a quasi-isotropic laminate has stiffness characteristics which are similar to aluminum and has similar in-plane load capacity. However, unlike aluminum, a quasi-isotropic laminate may delaminate, while aluminum does not have that problem. A quasi-isotropic laminate is susceptible to environmental degradation, while aluminum has less of a problem with this. The manufacture and repair of composite materials is less fully understood than the manufacture and repair of aluminum. The addition of more weight to a composite structure might alleviate these problems, but then the advantages of

using composite materials begin to decrease. Gains made in structural efficiency have been moderate while it seems the gains could be far greater. To make gains in structural efficiency by a factor of 2 or 3, the overly conservative utilization of a composite material must be disgarded and more innovative approaches must be developed. This particular study examines one departure from the conservative use of composite materials and develops an approach which may lead to step increases in structural performance.

Conventional design philosophies for fiber-reinforced composite structures are based on the idea of using multiple layers of fibers embedded in a matrix, the fibers in each layer being straight and parallel to each other, and aligned in a particular direction. Though each layer may have its own unique fiber orientation, the idea of allowing the fiber orientation within a layer to vary from point to point has not been considered seriously. The specific issue in this study is to use fiber reinforcement in such a way that the direction of the fibers, or at least some of the fibers, is a function of spatial position in the structure. This will be referred to herein as a curvilinear fiber format. The curvilinear format has the following advantage: A structural component may contain a geometric discontinuity, such as a hole, which interrupts fiber continuity in all of the layers and causes a concentration and realignment of stress. If the fibers are straight and parallel to each other, a

large number of fibers must be broken at this geometric discontinuity. The efficient way to use the fibers would be not to break the fiber continuity and thus use the fibers to greater advantage near the geometric discontinuty. The fibers should "flow" continuously around the discontinuity and be oriented in such a manner as to transmit the load efficiently around the discontinuity. Many issues must be studied to make this idea viable, the most important issue being fabrication. However, the availability of raw fiber, the increased power and flexibility of robotics, and new matrix development do provide promise for fabrication of components on a fiber-by-fiber basis with something other than a straightline format.

In considering the issue involved, this study focuses on the application of the concept to a particular problem. The particular problem studied here is a prime candidate for deviating from the straightline fiber format. The particular problem is a thin plate which contains a centrally located circular hole and is loaded uniaxially in its plane. The problem has been studied hundreds of times in the context of using isotropic and composite materials. However, it is an important problem. Aircraft structures contain many holes for access and fabrication, and commercial air transports contain numerous windows. The central question is: If the fibers are not to be used in a straightline fiber format, how should the orientation of the fibers vary

from point to point? The basic philosophy used here to design the plate will be to align the fibers with the principal stress directions. More specifically, in those layers which are allowed to have variable fiber orientation, the fibers will be aligned with the principal stress directions in those layers. The method focuses on the use of an iteration scheme to align the fibers with the principal stress directions. Several different stacking sequences of layers and four different geometries are considered to see how the curvilinear fiber format will compare with the straightline fiber format. The maximum strain and Tsai-Wu failure criteria are used to determine the comparative strengths and weaknesses of the various designs. Finally, the buckling strengths of the curvilinear designs are computed to determine if the curvilinear designs alter buckling strength.

The next chapter begins to address these issues by presenting a brief overview of classical laminated plate theory, casting these results within the framework of variational methods, and deriving the governing nonlinear partial differential equations and associated boundary conditions. Chapter III presents the specific plate geometries to be studied, and presents the governing equations developed in Chapter II in the context of those plates subjected to in-plane uniaxial tensile loading. The equations, by the nature of the problem, are linear partial differential equations with coefficients that are a function of the spa-

tial coordinates. The material properties vary from point to point and these material properties modify the differential equations. Because of the variable coefficients, an approximate numerical scheme is necessary to obtain numbers. Here the finite element method is used, and details of the particular finite element used are presented in Chapter III. Since the finite element method is well known, the discussion of the finite element approach is brief. The boundary conditions used in the tensile load analysis and the use of a one-quarter plate analysis are also discussed. Most importantly, the iteration scheme used to align the fiber directions with the principal stress directions is discussed. Finally, Chapter III includes an overview and discussion of the failure theories used.

Chapter IV focuses on the buckling analysis. The method of adjacent equilibrium is used to derive the equations which govern buckling. The buckling equations are based on the equations derived in Chapter II. Again these equations are partial differential equations with variable coefficients and solutions are obtained using the finite element method. Since this particular finite element analysis is based on use of the commercial code Engineering Analysis Language (EAL), the discussion centers on the characteristics of the element used. The boundary conditions used in the buckling analysis are presented along with reasons for analyzing the entire plate instead of only one-quarter

of the plate.

Chapter V presents the results for the tensile load problem. The failure loads and failure modes for 36 different plate designs are presented. Since the point of the work is improved performance with the curvilinear designs, gains in using this design are discussed in some detail. Through the use of contour plots, the basis for the improvement in terms of the redistribution of stress is discussed. Convergence and accuracy of the stress analysis for the laminates with the curvilinear layers is also addressed in Chapter V.

Chapter VI centers on the buckling resistance of the 36 different plate designs. As mentioned before, the purpose of the buckling analysis was not to design for improved buckling. Rather the buckling analysis was conducted to determine the influence of the curvilinear fiber format on the buckling capacity.

Finally, the last chapter, Chapter VII, includes a summary of the findings, discusses the limitations of the results, and makes recommendations for future research.

CHAPTER II

DERIVATION OF EQUATIONS GOVERNING GENERALLY ORTHOTROPIC THIN LAMINATED PLATES

General Considerations

Consider a thin laminated fiber-reinforced plate as shown in Figure 2.1. The x-y coordinate plane corresponds to the middle surface of the plate. The z-axis is perpendicular to the middle surface and z is measured relative to the middle surface. The total thickness of the plate is denoted by H.

The plate studied here is governed by the following set of assumptions based on classical thin-plate theory.

(1) The thickness of the plate is uniform and small compared to the other dimensions of the plate.

(2) The Kirchhoff hypothesis is assumed to be valid. The hypothesis states that at any point on the middle surface, line elements normal to the undeformed middle surface remain straight, normal to the surface, and do not extend or contract during the deformation of the plate. As a result, the transverse shear strain components are exactly zero. This is illustrated in Figure 2.2 where the orthogonality of the line element relative to the middle surface is shown.

(3) The strains are small compared to unity and the rotations about the x-axis and the y-axis are moderately small.

The strains are smaller than the rotations. The rotations about the z-axis are negligibly small. Essentially it is assumed that the von Karman thin-plate theory is valid for this problem, specifically the buckling problem.

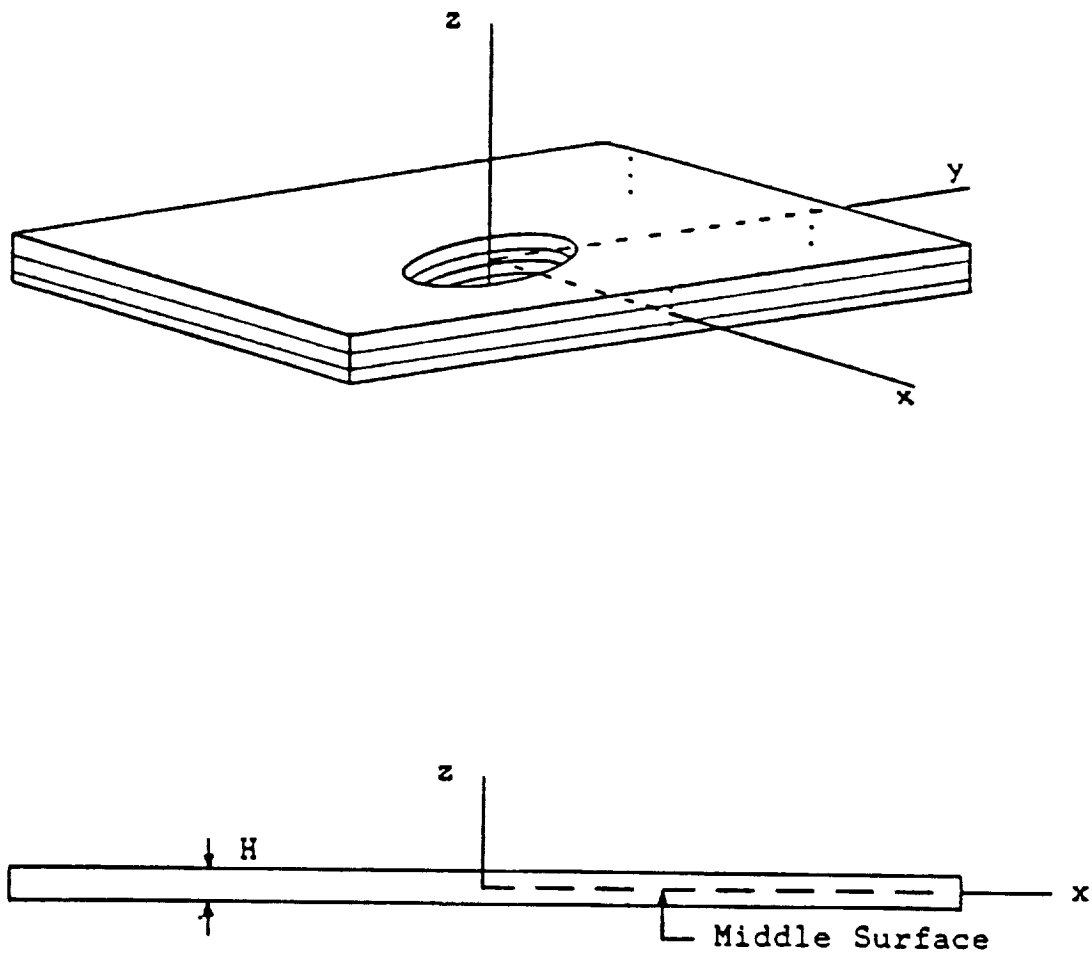

Figure 2.1 Thin Plate

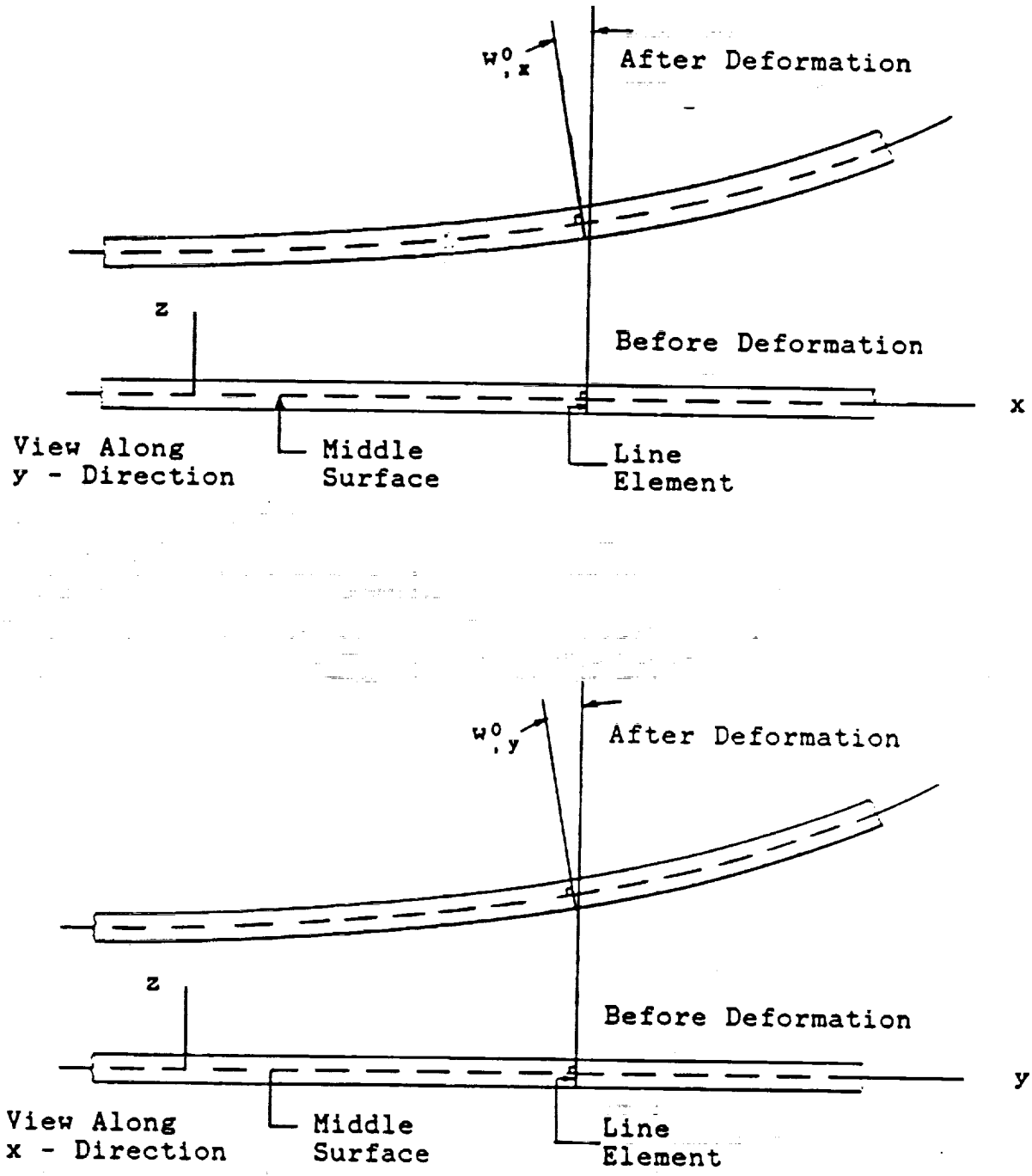

Figure 2.2 Kirchhoff Assumption

(4) The plate is constructed of multiple layers of fiber-reinforced material, each layer being bonded perfectly to the adjacent layer. Each layer is of thickness h and has its own fiber orientation.

(5) The plate is in a state of plane stress, i.e., at every point in the plate, $\sigma_z = \tau_{xz} = \tau_{yz} = 0$.

(6) The stiffness properties are uniform throughout the thickness of each layer, but the properties are a function of locations x and y in each layer. Each layer can also have different stiffness properties.

(7) Each layer exhibits linear elastic behavior.

(8) The material in each layer is orthotropic.

(9) There are no body forces acting in the plate.

Detailed Considerations For Layered Fiber-Reinforced Plates

In terms of plate displacements, the Kirchhoff assumption can be written as:

$$u(x,y,z) = u^0(x,y) - z\,(w^0(x,y))_{,x} \qquad (2.1a)$$

$$v(x,y,z) = v^0(x,y) - z\,(w^0(x,y))_{,y} \qquad (2.1b)$$

$$w(x,y,z) = w^0(x,y) \qquad (2.1c)$$

where u, v, and w denote the displacements at any point in the plate, and u^0, v^0, and w^0 denote the displacements of the middle surface of the plate. The quantity $w^0_{,x}$ is the rotation of the normal to the middle surface about the y-axis, as illustrated in Figure 2.2, and the quantity $w^0_{,y}$ is the rotation of the normal to the middle surface about the

x-axis, also illustrated in Figure 2.2.

The strain-displacement relations, including the effects of moderate rotations about the x and y axes are:

$$\epsilon_x (x,y,z) = (u(x,y,z))_{,x} + \tfrac{1}{2}[(w(x,y,z))_{,x}]^2 \quad (2.2a)$$

$$\epsilon_y (x,y,z) = (v(x,y,z))_{,y} + \tfrac{1}{2}[(w(x,y,z))_{,y}]^2 \quad (2.2b)$$

$$\Gamma_{xy}(x,y,z) = (u(x,y,z))_{,y} + (v(x,y,z))_{,x} + [(w(x,y,z))_{,x}(w(x,y,z))_{,y}] \quad (2.2c)$$

where ϵ_x, ϵ_y, Γ_{xy} are the strains at any point in the plate. Substituting the Kirchhoff displacements into the strain-displacement relations results in:

$$\epsilon_x = u^0{}_{,x} - z\, w^0{}_{,xx} + \tfrac{1}{2}[w^0{}_{,x}]^2 \quad (2.3a)$$

$$\epsilon_y = v^0{}_{,y} - z\, w^0{}_{,yy} + \tfrac{1}{2}[w^0{}_{,y}]^2 \quad (2.3b)$$

$$\Gamma_{xy} = u^0{}_{,y} + v^0{}_{,x} - 2\, z\, w^0{}_{,xy} + w^0{}_{,x} w^0{}_{,y} \quad (2.3c)$$

Written in more compact notation:

$$\epsilon_x (x,y,z) = \epsilon^0{}_x (x,y) + z\, K^0{}_x (x,y) \quad (2.4a)$$

$$\epsilon_y (x,y,z) = \epsilon^0{}_y (x,y) + z\, K^0{}_y (x,y) \quad (2.4b)$$

$$\Gamma_{xy}(x,y,z) = \Gamma^0{}_{xy}(x,y) + z\, K^0{}_{xy}(x,y) \quad (2.4c)$$

where the strains ϵ^0 of the middle surface of the plate are:

$$\epsilon^0{}_x = u^0{}_{,x} + \tfrac{1}{2}[w^0{}_{,x}]^2 \quad (2.5a)$$

$$\epsilon^0{}_y = v^0{}_{,y} + \tfrac{1}{2}[w^0{}_{,y}]^2 \quad (2.5b)$$

$$\Gamma^0{}_{xy} = u^0{}_{,y} + v^0{}_{,x} + w^0{}_{,x} w^0{}_{,y} \quad (2.5c)$$

and the curvatures K^0 of the middle surface of the plate are:

$$K^0{}_x = - w^0{}_{,xx} \quad (2.6a)$$

$$K^0_y = - w^0_{,yy} \quad (2.6b)$$

$$K^0_{xy} = - 2\, w^0_{,xy} \quad (2.6c)$$

A single layer within the plate is often referred to as a lamina. A lamina consists of many thousands of strong and stiff fibers embedded in a softer and weaker material. This second material is referred to as a matrix. The fibers carry most of the load while the matrix material transfers the load between the fibers and holds the fibers together. A laminate is a group of laminae or layers that, as stated before, are bonded perfectly together. The planes of the laminae are parallel to each other. This is shown in Figure 2.3. In Figure 2.3 the fiber directions of the various laminae are illustrated, and also as stated before, each lamina can have its fibers oriented in an arbitrary direction.

Because each layer can have its own fiber orientation, it is convenient to use a global or laminate coordinate system for the analysis. The global system is referred to here as the x-y-z coordinate system while the lamina system is denoted as the 1-2-3 coordinate system. The relationship between the 1-2-3 lamina coordinate system and the x-y-z laminate coordinate system is shown in Figure 2.4. The 1-axis corresponds to the fiber direction. The angle θ defines the orientation of the 1-axis with respect to the x-axis.

One of the most important aspects of laminated fiber-

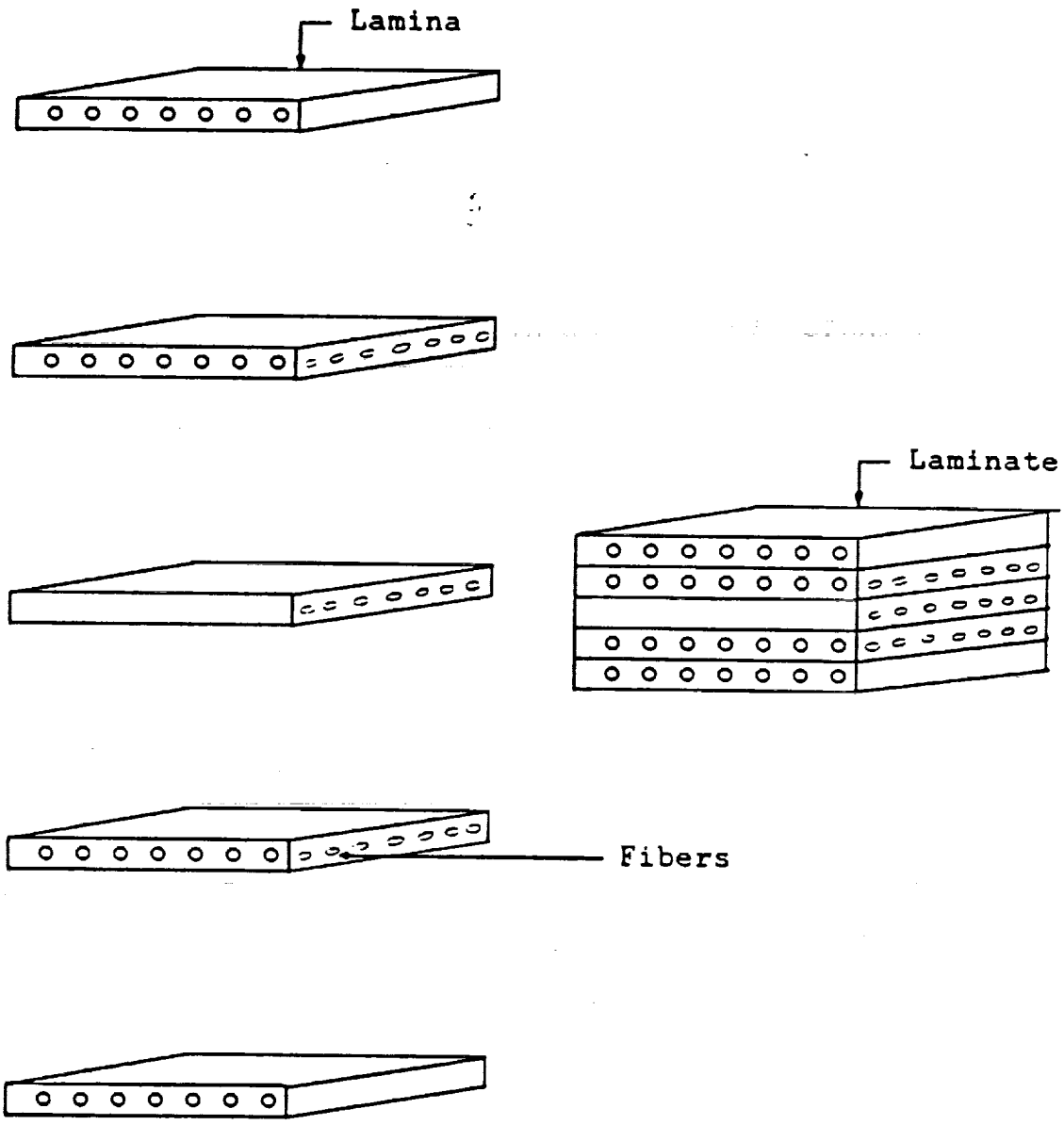

Figure 2.3 Lamina and Laminate

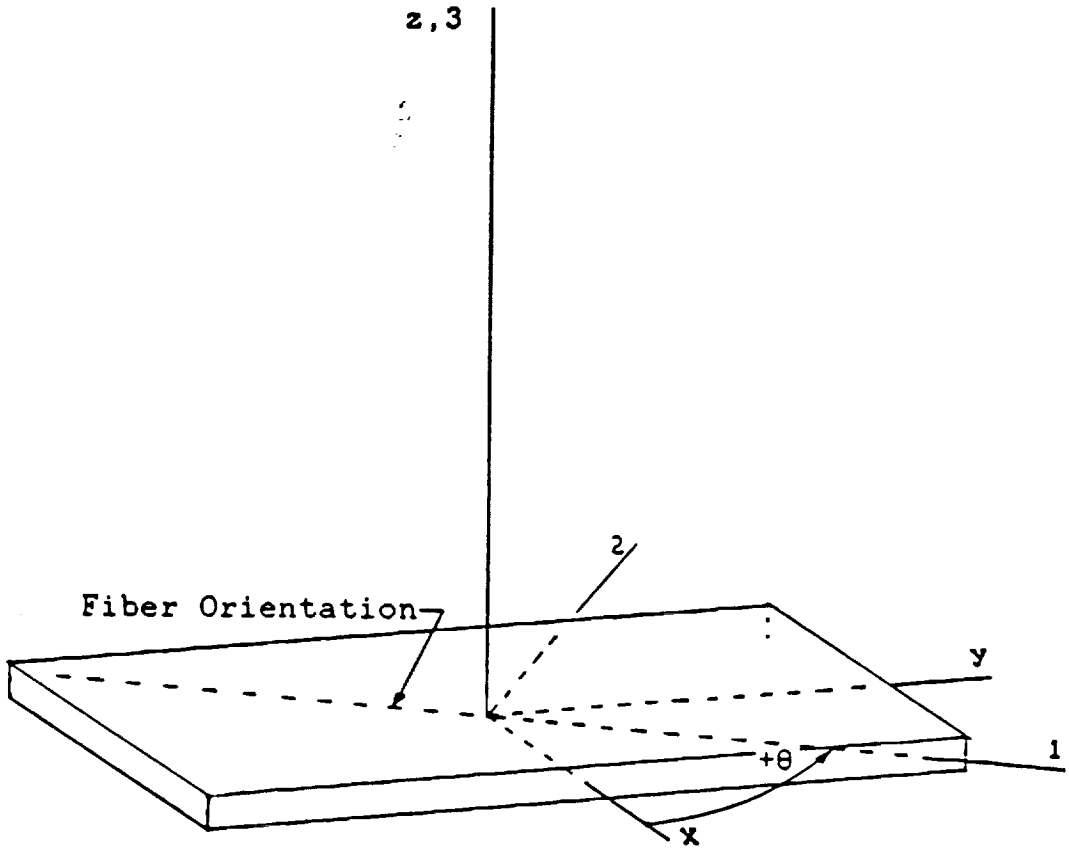

+ θ : Positive Rotation Of Coordinate Axes

Figure 2.4

Relationship Between 1-2-3 Lamina Coordinate System and x-y-z Laminate Coordinate System

reinforced composite plates, and one which distinguishes them from traditional isotropic plates, is the stress-strain behavior. As mentioned on page 11, it is assumed that the material in each layer is orthotropic and exhibits linear elastic behavior. Referring to Figure 2.5, which shows the stresses acting on an elemental unit cube in the 1-2-3 coordinate system, the stress-strain behavior of an orthotropic material in the 1-2-3 coordinate system is given by:

$$\begin{bmatrix} \sigma_1 \\ \sigma_2 \\ \sigma_3 \\ \tau_{23} \\ \tau_{31} \\ \tau_{12} \end{bmatrix} = \begin{bmatrix} C_{11} & C_{12} & C_{13} & 0 & 0 & 0 \\ C_{12} & C_{22} & C_{23} & 0 & 0 & 0 \\ C_{13} & C_{23} & C_{33} & 0 & 0 & 0 \\ 0 & 0 & 0 & C_{44} & 0 & 0 \\ 0 & 0 & 0 & 0 & C_{55} & 0 \\ 0 & 0 & 0 & 0 & 0 & C_{66} \end{bmatrix} \begin{bmatrix} \epsilon_1 \\ \epsilon_2 \\ \epsilon_3 \\ \Gamma_{23} \\ \Gamma_{31} \\ \Gamma_{12} \end{bmatrix} \qquad (2.7)$$

where the C 's are the stiffness coefficients of the material.

The stress-strain relations of Eqn. 2.7 reduce to the following form for an orthotropic lamina in a state of plane stress.

$$\begin{bmatrix} \sigma_1 \\ \sigma_2 \\ \tau_{12} \end{bmatrix} = \begin{bmatrix} Q_{11} & Q_{12} & 0 \\ Q_{12} & Q_{22} & 0 \\ 0 & 0 & Q_{66} \end{bmatrix} \begin{bmatrix} \epsilon_1 \\ \epsilon_2 \\ \Gamma_{12} \end{bmatrix} \qquad (2.8)$$

The Q's are the reduced stiffnesses in the 1-2 coordinate system. The Q's can be defined in terms of the

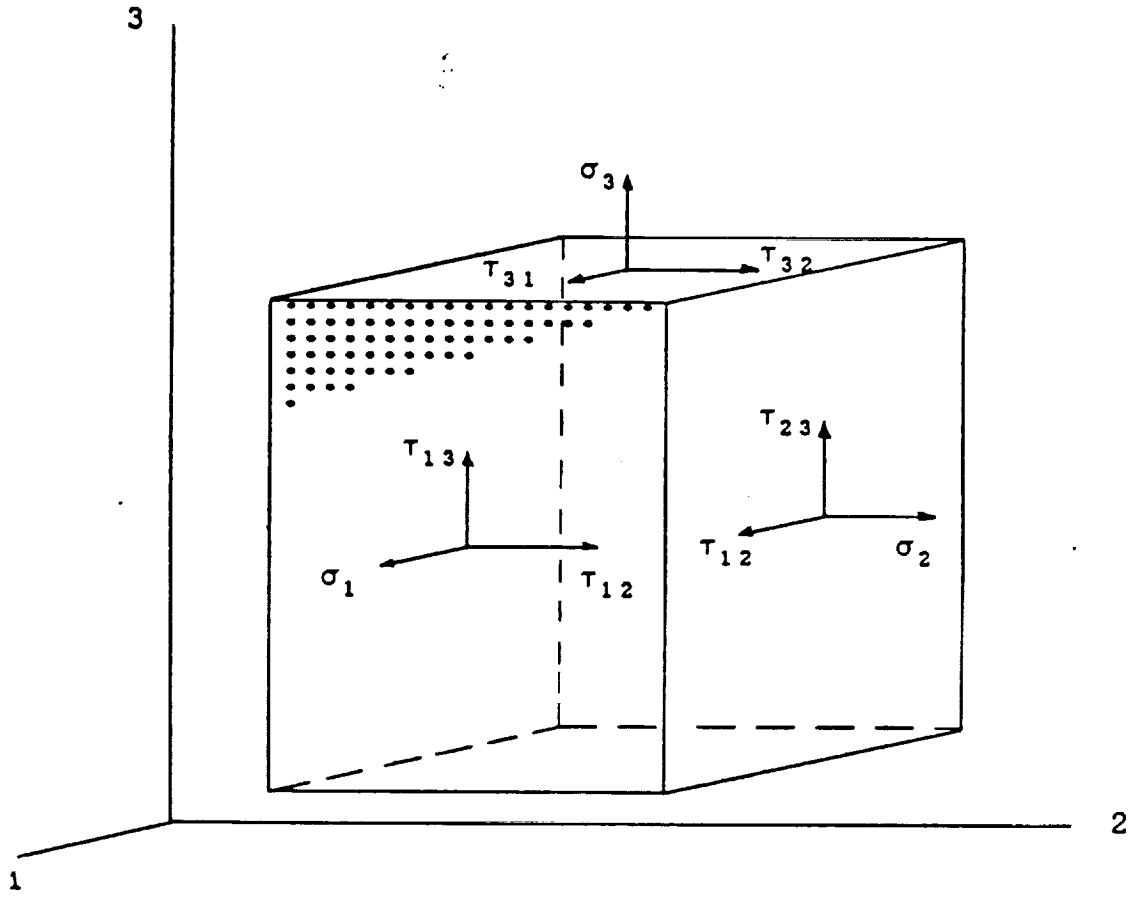

Figure 2.5

Stresses Acting On An Elemental Unit Cube

engineering constants E_1 , E_2 , μ_{12} , μ_{21} , and G_{12} as:

$$Q_{11} = \frac{E_1}{1 - \mu_{12}\mu_{21}} \tag{2.9a}$$

$$Q_{12} = \frac{E_2\mu_{12}}{1 - \mu_{12}\mu_{21}} = \frac{E_1\mu_{21}}{1 - \mu_{12}\mu_{21}} \tag{2.9b}$$

$$Q_{22} = \frac{E_2}{1 - \mu_{12}\mu_{21}} \tag{2.9c}$$

$$Q_{66} = G_{12} \tag{2.9d}$$

To completely describe the response of an orthotropic material in a state of plane stress, four independent material properties are required. These material properties are the elastic modulus in the fiber direction E_1 , the elastic modulus perpendicular to the fibers and in the plane of the of the lamina E_2 , the in-plane shear modulus G_{12} , and Poisson's ratio μ_{12}. The Poisson's ratio μ_{21} can be determined from the following reciprocal relation:

$$\frac{\mu_{12}}{E_1} = \frac{\mu_{21}}{E_2} \tag{2.10}$$

In general, Poisson's ratio μ_{ij} measures the contraction in the j-direction due to a stress applied in the i-direction.

The reduced stiffnesses in the x-y coordinate system are determined by transforming the reduced stiffnesses in the 1-2 coordinate system into the x-y coordinate system. The transformation matrix [T] needed for this is:

$$\begin{bmatrix} \cos^2\theta & \sin^2\theta & 2\sin\theta\cos\theta \\ \sin^2\theta & \cos^2\theta & -2\sin\theta\cos\theta \\ -\sin\theta\cos\theta & \sin\theta\cos\theta & \cos^2\theta - \sin^2\theta \end{bmatrix} \quad (2.11)$$

where θ denotes the angle from the x-axis to the 1-axis for a positive rotation in a Cartesian coordinate system. Given values of stress or strain with respect to the x-y coordinate system, these may be transformed to the 1-2 coordinate system according to the following:

$$\begin{bmatrix} \sigma_1 \\ \sigma_2 \\ \tau_{12} \end{bmatrix} = [\,T\,] \begin{bmatrix} \sigma_x \\ \sigma_y \\ \tau_{xy} \end{bmatrix} \qquad \begin{bmatrix} \epsilon_1 \\ \epsilon_2 \\ \frac{\Gamma_{12}}{2} \end{bmatrix} = [\,T\,] \begin{bmatrix} \epsilon_x \\ \epsilon_y \\ \frac{\Gamma_{xy}}{2} \end{bmatrix}$$

Conversely, given stress or strain in the 1-2 coordinate system, these may be transformed to the x-y coordinate system according to the following:

$$\begin{bmatrix} \sigma_x \\ \sigma_y \\ \tau_{xy} \end{bmatrix} = [\,T\,]^{-1} \begin{bmatrix} \sigma_1 \\ \sigma_2 \\ \tau_{12} \end{bmatrix} \qquad \begin{bmatrix} \epsilon_x \\ \epsilon_y \\ \frac{\Gamma_{xy}}{2} \end{bmatrix} = [\,T\,]^{-1} \begin{bmatrix} \epsilon_1 \\ \epsilon_2 \\ \frac{\Gamma_{12}}{2} \end{bmatrix}$$

The reduced stiffnesses in the x-y coordinate system for a lamina, given the reduced stiffnesses in the 1-2 coordinate system, can be determined using the following equation: (Jones [1], p. 50).

$$[\ \bar{Q}\ ] = [\ T\ ]^{-1}\ [\ Q\ ]\ [\ T\ ]^{-T} \qquad (2.12)$$

where:

$[\ \bar{Q}\ ]$ = reduced stiffnesses in the x-y coordinate system

$[\ T\ ]^{-1}$ = inverse of transformation matrix $[\ T\ ]$

$[\ Q\ ]$ = reduced stiffnesses in the 1-2 coordinate system

$[\ T\ ]^{-T}$ = transpose of inverse of matrix $[\ T\ ]$

The stress-strain relations in the x-y coordinate system for an orthotropic lamina in a state of plane stress then become:

$$\begin{bmatrix} \sigma_x \\ \sigma_y \\ \tau_{xy} \end{bmatrix} = [\ \bar{Q}\ ] \begin{bmatrix} \epsilon_x \\ \epsilon_y \\ \Gamma_{xy} \end{bmatrix}$$

$$\begin{bmatrix} \sigma_x \\ \sigma_y \\ \tau_{xy} \end{bmatrix} = \begin{bmatrix} \bar{Q}_{11} & \bar{Q}_{12} & \bar{Q}_{16} \\ \bar{Q}_{12} & \bar{Q}_{22} & \bar{Q}_{26} \\ \bar{Q}_{16} & \bar{Q}_{26} & \bar{Q}_{66} \end{bmatrix} \begin{bmatrix} \epsilon_x \\ \epsilon_y \\ \Gamma_{xy} \end{bmatrix} \qquad (2.13)$$

It is important to note that in the x-y coordinate system there is coupling between the shear strain and the normal stresses, and coupling between the shear stress and the normal strains. The lamina appears to be anisotropic in x-y coordinates. However, the lamina is orthotropic because there are still only four independent material properties. The lamina is designated as generally orthotropic and can be characterized by equation 2.13. (Jones [1], p. 51).

Force And Moment Resultants

The z-location of a layer in a laminate is shown in Figure 2.6. In particular, the k-th lamina is bounded by the coordinates z_k and z_{k-1}. When a plate is subjected to loads, stresses develop in each layer. To aid in deriving the governing differential equations, these stresses are lumped into equivalent forces and moments, commonly referred to as resultants. The force and moment resultants acting on an element of the plate are shown in Figure 2.7. These resultants have units of force per unit length or moment per unit length in the x and y directions. N_x and N_y are in-plane normal force resultants, N_{xy} is the in-plane shear force resultant, M_x and M_y are bending moment resultants, and M_{xy} is the twisting moment resultant.

The force and moment resultants are related to the stresses by the following equations:

$$N_x = \int_{-\frac{1}{2}H}^{+\frac{1}{2}H} \sigma_x \, dz \qquad (2.14a) \qquad M_x = \int_{-\frac{1}{2}H}^{+\frac{1}{2}H} \sigma_x \, z \, dz \qquad (2.14d)$$

$$N_y = \int_{-\frac{1}{2}H}^{+\frac{1}{2}H} \sigma_y \, dz \qquad (2.14b) \qquad M_y = \int_{-\frac{1}{2}H}^{+\frac{1}{2}H} \sigma_y \, z \, dz \qquad (2.14e)$$

$$N_{xy} = \int_{-\frac{1}{2}H}^{+\frac{1}{2}H} \tau_{xy} dz \qquad (2.14c) \qquad M_{xy} = \int_{-\frac{1}{2}H}^{+\frac{1}{2}H} \tau_{xy} z \, dz \qquad (2.14f)$$

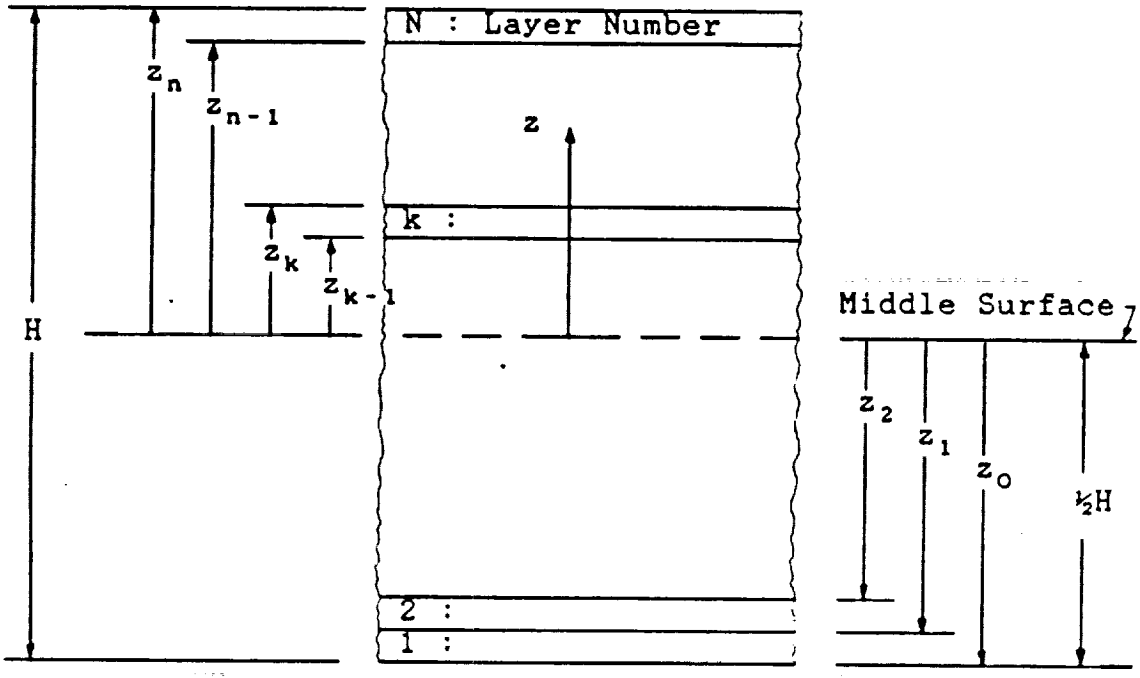

Figure 2.6 Geometry For Layers In A Laminate

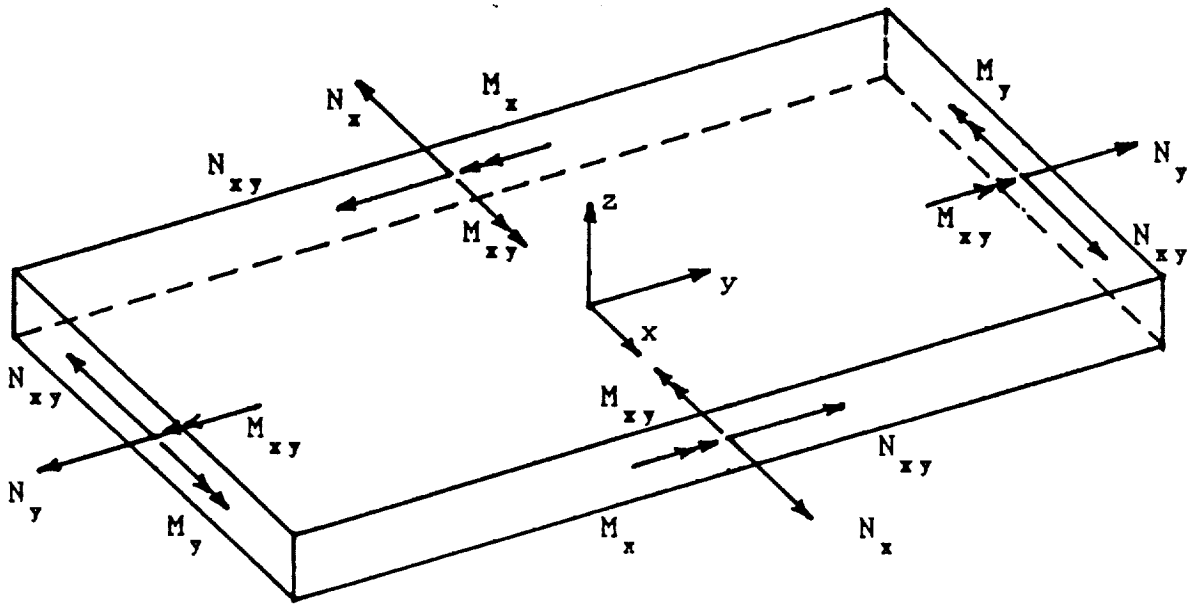

Figure 2.7 Plate Element With Force And Moment Resultants

Substituting equation 2.13 into equations 2.14a-f results in:

$$N_x = \int_{-\frac{1}{2}H}^{+\frac{1}{2}H} \bar{Q}_{11}\epsilon_x \, dz + \int_{-\frac{1}{2}H}^{+\frac{1}{2}H} \bar{Q}_{12}\epsilon_y \, dz + \int_{-\frac{1}{2}H}^{+\frac{1}{2}H} \bar{Q}_{16}\Gamma_{xy} \, dz \qquad (2.15a)$$

$$N_y = \int_{-\frac{1}{2}H}^{+\frac{1}{2}H} \bar{Q}_{12}\epsilon_x \, dz + \int_{-\frac{1}{2}H}^{+\frac{1}{2}H} \bar{Q}_{22}\epsilon_y \, dz + \int_{-\frac{1}{2}H}^{+\frac{1}{2}H} \bar{Q}_{26}\Gamma_{xy} \, dz \qquad (2.15b)$$

$$N_{xy} = \int_{-\frac{1}{2}H}^{+\frac{1}{2}H} \bar{Q}_{16}\epsilon_x \, dz + \int_{-\frac{1}{2}H}^{+\frac{1}{2}H} \bar{Q}_{26}\epsilon_y \, dz + \int_{-\frac{1}{2}H}^{+\frac{1}{2}H} \bar{Q}_{66}\Gamma_{xy} \, dz \qquad (2.15c)$$

$$M_x = \int_{-\frac{1}{2}H}^{+\frac{1}{2}H} \bar{Q}_{11}\epsilon_x z \, dz + \int_{-\frac{1}{2}H}^{+\frac{1}{2}H} \bar{Q}_{12}\epsilon_y z \, dz + \int_{-\frac{1}{2}H}^{+\frac{1}{2}H} \bar{Q}_{16}\Gamma_{xy} z \, dz \qquad (2.15d)$$

$$M_y = \int_{-\frac{1}{2}H}^{+\frac{1}{2}H} \bar{Q}_{12}\epsilon_x z \, dz + \int_{-\frac{1}{2}H}^{+\frac{1}{2}H} \bar{Q}_{22}\epsilon_y z \, dz + \int_{-\frac{1}{2}H}^{+\frac{1}{2}H} \bar{Q}_{26}\Gamma_{xy} z \, dz \qquad (2.15e)$$

$$M_{xy} = \int_{-\frac{1}{2}H}^{+\frac{1}{2}H} \bar{Q}_{16}\epsilon_x z \, dz + \int_{-\frac{1}{2}H}^{+\frac{1}{2}H} \bar{Q}_{26}\epsilon_y z \, dz + \int_{-\frac{1}{2}H}^{+\frac{1}{2}H} \bar{Q}_{66}\Gamma_{xy} z \, dz \qquad (2.15f)$$

The strains ϵ_x , ϵ_y , and Γ_{xy} can be expressed in terms of the middle surface strains $\epsilon^0{}_x$, $\epsilon^0{}_y$, and $\Gamma^0{}_{xy}$ and middle surface curvatures $K^0{}_x$, $K^0{}_y$, $K^0{}_{xy}$ using equations 2.4a-c. These expressions can be substituted into equations 2.15a-f. Since the middle surface laminate quantities are not functions of z , equations 2.15a-f become:

$$N_x = \epsilon^0_x \int_{-\frac{1}{2}H}^{+\frac{1}{2}H} \bar{Q}_{11}\, dz + K^0_x \int_{-\frac{1}{2}H}^{+\frac{1}{2}H} \bar{Q}_{11}\, z\, dz$$

$$+ \epsilon^0_y \int_{-\frac{1}{2}H}^{+\frac{1}{2}H} \bar{Q}_{12}\, dz + K^0_y \int_{-\frac{1}{2}H}^{+\frac{1}{2}H} \bar{Q}_{12}\, z\, dz$$

$$+ \Gamma^0_{xy} \int_{-\frac{1}{2}H}^{+\frac{1}{2}H} \bar{Q}_{16}\, dz + K^0_{xy} \int_{-\frac{1}{2}H}^{+\frac{1}{2}H} \bar{Q}_{16}\, z\, dz \qquad (2.16a)$$

$$N_y = \epsilon^0_x \int_{-\frac{1}{2}H}^{+\frac{1}{2}H} \bar{Q}_{12}\, dz + K^0_x \int_{-\frac{1}{2}H}^{+\frac{1}{2}H} \bar{Q}_{12}\, z\, dz$$

$$+ \epsilon^0_y \int_{-\frac{1}{2}H}^{+\frac{1}{2}H} \bar{Q}_{22}\, dz + K^0_y \int_{-\frac{1}{2}H}^{+\frac{1}{2}H} \bar{Q}_{22}\, z\, dz$$

$$+ \Gamma^0_{xy} \int_{-\frac{1}{2}H}^{+\frac{1}{2}H} \bar{Q}_{26}\, dz + K^0_{xy} \int_{-\frac{1}{2}H}^{+\frac{1}{2}H} \bar{Q}_{26}\, z\, dz \qquad (2.16b)$$

$$N_{xy} = \epsilon^0_x \int_{-\frac{1}{2}H}^{+\frac{1}{2}H} \bar{Q}_{16}\, dz + K^0_x \int_{-\frac{1}{2}H}^{+\frac{1}{2}H} \bar{Q}_{16}\, z\, dz$$

$$+ \epsilon^0_y \int_{-\frac{1}{2}H}^{+\frac{1}{2}H} \bar{Q}_{26}\, dz + K^0_y \int_{-\frac{1}{2}H}^{+\frac{1}{2}H} \bar{Q}_{26}\, z\, dz$$

$$+ \Gamma^0_{xy} \int_{-\frac{1}{2}H}^{+\frac{1}{2}H} \bar{Q}_{66}\, dz + K^0_{xy} \int_{-\frac{1}{2}H}^{+\frac{1}{2}H} \bar{Q}_{66}\, z\, dz \qquad (2.16c)$$

$$M_x = \epsilon^0_x \int_{-\frac{1}{2}H}^{+\frac{1}{2}H} \bar{Q}_{11}\, z\, dz + K^0_x \int_{-\frac{1}{2}H}^{+\frac{1}{2}H} \bar{Q}_{11}\, z^2\, dz$$

$$+ \epsilon^0_y \int_{-\frac{1}{2}H}^{+\frac{1}{2}H} \bar{Q}_{12}\, z\, dz + K^0_y \int_{-\frac{1}{2}H}^{+\frac{1}{2}H} \bar{Q}_{12}\, z^2\, dz$$

$$+ \Gamma^0_{xy} \int_{-\frac{1}{2}H}^{+\frac{1}{2}H} \bar{Q}_{16}\, z\, dz + K^0_{xy} \int_{-\frac{1}{2}H}^{+\frac{1}{2}H} \bar{Q}_{16}\, z^2\, dz \quad (2.16d)$$

$$M_y = \epsilon^0_x \int_{-\frac{1}{2}H}^{+\frac{1}{2}H} \bar{Q}_{12}\, z\, dz + K^0_x \int_{-\frac{1}{2}H}^{+\frac{1}{2}H} \bar{Q}_{12}\, z^2\, dz$$

$$+ \epsilon^0_y \int_{-\frac{1}{2}H}^{+\frac{1}{2}H} \bar{Q}_{22}\, z\, dz + K^0_y \int_{-\frac{1}{2}H}^{+\frac{1}{2}H} \bar{Q}_{22}\, z^2\, dz$$

$$+ \Gamma^0_{xy} \int_{-\frac{1}{2}H}^{+\frac{1}{2}H} \bar{Q}_{26}\, z\, dz + K^0_{xy} \int_{-\frac{1}{2}H}^{+\frac{1}{2}H} \bar{Q}_{26}\, z^2\, dz \quad (2.16e)$$

$$M_{xy} = \epsilon^0_x \int_{-\frac{1}{2}H}^{+\frac{1}{2}H} \bar{Q}_{16}\, z\, dz + K^0_x \int_{-\frac{1}{2}H}^{+\frac{1}{2}H} \bar{Q}_{16}\, z^2\, dz$$

$$+ \epsilon^0_y \int_{-\frac{1}{2}H}^{+\frac{1}{2}H} \bar{Q}_{26}\, z\, dz + K^0_y \int_{-\frac{1}{2}H}^{+\frac{1}{2}H} \bar{Q}_{26}\, z^2\, dz$$

$$+ \Gamma^0_{xy} \int_{-\frac{1}{2}H}^{+\frac{1}{2}H} \bar{Q}_{66}\, z\, dz + K^0_{xy} \int_{-\frac{1}{2}H}^{+\frac{1}{2}H} \bar{Q}_{66}\, z^2\, dz \quad (2.16f)$$

Each layer can have its own unique fiber orientation, so the $\bar{Q}$'s may be different for each layer. However, the $\bar{Q}$'s are constant within a single layer, so the integrals in equations 2.16a-f can be converted to sums over the layers.

The sums are defined to be:

$$A_{11} = \int_{-\frac{1}{2}H}^{+\frac{1}{2}H} \bar{Q}_{11}\, dz = \sum_{k=1}^{N} (\bar{Q}_{11})_k \, (z_k - z_{k-1}) \qquad (2.17a)$$

$$A_{12} = \int_{-\frac{1}{2}H}^{+\frac{1}{2}H} \bar{Q}_{12}\, dz = \sum_{k=1}^{N} (\bar{Q}_{12})_k \, (z_k - z_{k-1}) \qquad (2.17b)$$

$$A_{16} = \int_{-\frac{1}{2}H}^{+\frac{1}{2}H} \bar{Q}_{16}\, dz = \sum_{k=1}^{N} (\bar{Q}_{16})_k \, (z_k - z_{k-1}) \qquad (2.17c)$$

$$A_{22} = \int_{-\frac{1}{2}H}^{+\frac{1}{2}H} \bar{Q}_{22}\, dz = \sum_{k=1}^{N} (\bar{Q}_{22})_k \, (z_k - z_{k-1}) \qquad (2.17d)$$

$$A_{26} = \int_{-\frac{1}{2}H}^{+\frac{1}{2}H} \bar{Q}_{26}\, dz = \sum_{k=1}^{N} (\bar{Q}_{26})_k \, (z_k - z_{k-1}) \qquad (2.17e)$$

$$A_{66} = \int_{-\frac{1}{2}H}^{+\frac{1}{2}H} \bar{Q}_{66}\, dz = \sum_{k=1}^{N} (\bar{Q}_{66})_k \, (z_k - z_{k-1}) \qquad (2.17f)$$

$$B_{11} = \int_{-\frac{1}{2}H}^{+\frac{1}{2}H} \bar{Q}_{11}\, z\, dz = \sum_{k=1}^{N} (\bar{Q}_{11})_k \, \frac{(z^2_k - z^2_{k-1})}{2} \qquad (2.18a)$$

$$B_{12} = \int_{-\frac{1}{2}H}^{+\frac{1}{2}H} \bar{Q}_{12}\, z\, dz = \sum_{k=1}^{N} (\bar{Q}_{12})_k \, \frac{(z^2_k - z^2_{k-1})}{2} \qquad (2.18b)$$

$$B_{16} = \int_{-\frac{1}{2}H}^{+\frac{1}{2}H} \bar{Q}_{16}\, z\, dz = \sum_{k=1}^{N} (\bar{Q}_{16})_k \frac{(z^2_k - z^2_{k-1})}{2} \qquad (2.18c)$$

$$B_{22} = \int_{-\frac{1}{2}H}^{+\frac{1}{2}H} \bar{Q}_{22}\, z\, dz = \sum_{k=1}^{N} (\bar{Q}_{22})_k \frac{(z^2_k - z^2_{k-1})}{2} \qquad (2.18d)$$

$$B_{26} = \int_{-\frac{1}{2}H}^{+\frac{1}{2}H} \bar{Q}_{26}\, z\, dz = \sum_{k=1}^{N} (\bar{Q}_{26})_k \frac{(z^2_k - z^2_{k-1})}{2} \qquad (2.18e)$$

$$B_{66} = \int_{-\frac{1}{2}H}^{+\frac{1}{2}H} \bar{Q}_{66}\, z\, dz = \sum_{k=1}^{N} (\bar{Q}_{66})_k \frac{(z^2_k - z^2_{k-1})}{2} \qquad (2.18f)$$

$$D_{11} = \int_{-\frac{1}{2}H}^{+\frac{1}{2}H} \bar{Q}_{11}\, z^2\, dz = \sum_{k=1}^{N} (\bar{Q}_{11})_k \frac{(z^3_k - z^3_{k-1})}{3} \qquad (2.19a)$$

$$D_{12} = \int_{-\frac{1}{2}H}^{+\frac{1}{2}H} \bar{Q}_{12}\, z^2\, dz = \sum_{k=1}^{N} (\bar{Q}_{12})_k \frac{(z^3_k - z^3_{k-1})}{3} \qquad (2.19b)$$

$$D_{16} = \int_{-\frac{1}{2}H}^{+\frac{1}{2}H} \bar{Q}_{16}\, z^2\, dz = \sum_{k=1}^{N} (\bar{Q}_{16})_k \frac{(z^3_k - z^3_{k-1})}{3} \qquad (2.19c)$$

$$D_{22} = \int_{-\frac{1}{2}H}^{+\frac{1}{2}H} \bar{Q}_{22}\, z^2\, dz = \sum_{k=1}^{N} (\bar{Q}_{22})_k \frac{(z^3_k - z^3_{k-1})}{3} \qquad (2.19d)$$

$$D_{26} = \int_{-\frac{1}{2}H}^{+\frac{1}{2}H} \bar{Q}_{26}\, z^2\, dz = \sum_{k=1}^{N} (\bar{Q}_{26})_k \frac{(z^3_k - z^3_{k-1})}{3} \qquad (2.19e)$$

$$D_{66} = \int_{-\frac{1}{2}H}^{+\frac{1}{2}H} \bar{Q}_{66}\, z^2\, dz = \sum_{k=1}^{N} (\bar{Q}_{66})_k \frac{(z^3_k - z^3_{k-1})}{3} \qquad (2.19f)$$

The A's are the extentional stiffnesses for the laminate, the B's are the bending/extentional stiffnesses for the laminate, and the D's are the bending stiffnesses for the laminate. These stiffnesses, using index notation, are:

$$A_{ij} = \sum_{k=1}^{N} (\bar{Q}_{ij})_k \, (z_k - z_{k-1}) \qquad i,j = 1,2,6 \qquad (2.20)$$

$$B_{ij} = \sum_{k=1}^{N} (\bar{Q}_{ij})_k \, \frac{(z^2_k - z^2_{k-1})}{2} \qquad i,j = 1,2,6 \qquad (2.21)$$

$$D_{ij} = \sum_{k=1}^{N} (\bar{Q}_{ij})_k \, \frac{(z^3_k - z^3_{k-1})}{3} \qquad i,j = 1,2,6 \qquad (2.22)$$

Equations 2.16a-f in terms of the A's, B's, and D's, now become

$$N_x = A_{11}\,\epsilon^0_x + B_{11}\,K^0_x + A_{12}\,\epsilon^0_y + B_{12}\,K^0_y + A_{16}\,\Gamma^0_{xy} + B_{16}\,K^0_{xy} \qquad (2.23a)$$

$$N_y = A_{12}\,\epsilon^0_x + B_{12}\,K^0_x + A_{22}\,\epsilon^0_y + B_{22}\,K^0_y + A_{26}\,\Gamma^0_{xy} + B_{26}\,K^0_{xy} \qquad (2.23b)$$

$$N_{xy} = A_{16}\,\epsilon^0_x + B_{16}\,K^0_x + A_{26}\,\epsilon^0_y + B_{26}\,K^0_y + A_{66}\,\Gamma^0_{xy} + B_{66}\,K^0_{xy} \qquad (2.23c)$$

$$M_x = B_{11}\,\epsilon^0_x + D_{11}\,K^0_x + B_{12}\,\epsilon^0_y + D_{12}\,K^0_y + B_{16}\,\Gamma^0_{xy} + D_{16}\,K^0_{xy} \qquad (2.23d)$$

$$M_y = B_{12}\,\epsilon^0_x + D_{12}\,K^0_x + B_{22}\,\epsilon^0_y + D_{22}\,K^0_y + B_{26}\,\Gamma^0_{xy} + D_{26}\,K^0_{xy} \qquad (2.23e)$$

$$M_{xy} = B_{16}\,\epsilon^0_x + D_{16}\,K^0_x + B_{26}\,\epsilon^0_y + D_{26}\,K^0_y + B_{66}\,\Gamma^0_{xy} + D_{66}\,K^0_{xy} \qquad (2.23f)$$

Using matrix notation, equations 2.23a-f are:

$$\begin{bmatrix} N_x \\ N_y \\ N_{xy} \\ M_x \\ M_y \\ M_{xy} \end{bmatrix} = \begin{bmatrix} A_{11} & A_{12} & A_{16} & B_{11} & B_{12} & B_{16} \\ A_{12} & A_{22} & A_{26} & B_{12} & B_{22} & B_{26} \\ A_{16} & A_{26} & A_{66} & B_{16} & B_{26} & B_{66} \\ B_{11} & B_{12} & B_{16} & D_{11} & D_{12} & D_{16} \\ B_{12} & B_{22} & B_{26} & D_{12} & D_{22} & D_{26} \\ B_{16} & B_{26} & B_{66} & D_{16} & D_{26} & D_{66} \end{bmatrix} \begin{bmatrix} \epsilon^0{}_x \\ \epsilon^0{}_y \\ \Gamma^0{}_{xy} \\ K^0{}_x \\ K^0{}_y \\ K^0{}_{xy} \end{bmatrix} \quad (2.24)$$

The coupling stiffnesses B_{ij} are zero when the laminate is symmetrical. These terms imply that there is coupling between bending and extension. Subjecting a laminate which has coupling stiffnesses to extensional loads will cause the laminate to bend and/or twist in addition to stretching. Subjecting a laminate which has coupling stiffnesses to moments will cause the middle surface of the laminate to extend and shear, in addition to bending and/or twisting.

The coupling stiffnesses are equal to zero when the laminate is symmetric in both geometry and material properties about the middle surface of the laminate. (See Jones [1], page 160)

If the laminate is symmetric, equation 2.24 decouples and results in:

$$\begin{bmatrix} N_x \\ N_y \\ N_{xy} \end{bmatrix} = \begin{bmatrix} A_{11} & A_{12} & A_{16} \\ A_{12} & A_{22} & A_{26} \\ A_{16} & A_{26} & A_{66} \end{bmatrix} \begin{bmatrix} \epsilon^0{}_x \\ \epsilon^0{}_y \\ \Gamma^0{}_{xy} \end{bmatrix} \quad (2.25)$$

$$\begin{bmatrix} M_x \\ M_y \\ M_{xy} \end{bmatrix} \quad \begin{bmatrix} D_{11} & D_{12} & D_{16} \\ D_{12} & D_{22} & D_{26} \\ D_{16} & D_{26} & D_{66} \end{bmatrix} \begin{bmatrix} K^0{}_x \\ K^0{}_y \\ K^0{}_{xy} \end{bmatrix} \qquad (2.26)$$

The presence of the A_{16} and A_{26} stiffnesses in equation 2.25 shows that there is coupling between normal force resultants and shearing strain, and coupling between the shearing force resultant and normal strains. The presence of the D_{16} and D_{26} stiffnesses in equation 2.26 shows that there is coupling between bending moment resultants and twisting curvature, and coupling between the twisting moment resultant and normal curvatures.

Nonlinear Equilibrium Equations And Associated Boundary Conditions

Consider a portion of a laminated fiber-reinforced plate as shown in Figure 2.8. The x-y coordinate plane corresponds to the middle surface of the plate. The z-axis is perpendicular to the middle surface and, as stated before, z is measured relative to the middle surface. The total thickness of the plate is denoted by H. The interior region of the plate is denoted by Ω. The boundary of the hole in the plate as seen from the z-direction is denoted by Γ_1. For our case, the boundary Γ_1 does not have prescribed forces acting on it and no displacements are specified. The boundary around the plate as seen from the z-direction is

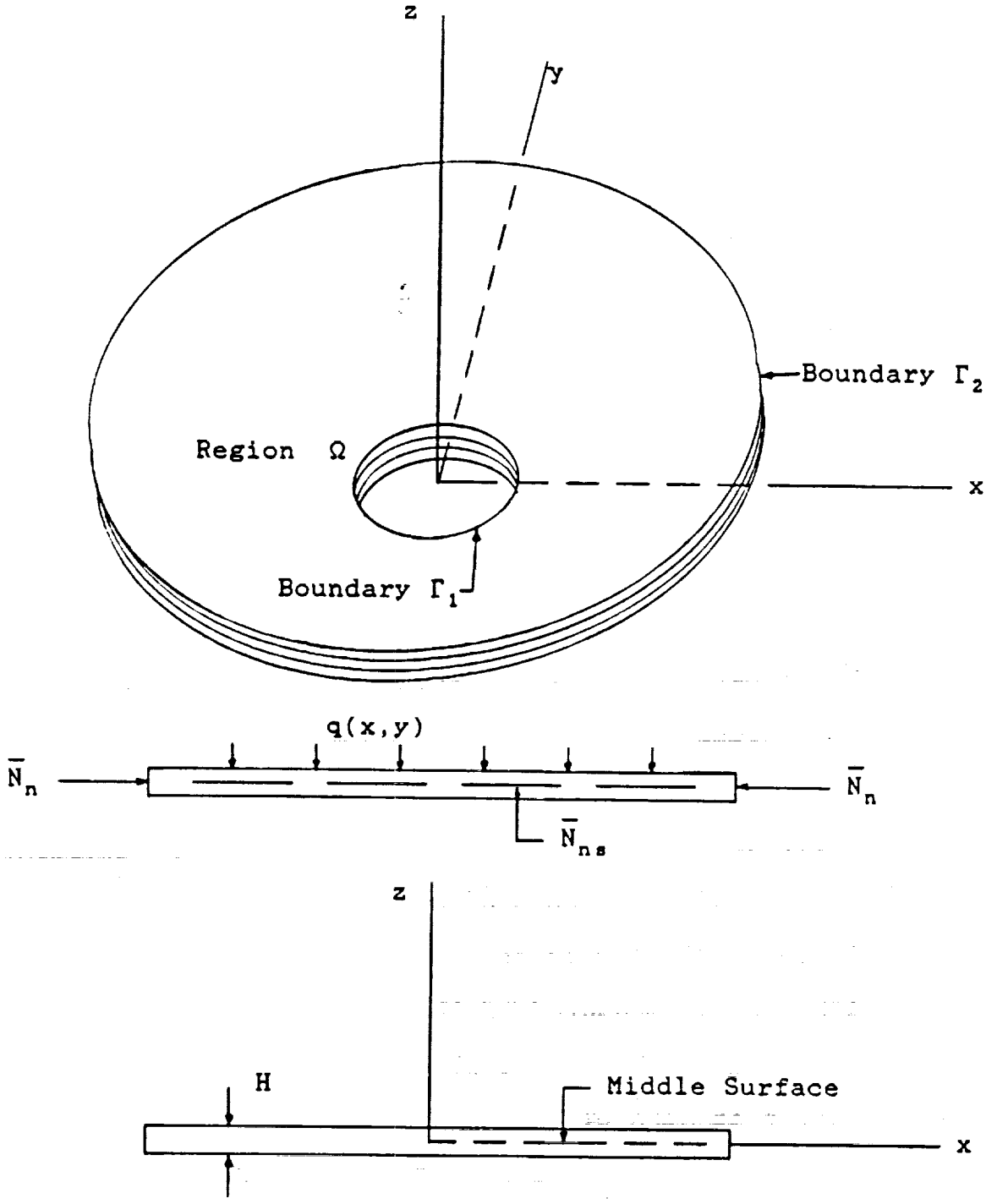

Figure 2.8 Thin Plate Prescribed Loading

denoted by Γ_2. For simplicity Γ_2 is considered at this point to be a smooth curve. In reality, Γ_2 is the boundary of a rectangular plate. The in-plane force resultants $\bar{N}_n$ and $\bar{N}_{ns}$ are prescribed on Γ_2. $\bar{N}_n$ acts in the direction normal to the boundary Γ_2 and $\bar{N}_{ns}$ acts in the direction tangential to the boundary Γ_2. The normal load distribution $q(x,y)$ acts downward on the region Ω perpendicular to the x-y plane of the plate.

The total potential energy of the loaded plate π, is defined as the sum of the total strain energy U and the potential of the applied force V.

$$\pi = U + V \tag{2.27}$$

The equilibrium equations and boundary conditions are determined by setting the first variation of the total potential equal to zero. (Shames and Dym [2], pp. 401-408). That is

$$\delta^{(1)}\pi = \delta^{(1)}(U + V) = 0 \tag{2.28}$$

The total strain energy is

$$U = \iiint_{\underline{V}} u \, d\underline{V} = \iiint_{\underline{V}} \left[\int_0^{\epsilon_{ij}} \tau_{ij} \, d\epsilon_{ij} \right] d\underline{V} \tag{2.29}$$

where: $$u = \int_0^{\epsilon_{ij}} \tau_{ij} \, d\epsilon_{ij} \tag{2.30}$$

This integral is a point function of the upper limit ϵ_{ij} if this integral is independent of the path taken between the limits 0 and ϵ_{ij}, meaning that $\tau_{ij} \, d\epsilon_{ij}$ must be a perfect differential. When these conditions are met, then

$$du = \tau_{ij}\, d\epsilon_{ij} \qquad (2.31)$$

Recall from page 11 the assumption that each layer exhibits linear elastic behavior, meaning that each stress component is linearly related to all of the strains by Hooke's Law which can be stated as:

$$\tau_{ij} = C_{ijkl}\, \epsilon_{kl} \qquad (2.32)$$

where $C_{ijkl} = C_{jikl}$ since $\tau_{ij} = \tau_{ji}$

and $C_{ijkl} = C_{ijlk}$ since $\epsilon_{kl} = \epsilon_{lk}$

Substituting equation 2.32 into equation 2.29 results in

$$U = \iiint_{\underline{V}} \left[\int C_{ijkl}\, \epsilon_{kl}\, d\epsilon_{ij} \right] d\underline{V} \qquad (2.33)$$

where the quantity inside the brackets is a perfect differential and the coefficients C_{ijkl} are constants. Equation 2.33 may now be expanded to take the form

$$U = \iiint_{\underline{V}} \left[\tfrac{1}{2} C_{ijkl}\, \epsilon_{kl}\, d\epsilon_{ij} + \tfrac{1}{2} C_{klij}\, \epsilon_{ij}\, d\epsilon_{kl} \right] d\underline{V}$$

if $C_{ijkl} = C_{klij}$

Thus, the following is established:

$$U = \iiint_{\underline{V}} \tfrac{1}{2} C_{ijkl}\, \epsilon_{kl}\, \epsilon_{ij}\, d\underline{V} \qquad (2.34)$$

Substituting τ_{ij} for $C_{ijkl}\, \epsilon_{kl}$ in equation 2.34 results in

$$U = \iiint_{\underline{V}} \tfrac{1}{2} \tau_{ij}\, \epsilon_{ij}\, d\underline{V} \qquad (2.35)$$

As stated on page 11, it is assumed that the plate is in a state of plane stress, so expanding equation 2.35 for this

case leads to

$$U = \tfrac{1}{2} \iiint_{\underline{V}} [\, \tau_{xx}\epsilon_{xx} + \tau_{yy}\epsilon_{yy} + 2\, \tau_{xy}\epsilon_{xy} \,]\, d\underline{V} \qquad (2.36)$$

Returning to contracted notation,

$$\tau_{xx} = \sigma_x \qquad \tau_{yy} = \sigma_y$$

$$\epsilon_{xx} = \epsilon_x \qquad \epsilon_{yy} = \epsilon_y$$

and noting that $\epsilon_{xy} = \tfrac{1}{2}\, \Gamma_{xy}$

Substituting these relations into equation 2.36 results in the following equation for the total strain energy for linear elastic behavior

$$U = \tfrac{1}{2} \iiint_{\underline{V}} [\, \sigma_x\, \epsilon_x + \sigma_y\, \epsilon_y + \tau_{xy}\, \Gamma_{xy} \,]\, d\underline{V} \qquad (2.37)$$

Using equations 2.8 and 2.9, the stress-strain relations in the x-y coordinate system for linear elastic behavior, an orthotropic material, and a state of plane stress, are:

$$\sigma_x = \frac{E_x}{1 - \mu_{xy}\mu_{yx}} (\epsilon_x + \mu_{yx}\epsilon_y) \qquad (2.38a)$$

$$\sigma_y = \frac{E_y}{1 - \mu_{xy}\mu_{yx}} (\epsilon_y + \mu_{xy}\epsilon_x) \qquad (2.38b)$$

$$\tau_{xy} = G_{xy}\Gamma_{xy} \qquad (2.38c)$$

From equation 2.9b

$$\frac{E_y\mu_{xy}}{1 - \mu_{xy}\mu_{yx}} = \frac{E_x\mu_{yx}}{1 - \mu_{xy}\mu_{yx}} \qquad (2.39)$$

Substitute equations 2.38a-c into equation 2.37 to obtain

$$U = \tfrac{1}{2} \iiint_{\underline{V}} \left[\frac{E_x}{1 - \mu_{xy}\mu_{yx}} (\epsilon_x + \mu_{yx}\epsilon_y)\epsilon_x \right.$$

$$\left. + \frac{E_y}{1 - \mu_{xy}\mu_{yx}} (\epsilon_y + \mu_{xy}\epsilon_x)\epsilon_y + (G_{xy}\Gamma_{xy})\Gamma_{xy} \right] d\underline{V}$$

Combining terms in the equation above, obtain:

$$U = \tfrac{1}{2} \iiint_{\underline{V}} \left[\frac{E_x}{1 - \mu_{xy}\mu_{yx}} \epsilon_x^2 + \frac{E_x\mu_{yx}}{1 - \mu_{xy}\mu_{yx}} \epsilon_y\epsilon_x \right.$$

$$+ \frac{E_y}{1 - \mu_{xy}\mu_{yx}} \epsilon_y^2 + \frac{E_y\mu_{xy}}{1 - \mu_{xy}\mu_{yx}} \epsilon_x\epsilon_y$$

$$\left. + G_{xy}\Gamma_{xy}^2 \right] d\underline{V} \qquad (2.40)$$

The number of terms in equation 2.40 may be simplified using equation 2.39 to obtain:

$$U = \tfrac{1}{2} \iiint_{\underline{V}} \left[\frac{E_x}{1 - \mu_{xy}\mu_{yx}} \epsilon_x^2 + \frac{2\,E_x\mu_{yx}}{1 - \mu_{xy}\mu_{yx}} \epsilon_y\epsilon_x \right.$$

$$\left. + \frac{E_y}{1 - \mu_{xy}\mu_{yx}} \epsilon_y^2 + G_{xy}\Gamma_{xy}^2 \right] d\underline{V} \qquad (2.41)$$

The first variation of the total strain energy is taken with respect to the strains as extremal functions, noting first that in principle:

$$\delta(\alpha^2) = 2\,\alpha(\delta\alpha) \tag{2.42a}$$

$$\delta(\alpha\beta) = \alpha(\delta\beta) + \beta(\delta\alpha) \tag{2.42b}$$

Therefore,

$$\delta^{(1)}U = \tfrac{1}{2}\iiint_{\underline{V}}\left[\frac{2\,E_x}{1-\mu_{xy}\mu_{yx}}\epsilon_x\delta\epsilon_x + \frac{2\,E_x\mu_{yx}}{1-\mu_{xy}\mu_{yx}}\epsilon_y\delta\epsilon_x + \frac{2\,E_x\mu_{yx}}{1-\mu_{xy}\mu_{yx}}\epsilon_x\delta\epsilon_y + \frac{2\,E_y}{1-\mu_{xy}\mu_{yx}}\epsilon_y\delta\epsilon_y + 2\,G_{xy}\Gamma_{xy}\delta\Gamma_{xy}\right]d\underline{V} \tag{2.43}$$

The factor $\tfrac{1}{2}$ is cancelled in the process and again using equation 2.39 to change the third term in equation 2.43 to obtain the desired form for a recombination of terms:

$$\delta^{(1)}U = \iiint_{\underline{V}}\left[\frac{E_x}{1-\mu_{xy}\mu_{yx}}\epsilon_x\delta\epsilon_x + \frac{E_x\mu_{yx}}{1-\mu_{xy}\mu_{yx}}\epsilon_y\delta\epsilon_x + \frac{E_y\mu_{xy}}{1-\mu_{xy}\mu_{yx}}\epsilon_x\delta\epsilon_y + \frac{E_y}{1-\mu_{xy}\mu_{yx}}\epsilon_y\delta\epsilon_y + G_{xy}\Gamma_{xy}\delta\Gamma_{xy}\right]d\underline{V} \tag{2.44}$$

$$\delta^{(1)}U = \iiint_{\underline{V}}\left[\frac{E_x}{1-\mu_{xy}\mu_{yx}}(\epsilon_x + \mu_{yx}\epsilon_y)\,\delta\epsilon_x + \frac{E_y}{1-\mu_{xy}\mu_{yx}}(\mu_{xy}\epsilon_x + \epsilon_y)\,\delta\epsilon_y + G_{xy}\Gamma_{xy}\delta\Gamma_{xy}\right]d\underline{V} \tag{2.45}$$

Using equations 2.38a-c, the first variation in the total strain energy is expressed as:

$$\delta^{(1)}U = \iiint_{\underline{V}} [\, \sigma_x \delta\epsilon_x + \sigma_y \delta\epsilon_y + \tau_{xy} \delta\Gamma_{xy} \,]\, d\underline{V} \qquad (2.46)$$

To express the first variation in the total strain energy in terms of stress and displacement, substitute the strain-displacement relations in equations 2.3a-c into equation 2.46 to obtain:

$$\begin{aligned}\delta^{(1)}U = \iiint_{\underline{V}} [\, & \sigma_x \delta(u^0_{,x} - z\, w^0_{,xx} + \tfrac{1}{2}\,[w^0_{,x}]^2) \\ & + \sigma_y \delta(v^0_{,y} - z\, w^0_{,yy} + \tfrac{1}{2}\,[w^0_{,y}]^2) \\ & + \tau_{xy} \delta(u^0_{,y} + v^0_{,x} - 2\, z\, w^0_{,xy} + w^0_{,x}\, w^0_{,y}) \,]\, d\underline{V} \end{aligned} \qquad (2.47)$$

Noting that the delta operator and differential operator are commutative as shown by the following in principle:

$$\delta(\alpha_{,x}) = (\delta\alpha)_{,x} \qquad (2.48a)$$

$$\delta(\alpha_{,y}) = (\delta\alpha)_{,y} \qquad (2.48b)$$

Using equations 2.42a-b and 2.48a-b, equation 2.47 becomes

$$\begin{aligned}\delta^{(1)}U = \iiint_{\underline{V}} [\, & \sigma_x \{(\delta u^0)_{,x} - z\, (\delta w^0)_{,xx} + w^0_{,x} (\delta w^0)_{,x}\} \\ & + \sigma_y \{(\delta v^0)_{,y} - z\, (\delta w^0)_{,yy} + w^0_{,y} (\delta w^0)_{,y}\} \\ & + \tau_{xy} \{(\delta u^0)_{,y} + (\delta v^0)_{,x} - 2\, z\, (\delta w^0)_{,xy} + w^0_{,x} (\delta w^0)_{,y} + w^0_{,y} (\delta w^0)_{,x}\} \,]\, d\underline{V} \end{aligned} \qquad (2.49)$$

Expressing the volume integral in equation 2.49 in terms of plate thickness and the area of region Ω , or middle surface of the plate (x-y plane), results in:

$$\delta^{(1)}U = \iint_{\Omega} \int_{-\frac{1}{2}H}^{+\frac{1}{2}H} [\, \sigma_x\{(\delta u^0)_{,x} - z\,(\delta w^0)_{,xx} + w^0_{,x}(\delta w^0)_{,x}\}$$

$$+ \sigma_y\{(\delta v^0)_{,y} - z\,(\delta w^0)_{,yy} + w^0_{,y}(\delta w^0)_{,y}\}$$

$$+ \tau_{xy}\{(\delta u^0)_{,y} + (\delta v^0)_{,x} - 2\,z\,(\delta w^0)_{,xy}\}$$

$$+ \tau_{xy}\{w^0_{,x}(\delta w^0)_{,y} + w^0_{,y}(\delta w^0)_{,x}\}\,]\, dz\, dx\, dy \quad (2.50)$$

The middle surface displacements u^0, v^0, and w^0 are not functions of z. Therefore those displacements may be placed outside of the integral over the thickness of the plate. The result is

$$\delta^{(1)}U = \iint_{\Omega} [\{(\delta u^0)_{,x} + w^0_{,x}(\delta w^0)_{,x}\} \int_{-\frac{1}{2}H}^{+\frac{1}{2}H} \sigma_x\, dz - (\delta w^0)_{,xx} \int_{-\frac{1}{2}H}^{+\frac{1}{2}H} \sigma_x z\, dz$$

$$+ \{(\delta v^0)_{,y} + w^0_{,y}(\delta w^0)_{,y}\} \int_{-\frac{1}{2}H}^{+\frac{1}{2}H} \sigma_y\, dz - (\delta w^0)_{,yy} \int_{-\frac{1}{2}H}^{+\frac{1}{2}H} \sigma_y z\, dz$$

$$+ \{(\delta u^0)_{,y} + (\delta v^0)_{,x}\} \int_{-\frac{1}{2}H}^{+\frac{1}{2}H} \tau_{xy}\, dz - 2\,(\delta w^0)_{,xy} \int_{-\frac{1}{2}H}^{+\frac{1}{2}H} \tau_{xy} z\, dz$$

$$+ \{w^0_{,x}(\delta w^0)_{,y} + w^0_{,y}(\delta w^0)_{,x}\} \int_{-\frac{1}{2}H}^{+\frac{1}{2}H} \tau_{xy} dz\,]\, dx\, dy \quad (2.51)$$

Substituting equations 2.14a-f, the force and moment resultants, into equation 2.51 results in

$$\delta^{(1)}U = \iint_{\Omega} [\, N_x\{(\delta u^0)_{,x} + w^0_{,x}(\delta w^0)_{,x}\} - M_x(\delta w^0)_{,xx}$$

$$+ N_y\{(\delta v^0)_{,y} + w^0_{,y}(\delta w^0)_{,y}\} - M_y(\delta w^0)_{,yy}$$

$$+ N_{xy}\{(\delta u^0)_{,y} + (\delta v^0)_{,x}\} - 2\,M_{xy}(\delta w^0)_{,xy}$$

$$+ N_{xy}\{w^0_{,x}(\delta w^0)_{,y} + w^0_{,y}(\delta w^0)_{,x}\}\,]\, dx\, dy \quad (2.52)$$

The first variation of the potential of the applied forces and the normal load distribution is

$$\delta^{(1)}V = \oint_{\Gamma_2} \bar{N}_n \, \delta u^0{}_n ds + \oint_{\Gamma_2} \bar{N}_{ns} \delta u^0{}_s ds - \iint_{\Omega} q \, \delta w^0 \, dx \, dy \quad (2.53)$$

Note that $\bar{N}_n$ is taken as positive in compression as shown in Figure 2.8.

Using equations 2.52 and 2.53 to form the first variation of the total potential energy π and setting that variation equal to zero to satisfy the necessary requirement for extremization of π, leads to

$$\delta^{(1)}\pi = \delta^{(1)}U + \delta^{(1)}V = 0$$

$$\begin{aligned}\delta^{(1)}\pi = \iint_{\Omega} \Big[& N_x\{(\delta u^0)_{,x} + w^0_{,x}(\delta w^0)_{,x}\} - M_x(\delta w^0)_{,xx} \\ & + N_y\{(\delta v^0)_{,y} + w^0_{,y}(\delta w^0)_{,y}\} - M_y(\delta w^0)_{,yy} \\ & + N_{xy}\{(\delta u^0)_{,y} + (\delta v^0)_{,x}\} - 2 M_{xy}(\delta w^0)_{,xy} \\ & + N_{xy}\{w^0_{,x}(\delta w^0)_{,y} + w^0_{,y}(\delta w^0)_{,x}\} \Big] \, dx \, dy \\ & + \oint_{\Gamma_2} \bar{N}_n \, \delta u^0{}_n ds + \oint_{\Gamma_2} \bar{N}_{ns} \delta u^0{}_s ds - \iint_{\Omega} q \, \delta w^0 \, dx \, dy \\ = \; & 0 \end{aligned} \quad (2.54)$$

Referring to Figure 2.9, and using the chain rule for differentiation to establish a relation between the partial derivatives in x-y coordinates and the partial derivatives in n-s coordinates, results in

$$( )_{,x} = (n)_{,x} ( )_n + (s)_{,x} ( )_s \quad (2.55a)$$

$$( )_{,y} = (n)_{,y} ( )_n + (s)_{,y} ( )_s \quad (2.55b)$$

Using Figure 2.9, equations 2.55a-b can be re-written to be

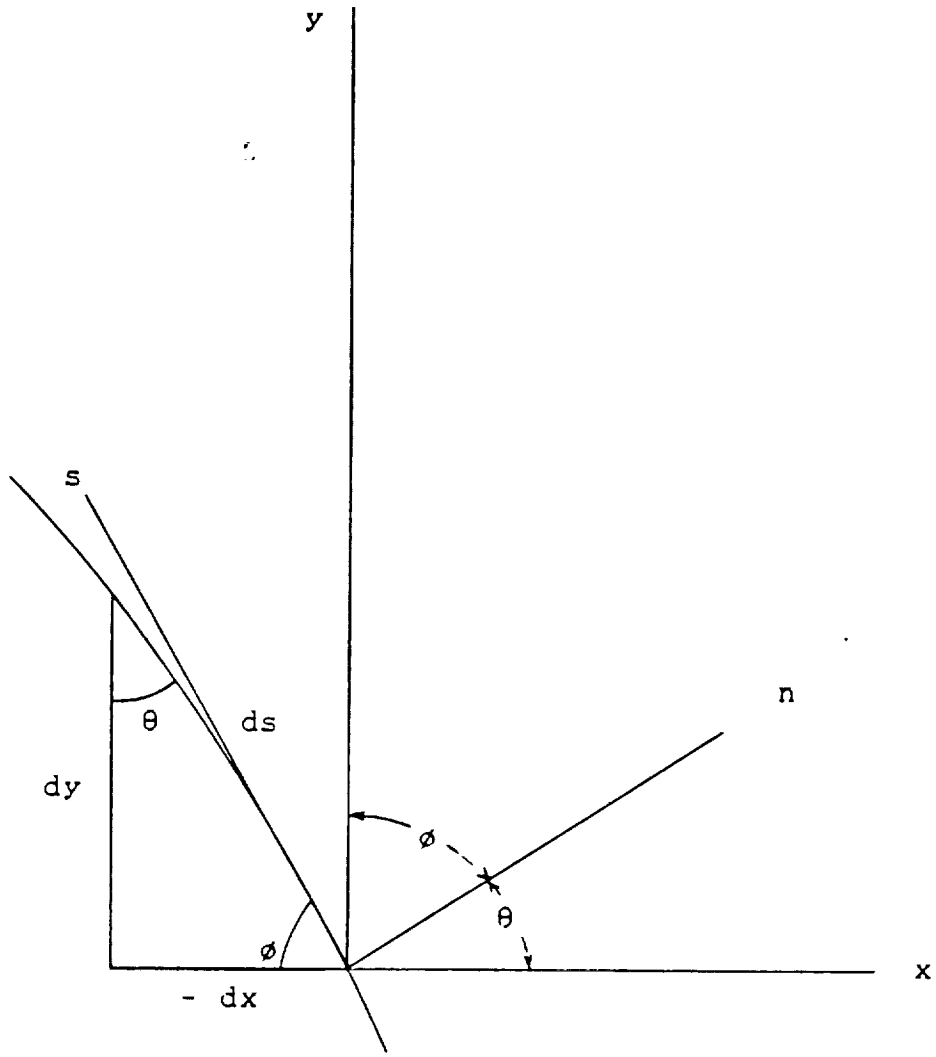

$$dx = - \cos \phi \, ds = - a_{ny} \, ds$$

$$dy = \cos \theta \, ds = a_{nx} \, ds$$

Figure 2.9 Relation Of Differentials At Boundary

$$( )_{,x} = a_{nx}( )_{,n} + a_{sx}( )_{,s} \quad (2.56a)$$

$$( )_{,y} = a_{ny}( )_{,n} + a_{sy}( )_{,s} \quad (2.56b)$$

From the geometry of Figure 2.9, considering n and s to be a rectangular set of coordinates at a point on the boundary

$$a_{nx} = \cos(n,x) = \cos\theta = (n)_{,x} \quad (2.57a)$$

$$a_{sx} = \cos(s,x) = \cos(\pi/2 + \theta) = -\sin\theta = (s)_{,x} \quad (2.57b)$$

$$a_{ny} = \cos(n,y) = \cos\phi = \sin\theta = (n)_{,y} \quad (2.57c)$$

$$a_{sy} = \cos(s,y) = \cos\theta = (s)_{,y} \quad (2.57d)$$

where by definition:

cos(n,x) is the cosine of the angle between the n and x axes

cos(s,x) is the cosine of the angle between the s and x axes

cos(n,y) is the cosine of the angle between the n and y axes

cos(s,y) is the cosine of the angle between the s and y axes

From equations 2.57a-d

$$a_{sx} = -a_{ny} \quad (2.58a)$$

$$a_{sy} = a_{nx} \quad (2.58b)$$

Using equations 2.58a-b, equations 2.56a-b can be re-written as

$$( )_{,x} = a_{nx}( )_{,n} - a_{ny}( )_{,s} \quad (2.59a)$$

$$( )_{,y} = a_{ny}( )_{,n} + a_{nx}( )_{,s} \quad (2.59b)$$

From the geometry of Figure 2.9

$$a_{nx} = \cos\theta = \frac{dy}{ds} \quad (2.60a)$$

$$a_{ny} = \cos\phi = -\frac{dx}{ds} \quad (2.60b)$$

In the x-y coordinate system, u^0 and v^0 are the middle surface displacements. In the n-s coordinate system, u^0_n and u^0_s are the middle surface displacements. From the

geometry of Figure 2.9, transformation from the x-y coordinate system to the n-s coordinate system yields

$$u^0_n = a_{nx}\, u^0 + a_{ny}\, v^0 \qquad (2.61a)$$

$$u^0_s = - a_{ny}\, u^0 + a_{nx}\, v^0 \qquad (2.61b)$$

Transformation from the n-s coordinate system to the x-y coordinate system yields

$$u^0 = a_{nx}\, u^0_n - a_{ny}\, u^0_s \qquad (2.62a)$$

$$v^0 = a_{ny}\, u^0_n + a_{nx}\, u^0_s \qquad (2.62b)$$

Green's Theorem for integration by parts in two dimensions may be expressed in general as follows:

$$\iint \alpha\, \beta_{,x}\, dx\, dy = - \iint \alpha_{,x} \beta\, dx\, dy + \oint (\alpha\beta)\, a_{nx} ds \qquad (2.63a)$$

$$\iint \alpha\, \beta_{,y}\, dx\, dy = - \iint \alpha_{,y} \beta\, dx\, dy + \oint (\alpha\beta)\, a_{ny} ds \qquad (2.63b)$$

Applying Green's Theorem as expressed by equations 2.63 to change the terms in equation 2.54 which involve partial derivatives of the variations in u^0, v^0, and w^0, and to permit extraction of those terms from the area integrals, results in the following:

$$\iint_\Omega N_x (\delta u^0)_{,x}\, dx\, dy = - \iint_\Omega N_{x,x} \delta u^0\, dx\, dy + \oint_{\Gamma_2} N_x \delta u^0\, a_{nx} ds$$

$$\iint_\Omega N_x w^0_{,x} (\delta w^0)_{,x}\, dx\, dy = - \iint_\Omega (N_x w^0_{,x})_{,x} \delta w^0\, dx\, dy + \oint_{\Gamma_2} N_x w^0_{,x} \delta w^0\, a_{nx} ds$$

$$\iint_\Omega M_x (\delta w^0)_{,xx}\, dx\, dy = - \iint_\Omega M_{x,x} (\delta w^0)_{,x}\, dx\, dy + \oint_{\Gamma_2} M_x (\delta w^0)_{,x} a_{nx} ds$$

$$= \iint_\Omega M_{x,xx} \delta w^0\, dx\, dy - \oint_{\Gamma_2} M_{x,x} \delta w^0\, a_{nx} ds + \oint_{\Gamma_2} M_x (\delta w^0)_{,x} a_{nx} ds$$

Note that Green's Theorem is applied for two successive integrations to extract the second-order partial derivative of

the variation in w^0 whereas one integration is required to extract first-order partial derivatives of the variations in u^0, v^0, or w^0.

$$\iint_\Omega N_y(\delta v^0)_{,y}dx\,dy = -\iint_\Omega N_{y,y}\delta v^0\,dx\,dy + \oint_{\Gamma_2} N_y\delta v^0\,a_{ny}ds$$

$$\iint_\Omega N_y w^0_{,y}(\delta w^0)_{,y}dx\,dy = -\iint_\Omega (N_y w^0_{,y})_{,y}\delta w^0\,dx\,dy + \oint_{\Gamma_2} N_y w^0_{,y}\delta w^0\,a_{ny}ds$$

$$\iint_\Omega M_y(\delta w^0)_{,yy}dx\,dy = -\iint_\Omega M_{y,y}(\delta w^0)_{,y}dx\,dy + \oint_{\Gamma_2} M_y(\delta w^0)_{,y}a_{ny}ds$$

$$= \iint_\Omega M_{y,yy}\delta w^0\,dx\,dy - \oint_{\Gamma_2} M_{y,y}\delta w^0\,a_{ny}ds + \oint_{\Gamma_2} M_y(\delta w^0)_{,y}a_{ny}ds$$

$$\iint_\Omega N_{xy}(\delta u^0)_{,y}dx\,dy = -\iint_\Omega N_{xy,y}\delta u^0\,dx\,dy + \oint_{\Gamma_2} N_{xy}\delta u^0\,a_{ny}ds$$

$$\iint_\Omega N_{xy}(\delta v^0)_{,x}dx\,dy = -\iint_\Omega N_{xy,x}\delta v^0\,dx\,dy + \oint_{\Gamma_2} N_{xy}\delta v^0\,a_{nx}ds$$

$$\iint_\Omega N_{xy}w^0_{,x}(\delta w^0)_{,y}dx\,dy = -\iint_\Omega (N_{xy}w^0_{,x})_{,y}\delta w^0\,dx\,dy + \oint_{\Gamma_2} N_{xy}w^0_{,x}\delta w^0\,a_{ny}ds$$

$$\iint_\Omega N_{xy}w^0_{,y}(\delta w^0)_{,x}dx\,dy = -\iint_\Omega (N_{xy}w^0_{,y})_{,x}\delta w^0\,dx\,dy + \oint_{\Gamma_2} N_{xy}w^0_{,y}\delta w^0\,a_{nx}ds$$

$$\iint_\Omega M_{xy}(\delta w^0)_{,xy}dx\,dy = -\iint_\Omega M_{xy,x}(\delta w^0)_{,y}dx\,dy + \oint_{\Gamma_2} M_{xy}(\delta w^0)_{,y}a_{nx}ds$$

$$= \iint_\Omega M_{xy,xy}\delta w^0\,dx\,dy - \oint_{\Gamma_2} M_{xy,x}\delta w^0\,a_{ny}ds + \oint_{\Gamma_2} M_{xy}(\delta w^0)_{,y}a_{nx}ds$$

The equation immediately above was integrated first with respect to x and then integrated with respect to y. Reversing the order of integration provides a result which may be used additionally in view of the factor 2 in equation 2.54 for the term involving the moment resultant M_{xy}.

$$\iint_{\Omega} M_{xy}(\delta w^0)_{,xy}\,dx\,dy = -\iint_{\Omega} M_{xy,y}(\delta w^0)_{,x}\,dx\,dy + \oint_{\Gamma_2} M_{xy}(\delta w^0)_{,x}a_{ny}\,ds$$

$$= \iint_{\Omega} M_{xy,yx}\delta w^0\,dx\,dy - \oint_{\Gamma_2} M_{xy,y}\delta w^0\,a_{nx}\,ds + \oint_{\Gamma_2} M_{xy}(\delta w^0)_{,x}a_{ny}\,ds$$

The results of having applied Green's Theorem to equation 2.54 may be combined and written as follows for extremization of the first variation of the total potential energy.

$$- \iint_{\Omega} N_{x,x}\delta u^0\,dx\,dy + \oint_{\Gamma_2} N_x\delta u^0\,a_{nx}\,ds$$

$$- \iint_{\Omega} (N_x w^0_{,x})_{,x}\delta w^0\,dx\,dy + \oint_{\Gamma_2} N_x w^0_{,x}\delta w^0\,a_{nx}\,ds$$

$$- \iint_{\Omega} N_{y,y}\delta v^0\,dx\,dy + \oint_{\Gamma_2} N_y\delta v^0\,a_{ny}\,ds$$

$$- \iint_{\Omega} (N_y w^0_{,y})_{,y}\delta w^0\,dx\,dy + \oint_{\Gamma_2} N_y w^0_{,y}\delta w^0\,a_{ny}\,ds$$

$$- \iint_{\Omega} N_{xy,y}\delta u^0\,dx\,dy + \oint_{\Gamma_2} N_{xy}\delta u^0\,a_{ny}\,ds$$

$$- \iint_{\Omega} N_{xy,x}\delta v^0\,dx\,dy + \oint_{\Gamma_2} N_{xy}\delta v^0\,a_{nx}\,ds$$

$$- \iint_{\Omega} (N_{xy}w^0_{,x})_{,y}\delta w^0\,dx\,dy + \oint_{\Gamma_2} N_{xy}w^0_{,x}\delta w^0\,a_{ny}\,ds$$

$$- \iint_{\Omega} (N_{xy}w^0_{,y})_{,x}\delta w^0\,dx\,dy + \oint_{\Gamma_2} N_{xy}w^0_{,y}\delta w^0\,a_{nx}\,ds$$

$$- \iint_{\Omega} M_{x,xx}\delta w^0\,dx\,dy + \oint_{\Gamma_2} M_{x,x}\delta w^0\,a_{nx}\,ds - \oint_{\Gamma_2} M_x(\delta w^0)_{,x}a_{nx}\,ds$$

$$- \iint_{\Omega} M_{y,yy}\delta w^0\,dx\,dy + \oint_{\Gamma_2} M_{y,y}\delta w^0\,a_{ny}\,ds - \oint_{\Gamma_2} M_y(\delta w^0)_{,y}a_{ny}\,ds$$

$$- \iint_{\Omega} M_{xy,xy}\delta w^0\,dx\,dy + \oint_{\Gamma_2} M_{xy,x}\delta w^0\,a_{ny}\,ds - \oint_{\Gamma_2} M_{xy}(\delta w^0)_{,y}a_{nx}\,ds$$

$$- \iint_{\Omega} M_{xy,yx}\delta w^0\,dx\,dy + \oint_{\Gamma_2} M_{xy,y}\delta w^0\,a_{nx}\,ds - \oint_{\Gamma_2} M_{xy}(\delta w^0)_{,x}a_{ny}\,ds$$

$$+ \oint_{\Gamma_2} \bar{N}_n\,\delta u^0{}_n\,ds + \oint_{\Gamma_2} \bar{N}_{ns}\delta u^0{}_s\,ds - \iint_{\Omega} q\,\delta w^0\,dx\,dy = 0 \qquad (2.64)$$

Equation 2.64 is expressed in terms referred to the x-y coordinate system and provides a basis with which to determine plate equilibrium equations and the associated boundary conditions. The equation is complicated but may be simplified if a selection of terms is expressed with respect to the n-s coordinate system.

Stress components in the x-y coordinate system transform as a second-order tensor to the n-s coordinate system as expressed by the following equation:

$$\tau_{pk}^{(ns)} = a_{pj}\, a_{ki}\, \tau_{ji}^{(xy)} \qquad p,k = n,s \quad j,i = x,y \qquad (2.65)$$

The stress component τ_{nn} is

$$\tau_{nn} = a_{nj}\, a_{ni}\, \tau_{ji}$$

$$\tau_{nn} = a_{nx}\, a_{nx}\, \tau_{xx} + a_{nx}\, a_{ny}\, \tau_{xy} + a_{ny}\, a_{nx}\, \tau_{yx} + a_{ny}\, a_{ny}\, \tau_{yy} \qquad (2.66a)$$

The stress component τ_{ns} is

$$\tau_{ns} = a_{nj}\, a_{si}\, \tau_{ji}$$

$$\tau_{ns} = a_{nx}\, a_{sx}\, \tau_{xx} + a_{nx}\, a_{sy}\, \tau_{xy} + a_{ny}\, a_{sx}\, \tau_{yx} + a_{ny}\, a_{sy}\, \tau_{yy} \qquad (2.66b)$$

The stress tensor is symmetric (equation 2.32) so that equations 2.66a-b can be re-written as follows:

$$\tau_{nn} = a_{nx}^2\, \tau_{xx} + 2\, a_{nx}\, a_{ny}\, \tau_{xy} + a_{ny}^2\, \tau_{yy} \qquad (2.67a)$$

$$\tau_{ns} = a_{nx}\, a_{sx}\, \tau_{xx} + a_{nx}\, a_{sy}\, \tau_{xy} + a_{ny}\, a_{sx}\, \tau_{xy} + a_{ny}\, a_{sy}\, \tau_{yy} \qquad (2.67b)$$

Using the following relations

$$\tau_{nn} = \sigma_n \qquad \tau_{xx} = \sigma_x \qquad \tau_{yy} = \sigma_y$$

$$a_{ny} = -\, a_{sx} \qquad a_{nx} = a_{sy}$$

Equations 2.67a-b may be expressed as follows:

$$\sigma_n = a_{nx}^2 \sigma_x + 2 a_{nx} a_{ny} \tau_{xy} + a_{ny}^2 \sigma_y \qquad (2.68a)$$

$$\tau_{ns} = - a_{nx} a_{ny} \sigma_x + a_{nx}^2 \tau_{xy} - a_{ny}^2 \tau_{xy} + a_{nx} a_{ny} \sigma_y \qquad (2.68b)$$

The force and moment resultants in the n-s coordinate system may be expressed in terms of stress by the following equations:

$$N_n = \int_{-\frac{1}{2}H}^{+\frac{1}{2}H} \sigma_n \, dz \qquad (2.69a) \qquad M_n = \int_{-\frac{1}{2}H}^{+\frac{1}{2}H} \sigma_n \, z \, dz \qquad (2.69c)$$

$$N_{ns} = \int_{-\frac{1}{2}H}^{+\frac{1}{2}H} \tau_{ns} \, dz \qquad (2.69b) \qquad M_{ns} = \int_{-\frac{1}{2}H}^{+\frac{1}{2}H} \tau_{ns} \, z \, dz \qquad (2.69d)$$

The force resultants in the n-s coordinate system may be expressed in terms of the force resultants referred to the x-y coordinate system by integrating equations 2.68a-b over the plate thickness and using the definitions given by equations 2.69a-b and equations 2.14a-c which yields the following force resultant transformation equations:

$$N_n = a_{nx}^2 N_x + 2 a_{nx} a_{ny} N_{xy} + a_{ny}^2 N_y \qquad (2.70a)$$

$$N_{ns} = - a_{nx} a_{ny} N_x + a_{nx}^2 N_{xy} - a_{ny}^2 N_{xy} + a_{nx} a_{ny} N_y \qquad (2.70b)$$

The moment resultants in the n-s coordinate system may be expressed in terms of the moment resultants referred to the x-y coordinate system by multiplying equations 2.68a-b by z, integrating over the plate thickness, and using the definitions given by equations 2.69c-d and equations 2.14d-f which yields the following moment resultant transformation equations:

$$M_n = a_{nx}^2 M_x + 2 a_{nx} a_{ny} M_{xy} + a_{ny}^2 M_y \quad (2.71a)$$

$$M_{ns} = - a_{nx} a_{ny} M_x + a_{nx}^2 M_{xy} - a_{ny}^2 M_{xy} + a_{nx} a_{ny} M_y \quad (2.71b)$$

Proceeding with a selection of terms in equation 2.64 to be referred to the n-s coordinate system, and first considering the boundary integrals, equations 2.62a-b may be used to express variations in u^0 and v^0 as follows:

$$\delta u^0 = a_{nx} \delta u^0{}_n - a_{ny} \delta u^0{}_s \quad (2.72a)$$

$$\delta v^0 = a_{ny} \delta u^0{}_n + a_{nx} \delta u^0{}_s \quad (2.72b)$$

Selecting boundary integrals which include variations in u^0 and v^0 from equation 2.64, those integrals are referred to the n-s coordinate system as follows:

$$\begin{aligned}
&\oint_{\Gamma_2} N_x \delta u^0 a_{nx} ds + \oint_{\Gamma_2} N_{xy} \delta u^0 a_{ny} ds \\
&\qquad + \oint_{\Gamma_2} N_{xy} \delta v^0 a_{nx} ds + \oint_{\Gamma_2} N_y \delta v^0 a_{ny} ds \\
&= \oint_{\Gamma_2} (N_x a_{nx} + N_{xy} a_{ny})(a_{nx} \delta u^0{}_n - a_{ny} \delta u^0{}_s) ds \\
&\qquad + \oint_{\Gamma_2} (N_{xy} a_{nx} + N_y a_{ny})(a_{ny} \delta u^0{}_n + a_{nx} \delta u^0{}_s) ds \\
&= \oint_{\Gamma_2} (N_x a_{nx}^2 + 2 N_{xy} a_{nx} a_{ny} + N_y a_{ny}^2) \delta u^0{}_n ds \\
&\qquad + \oint_{\Gamma_2} (- N_x a_{nx} a_{ny} + N_{xy} a_{nx}^2 - N_{xy} a_{ny}^2 + N_y a_{nx} a_{ny}) \delta u^0{}_s ds \\
&= \oint_{\Gamma_2} N_n \delta u^0{}_n ds + \oint_{\Gamma_2} N_{ns} \delta u^0{}_s ds
\end{aligned} \quad (2.73)$$

Equations 2.70a-b were used to obtain the final result.

Equations 2.59a-b may be used to express derivatives of w^0 as follows:

$$(w^0)_{,x} = a_{nx} (w^0)_{,n} - a_{ny} (w^0)_{,s} \quad (2.74a)$$

$$(w^0)_{,y} = a_{ny}(w^0)_{,n} + a_{nx}(w^0)_{,s} \qquad (2.74b)$$

Selecting boundary integrals which include derivatives of and variations in w^0 from equation 2.64, those integrals are referred to the n-s coordinate system as follows:

$$\oint_{\Gamma_2} N_x w^0_{,x}\delta w^0\, a_{nx}ds + \oint_{\Gamma_2} N_{xy} w^0_{,x}\delta w^0\, a_{ny}ds$$

$$+ \oint_{\Gamma_2} N_{xy} w^0_{,y}\delta w^0\, a_{nx}ds + \oint_{\Gamma_2} N_y w^0_{,y}\delta w^0\, a_{ny}ds$$

$$= \oint_{\Gamma_2} (N_x a_{nx} + N_{xy}a_{ny})(a_{nx}(w^0)_{,n} - a_{ny}(w^0)_{,s})\,\delta w^0\, ds$$

$$+ \oint_{\Gamma_2} (N_{xy}a_{nx} + N_y a_{ny})(a_{ny}(w^0)_{,n} + a_{nx}(w^0)_{,s})\,\delta w^0\, ds$$

$$= \oint_{\Gamma_2} (N_x a_{nx}^2 + 2\,N_{xy}a_{nx}a_{ny} + N_y a_{ny}^2)(w^0)_{,n}\delta w^0\, ds$$

$$+ \oint_{\Gamma_2} (-N_x a_{nx}a_{ny} + N_{xy}a_{nx}^2 - N_{xy}a_{ny}^2 + N_y a_{nx}a_{ny})(w^0)_{,s}\delta w^0\, ds$$

$$= \oint_{\Gamma_2} N_n (w^0)_{,n}\delta w^0\, ds + \oint_{\Gamma_2} N_{ns}(w^0)_{,s}\delta w^0\, ds \qquad (2.75)$$

Equations 2.70a-b were used to obtain the final result.

Equations 2.62a-b may be used to express variations in w^0 as follows:

$$\delta w^0 = a_{nx}\,\delta w^0{}_n - a_{ny}\,\delta w^0{}_s \qquad (2.76a)$$

$$\delta w^0 = a_{ny}\,\delta w^0{}_n + a_{nx}\,\delta w^0{}_s \qquad (2.76b)$$

Selecting boundary integrals which include derivatives of the moment resultants and variations in w^0 from equation 2.64, those integrals are referred to the n-s coordinate system as follows:

$$\oint_{\Gamma_2} M_{x,x}\delta w^0\, a_{nx}ds + \oint_{\Gamma_2} M_{xy,y}\delta w^0\, a_{nx}ds$$

$$+ \oint_{\Gamma_2} M_{xy,x}\delta w^0\, a_{ny} ds \;+\; \oint_{\Gamma_2} M_{y,y}\delta w^0\, a_{ny} ds$$

$$= \oint_{\Gamma_2} (M_{x,x}a_{nx} + M_{xy,y}a_{nx})\, \delta w^0\, ds$$

$$+ \oint_{\Gamma_2} (M_{xy,x}a_{ny} + M_{y,y}a_{ny})\, \delta w^0\, ds$$

$$= \oint_{\Gamma_2} [\, (M_{x,x} + M_{xy,y})\, a_{nx} + (M_{xy,x} + M_{y,y})\, a_{ny}]\, \delta w^0\, ds$$

Multiplication of the three-dimensional equilibrium equations of elasticity by z and then integrating over the plate thickness, in the absence of body forces, establishes relations among the quantities M_x , M_y , M_{xy} , Q_x , and Q_y , where the latter two quantities are defined as the transverse shear force resultants from classical plate theory. The resulting equilibrium equations are:

$$M_{x,x} + M_{xy,y} = Q_x \qquad (2.78a)$$

$$M_{xy,x} + M_{y,y} = Q_y \qquad (2.78b)$$

$$Q_{x,x} + Q_{y,y} + q(x,y) = 0 \qquad (2.78c)$$

where $q(x,y)$ is a normal load distribution on the plate.

The right sides of equations 2.78a-b may be substituted into the boundary integral immediately above.

$$\oint_{\Gamma_2} [\, (M_{x,x} + M_{xy,y})\, a_{nx} + (M_{xy,x} + M_{y,y})\, a_{ny}]\, \delta w^0\, ds$$

$$= \oint_{\Gamma_2} [\; Q_x\, a_{nx} + Q_y\, a_{ny}\;]\, \delta w^0\, ds$$

$$= \oint_{\Gamma_2} [\, Q_n\,]\, \delta w^0\, ds \qquad (2.79)$$

Equation 2.61a, which transforms quantities in the x-y coordinate system to the n-s coordinate system, was used to

obtain the final result given in equation 2.79.

Equations 2.59a-b may be used to express derivatives of variations in w^0 as follows:

$$(\delta w^0)_{,x} = a_{nx}(\delta w^0)_{,n} - a_{ny}(\delta w^0)_{,s} \qquad (2.80a)$$

$$(\delta w^0)_{,y} = a_{ny}(\delta w^0)_{,n} + a_{nx}(\delta w^0)_{,s} \qquad (2.80b)$$

Selecting boundary integrals which include the moment resultants and derivatives of variations in w^0 from equation 2.64, those integrals are referred to the n-s coordinate system as follows:

$$\begin{aligned}
&-\oint_{\Gamma_2} M_x(\delta w^0)_{,x}a_{nx}ds - \oint_{\Gamma_2} M_{xy}(\delta w^0)_{,x}a_{ny}ds \\
&\qquad - \oint_{\Gamma_2} M_{xy}(\delta w^0)_{,y}a_{nx}ds - \oint_{\Gamma_2} M_y(\delta w^0)_{,y}a_{ny}ds \\
&= -\oint_{\Gamma_2} (M_x a_{nx} + M_{xy}a_{ny})(a_{nx}(\delta w^0)_{,n} - a_{ny}(\delta w^0)_{,s})\, ds \\
&\qquad - \oint_{\Gamma_2} (M_{xy}a_{nx} + M_y a_{ny})(a_{ny}(\delta w^0)_{,n} + a_{nx}(\delta w^0)_{,s})\, ds \\
&= -\oint_{\Gamma_2} (M_x a_{nx}^2 + 2\, M_{xy}a_{nx}a_{ny} + M_y a_{ny}^2)(\delta w^0)_{,n} ds \\
&\qquad - \oint_{\Gamma_2} (-\, M_x a_{nx}a_{ny} + M_{xy}a_{nx}^2 - M_{xy}a_{ny}^2 + M_y a_{nx}a_{ny})(\delta w^0)_{,s} ds \\
&= -\oint_{\Gamma_2} M_n\, (\delta w^0)_{,n}\, ds - \oint_{\Gamma_2} M_{ns}\, (\delta w^0)_{,s}\, ds
\end{aligned} \qquad (2.81)$$

Equations 2.71a-b were used to obtain the final result.

The second integral in equation 2.81 can be considered further. If the moment resultant is continuous and the boundary is smooth, then an integration by parts yields

$$\int_1^2 M_{ns}(\delta w^0)_{,s} ds = -\int_1^2 M_{ns,s}\delta w^0\, ds + [\, M_{ns}\delta w^0\,]\,|_1^2 \qquad (2.82)$$

For the case where the boundary is a smooth closed curve, the expression in brackets is equal to zero and the result obtained in equation 2.81 may be written as follows:

$$- \oint_{\Gamma_2} M_n \, (\delta w^0)_{,n} \, ds \; - \oint_{\Gamma_2} M_{ns} \, (\delta w^0)_{,s} \, ds$$

$$= \; - \oint_{\Gamma_2} M_n \, (\delta w^0)_{,n} \, ds \; + \oint_{\Gamma_2} M_{ns,s} \delta w^0 \, ds \qquad (2.83)$$

For the case where the boundary is not smooth, such as a plate with four smooth sides which terminate at corners, or discontinuous points, then the expression in brackets in equation 2.82 must be evaluated over each section of smooth continuous boundary.

Having simplified the boundary integrals, equation 2.64 may be rewritten as follows for extremization of the first variation of the total potential energy.

$$- \iint_{\Omega} [M_{x,xx} + 2 \, M_{xy,xy} + M_{y,yy} + q \,] \delta w^0 \, dx \, dy$$

$$- \iint_{\Omega} [(N_x w^0_{,x})_{,x} + (N_{xy} w^0_{,x})_{,y} + (N_{xy} w^0_{,y})_{,x} + (N_y w^0_{,y})_{,y}] \delta w^0 \, dx \, dy$$

$$- \iint_{\Omega} [N_{x,x} + N_{xy,y}] \delta u^0 \, dx \, dy \; - \iint_{\Omega} [N_{xy,x} + N_{y,y}] \delta v^0 \, dx \, dy$$

$$+ \oint_{\Gamma_2} [M_{ns,s} + N_n (w^0)_{,n} + N_{ns} (w^0)_{,s} + Q_n] \, \delta w^0 \, ds$$

$$+ \oint_{\Gamma_2} (\bar{N}_n + N_n) \delta u^0{}_n ds \; + \oint_{\Gamma_2} (\bar{N}_{ns} + N_{ns}) \delta u^0{}_s ds$$

$$- \oint_{\Gamma_2} M_n (\delta w^0)_{,n} \, ds \; - \; [\, M_{ns} \delta w^0 \,] \, |_{\Gamma_2} \; = \; 0 \qquad (2.84)$$

where the last term must be evaluated over each portion of the boundary between discontinuities. If the boundary is smooth and continuous, that term equals zero.

Having satisfied the requirement for extremization of the total potential energy by equating its first variation to zero, resulting in equation 2.84, a basis has been established for a series of deductions to be made. The middle surface displacements u^0, v^0, and w^0, were specified to be arbitrary in the region Ω. This means that variations in the surface displacements are not equal to zero in the region Ω. If equation 2.84 is to be satisfied, then those expressions in brackets in the surface integrals which are multiplied by δu^0, δv^0, or δw^0, must be equal to zero. Those expressions are the equations of equilibrium and are written as

$$M_{x,xx} + 2\,M_{xy,xy} + M_{y,yy} + (N_x w^0_{,x})_{,x} + (N_{xy} w^0_{,x})_{,y} + (N_{xy} w^0_{,y})_{,x} + (N_y w^0_{,y})_{,y} + q = 0 \qquad (2.85)$$

$$N_{x,x} + N_{xy,y} = 0 \qquad (2.86)$$

$$N_{xy,x} + N_{y,y} = 0 \qquad (2.87)$$

Equations 2.86 and 2.87 can be identified with the equilibrium equations for plane stress. Equation 2.85 may be simplified by using equations 2.86 and 2.87 to eliminate some terms when its product terms are expanded. Expansion of the product terms are written as

$$(N_x\, w^0_{,x})_{,x} = N_x\, w^0_{,xx} + N_{x,x}\, w^0_{,x} \qquad (2.88a)$$

$$(N_{xy}\, w^0_{,x})_{,y} = N_{xy}\, w^0_{,xy} + N_{xy,y}\, w^0_{,x} \qquad (2.88b)$$

$$(N_{xy}\, w^0_{,y})_{,x} = N_{xy}\, w^0_{,yx} + N_{xy,x}\, w^0_{,y} \qquad (2.88c)$$

$$(N_y\, w^0_{,y})_{,y} = N_y\, w^0_{,yy} + N_{y,y}\, w^0_{,y} \qquad (2.88d)$$

Terms from each of equations 2.88a-b and equations 2.88c-d

can be combined and eliminated on the basis of equation 2.86 and equation 2.87 as follows

$$(N_{x,x} + N_{xy,y})\, w^0_{,x} = 0 \qquad (2.89)$$

$$(N_{xy,x} + N_{y,y})\, w^0_{,y} = 0 \qquad (2.90)$$

The terms in equations 2.88a-d which remain are

$$N_x\, w^0_{,xx} \;,\quad N_{xy}\, w^0_{,xy} \;,\quad N_{xy}\, w^0_{,yx} \;,\quad N_y\, w^0_{,yy}$$

and the second and third terms may be combined.

Equation 2.85 can be rewritten as

$$M_{x,xx} + 2\, M_{xy,xy} + M_{y,yy} + N_x w^0_{,xx} + 2\, N_{xy} w^0_{,xy} + N_y w^0_{,yy} + q = 0 \qquad (2.91)$$

This equation of equilibrium, opposed to the linear differential equation of classical plate theory, is nonlinear. It contains the nonlinear terms consisting of products of the force resultants and curvatures.

In addition to the means to determine the equations of equilibrium, equation 2.84 contains the natural (or force) and the kinematic (or geometric) boundary conditions which must be satisfied or specified on the boundary Γ_2. These boundary conditions are

Either $N_n = -\bar{N}_n$ or, $u^0{}_n$ is specified (2.92a)

Either $N_{ns} = -\bar{N}_{ns}$ or, $u^0{}_s$ is specified (2.92b)

Either $M_n = 0$ or, $w^0_{,n}$ is specified (2.92c)

Either $Q_n + M_{ns,s} + N_n w^0_{,n} + N_{ns} w^0_{,s} = 0$ or, w^0 is specified (2.92d)

And, at discontinuities $[\, M_{ns} \delta w^0 \,] = 0$ (2.92e)

The last three conditions contain those terms which are

characteristic of conditions embodied in classical plate theory. However, the effective shear force condition in equation 2.92d, consisting of the shear force resultant term and the moment resultant term, has been made more complicated by the addition of product terms (in-plane force resultants multiplied by the slope at the boundary).

The equilibrium equations 2.86, 2.87, and 2.91 can be written using equations 2.25 and 2.26 as follows:

$$[A_{11}\epsilon_x^0 + A_{12}\epsilon_y^0 + A_{16}\Gamma_{xy}^0]_{,x} + [A_{16}\epsilon_x^0 + A_{26}\epsilon_y^0 + A_{66}\Gamma_{xy}^0]_{,y} = 0 \tag{2.93}$$

$$[A_{16}\epsilon_x^0 + A_{26}\epsilon_y^0 + A_{66}\Gamma_{xy}^0]_{,x} + [A_{12}\epsilon_x^0 + A_{22}\epsilon_y^0 + A_{26}\Gamma_{xy}^0]_{,y} = 0 \tag{2.94}$$

$$\begin{aligned}&[D_{11}K_x^0 + D_{12}K_y^0 + D_{16}K_{xy}^0]_{,xx} \\ &\quad + 2\,[D_{16}K_x^0 + D_{26}K_y^0 + D_{66}K_{xy}^0]_{,xy} \\ &\quad + [D_{12}K_x^0 + D_{22}K_y^0 + D_{26}K_{xy}^0]_{,yy} \\ &+ [A_{11}\epsilon_x^0 + A_{12}\epsilon_y^0 + A_{16}\Gamma_{xy}^0]w_{,xx}^0 \\ &\quad + 2\,[A_{16}\epsilon_x^0 + A_{26}\epsilon_y^0 + A_{66}\Gamma_{xy}^0]w_{,xy}^0 \\ &\quad + [A_{12}\epsilon_x^0 + A_{22}\epsilon_y^0 + A_{26}\Gamma_{xy}^0]w_{,yy}^0 + q = 0\end{aligned} \tag{2.95}$$

The equilibrium equations 2.93, 2.94, and 2.95 can be written in terms of the surface displacements using equations 2.5a-c and 2.6a-c in substitution resulting in

$$\begin{aligned}&[A_{11}\{u_{,x}^0 + \tfrac{1}{2}(w_{,x}^0)^2\} + A_{12}\{v_{,y}^0 + \tfrac{1}{2}(w_{,y}^0)^2\} \\ &\quad + A_{16}\{u_{,y}^0 + v_{,x}^0 + w_{,x}^0 w_{,y}^0\}]_{,x} \\ &+ [A_{16}\{u_{,x}^0 + \tfrac{1}{2}(w_{,x}^0)^2\} + A_{26}\{v_{,y}^0 + \tfrac{1}{2}(w_{,y}^0)^2\} \\ &\quad + A_{66}\{u_{,y}^0 + v_{,x}^0 + w_{,x}^0 w_{,y}^0\}]_{,y} = 0\end{aligned} \tag{2.96}$$

$$[A_{16}\{u^0_{,x} + \tfrac{1}{2}(w^0_{,x})^2\} + A_{26}\{v^0_{,y} + \tfrac{1}{2}(w^0_{,y})^2\} + A_{66}\{u^0_{,y} + v^0_{,x} + w^0_{,x}w^0_{,y}\}]_{,x}$$
$$+ [A_{12}\{u^0_{,x} + \tfrac{1}{2}(w^0_{,x})^2\} + A_{22}\{v^0_{,y} + \tfrac{1}{2}(w^0_{,y})^2\} + A_{26}\{u^0_{,y} + v^0_{,x} + w^0_{,x}w^0_{,y}\}]_{,y} = 0 \quad (2.97)$$

$$[A_{11}\{u^0_{,x} + \tfrac{1}{2}(w^0_{,x})^2\} + A_{12}\{v^0_{,y} + \tfrac{1}{2}(w^0_{,y})^2\} + A_{16}\{u^0_{,y} + v^0_{,x} + w^0_{,x}w^0_{,y}\}]\, w^0_{,xx}$$
$$+ 2\,[A_{16}\{u^0_{,x} + \tfrac{1}{2}(w^0_{,x})^2\} + A_{26}\{v^0_{,y} + \tfrac{1}{2}(w^0_{,y})^2\} + A_{66}\{u^0_{,y} + v^0_{,x} + w^0_{,x}w^0_{,y}\}]\, w^0_{,xy}$$
$$+ [A_{12}\{u^0_{,x} + \tfrac{1}{2}(w^0_{,x})^2\} + A_{22}\{v^0_{,y} + \tfrac{1}{2}(w^0_{,y})^2\} + A_{26}\{u^0_{,y} + v^0_{,x} + w^0_{,x}w^0_{,y}\}]\, w^0_{,yy}$$
$$- [D_{11}w^0_{,xx} + D_{12}w^0_{,yy} + 2\,D_{16}w^0_{,xy}]_{,xx}$$
$$- 2\,[D_{16}w^0_{,xx} + D_{26}w^0_{,yy} + 2\,D_{66}w^0_{,xy}]_{,xy}$$
$$- [D_{12}w^0_{,xx} + D_{22}w^0_{,yy} + 2\,D_{26}w^0_{,xy}]_{,yy}$$
$$+ q(x,y) = 0 \quad (2.98)$$

The laminate extentional stiffness properties A_{ij} and the laminate bending stiffness properties D_{ij} are functions of the spatial coordinates in equations 2.93, 2.94, and 2.95. These equations are partial differential equations in x and y and may not be solved exactly. A finite element method will be used to obtain solutions for these equations. This will be discussed in detail in Chapter III.

CHAPTER III

PROBLEM FORMULATION AND METHOD OF ANALYSIS FOR TENSILE RESPONSE

Plate Geometries

The geometric configuration of the plate under consideration is illustrated in Figure 3.1. The plate width is designated by W , the plate length by L , and the plate hole diameter by D . The positive horizontal x-axis is to the right and the positive vertical y-axis is 90° counterclockwise from the x-axis. The plate is loaded by in-plane tensile forces in the x-direction distributed uniformly over each end.

Four discrete plate geometries are considered. Two values of D/W equal to 1/3 and 1/6 are used along with two values of L/W equal to 1 and 2. The reason for considering various geometries is to ascertain whether an improvement in structural efficiency with the curvilinear fiber design is or is not a function of plate geometry.

Equations Governing In-Plane Tensile Response

A thin symmetrically laminated plate in a state of plane stress is considered. If the plate is subjected only to an in-plane tensile loading, the displacements developed due to that loading are only in-plane displacements. The out-of-plane displacements equal zero. For that situation,

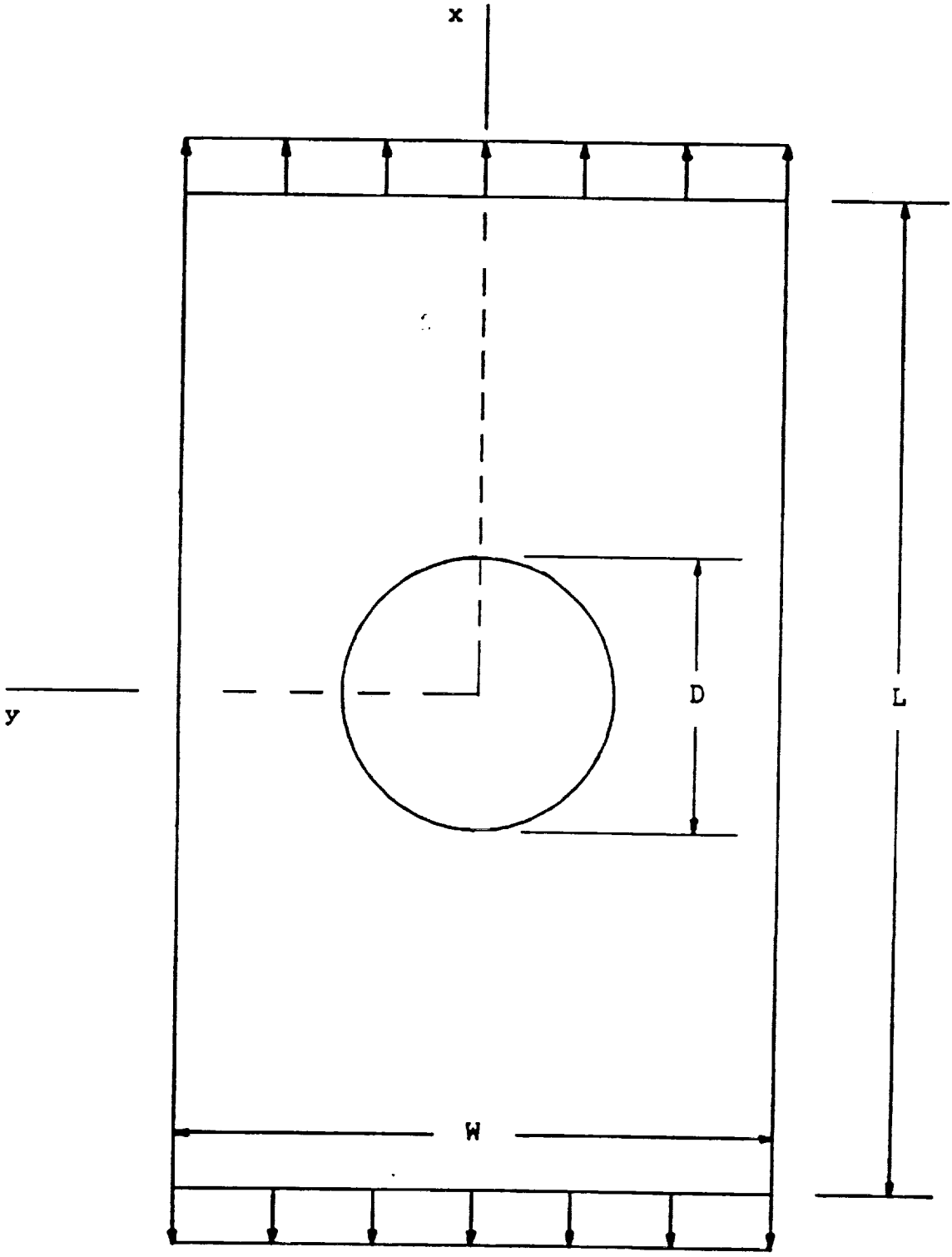

Figure 3.1 Plate Geometry And Loading

equations 2.96 and 2.97 reduce to

$$[A_{11}u^0_{,x} + A_{12}v^0_{,y} + A_{16}(u^0_{,y} + v^0_{,x})]_{,x} + [A_{16}u^0_{,x} + A_{26}v^0_{,y} + A_{66}(u^0_{,y} + v^0_{,x})]_{,y} = 0 \qquad (3.1)$$

$$[A_{16}u^0_{,x} + A_{26}v^0_{,y} + A_{66}(u^0_{,y} + v^0_{,x})]_{,x} + [A_{12}u^0_{,x} + A_{22}v^0_{,y} + A_{26}(u^0_{,y} + v^0_{,x})]_{,y} = 0 \qquad (3.2)$$

These equations are linear partial differential equations and the coefficients A_{ij} $(i,j = 1,2,6)$ are functions of the coordinates x and y. These equations can not be solved exactly. A finite element method will be used to determine solutions. The type of boundary conditions considered are those associated with simply supported plate edges.

Finite Element Model, Finite Element Meshes, And Boundary Constraints

The plates are analyzed using a finite element code written previously to this study. As shown in Figure 3.2, the basic element is an eight-node isoparametric element with nine Gauss integration points. A relationship is needed between the element displacements at any point within the element and the element nodal point displacements, since results are obtained with reference to the nodal point positions. This is accomplished directly through the use of interpolation functions which are defined in a natural coordinate system. Coordinates of any point in the element in a global x-y coordinate system may be related to coordinates

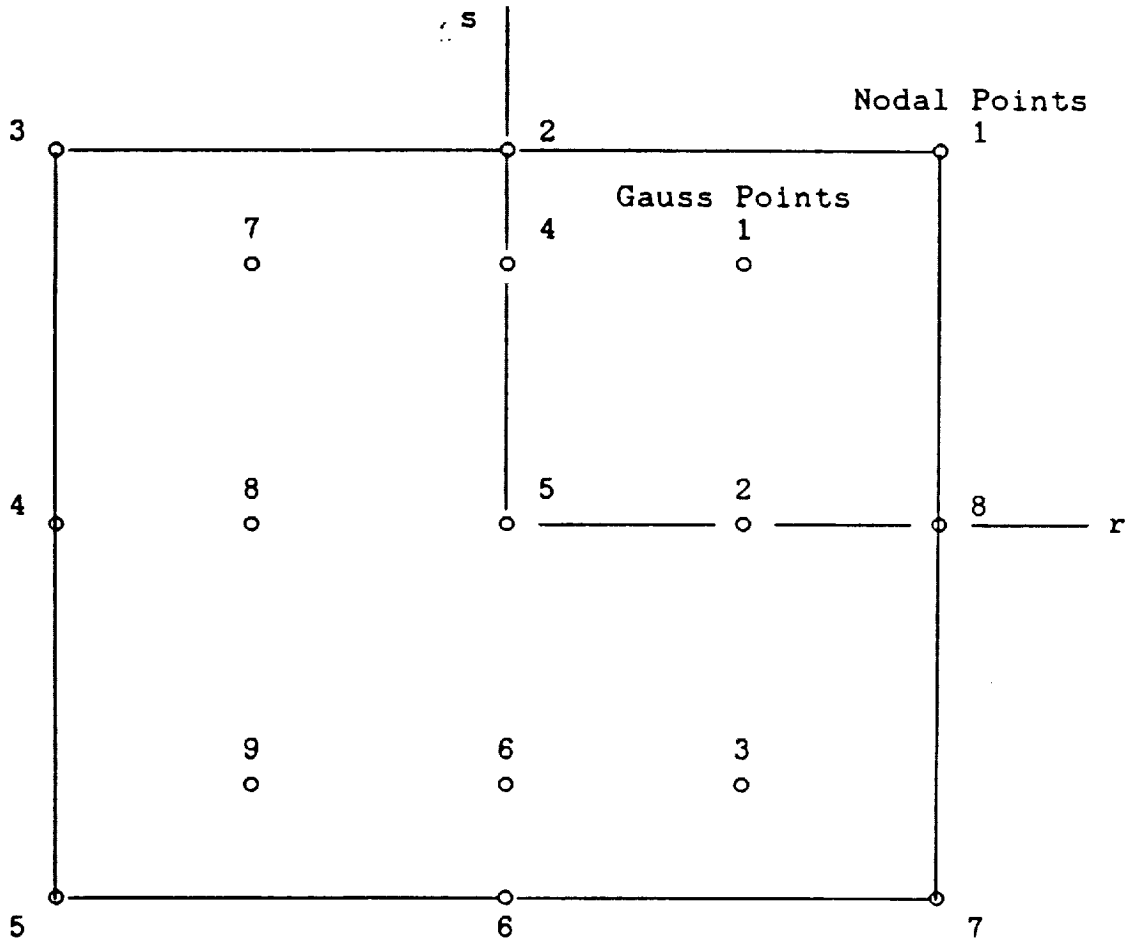

Figure 3.2 Eight-Node Isoparametric Element

of the nodal points through functions expressed in a natural r-s coordinate system.

The element shown in Figure 3.2 lies in the global x-y coordinate system. A transformation between positions of the nodal points and positions of any other points in the element is given by the relations

$$x = \sum_{i=1}^{8} \Phi_i(r,s)\, x_i \qquad (3.3a)$$

$$y = \sum_{i=1}^{8} \Phi_i(r,s)\, y_i \qquad (3.3b)$$

where Φ_i are the interpolation functions, x and y are the coordinates of any point of the element, and x_i and y_i are the coordinates of the element nodes.

Interpolation of the element displacements is accomplished in the same manner as interpolation of the element coordinates as expressed by

$$u = \sum_{i=1}^{8} \Phi_i(r,s)\, u_i \qquad (3.4a)$$

$$v = \sum_{i=1}^{8} \Phi_i(r,s)\, v_i \qquad (3.4b)$$

where u and v are displacements of any point of the element, and u_i and v_i are displacements of the nodes. The same interpolation functions are used to interpolate the element displacements and the element coordinates. This is the basis for the isoparametric finite element formulation. The interpolation functions for the eight-node element shown in Figure 3.2 are

$$\Phi_1(r,s) = 1/4\ (1 + r)(1 + s)(-1 + r + s) \qquad (3.5a)$$

$$\Phi_2(r,s) = 1/2\ (1 - r^2)(1 + s) \qquad (3.5b)$$

$$\Phi_3(r,s) = 1/4\ (1 - r)(1 + s)(-1 - r + s) \qquad (3.5c)$$

$$\Phi_4(r,s) = 1/2\ (1 - r)(1 - s^2) \qquad (3.5d)$$

$$\Phi_5(r,s) = 1/4\ (1 - r)(1 - s)(-1 - r - s) \qquad (3.5e)$$

$$\Phi_6(r,s) = 1/2\ (1 - r^2)(1 - s) \qquad (3.5f)$$

$$\Phi_7(r,s) = 1/4\ (1 + r)(1 - s)(-1 + r - s) \qquad (3.5g)$$

$$\Phi_8(r,s) = 1/2\ (1 + r)(1 - s^2) \qquad (3.5h)$$

The function Φ and its subscript in equations 3.5a-h correspond to the sequence and position of nodal numbers in Figure 3.2. (Reddy [3], pp. 242-254).

The finite element meshes for the 4 geometries considered in the tensile analysis are depicted in Figures 3.3 through 3.6. The plate geometry, loading and material properties are symmetric about the midspan of the plate in the x and y directions, so only one quarter of the plate is used in the analysis. Each quarter plate mesh consists of 192 elements with 12 elements placed around the hole edge.

The boundary constraints for the finite element mesh are depicted in Figure 3.7. The nodes at the edge of the hole are traction free. The displacements v^0 in the y-direction equal zero for the nodes on the edge which corresponds to $D/2 \le x \le L/2$ and $y = 0$, and that edge is traction free in the x-direction. The displacements u^0 in the x-direction equal zero for the nodes on the edge which corresponds to $x = 0$ and $D/2 \le y \le W/2$, and that edge is traction free in the y-direction. Tensile forces are prescribed in the x-direction at the nodes on the edge which corresponds to $x = L/2$ and $0 \le y \le W/2$, and that edge is traction free

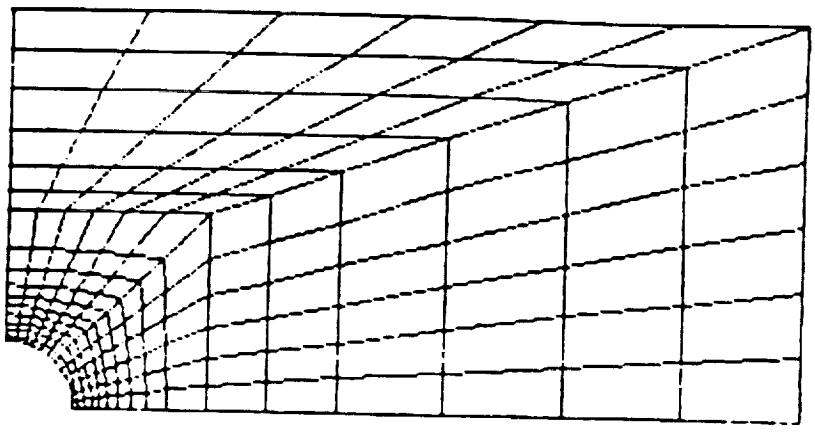

Figure 3.3 One-Quarter Finite Element Mesh For The Case L/W = 2 And D/W = 1/6

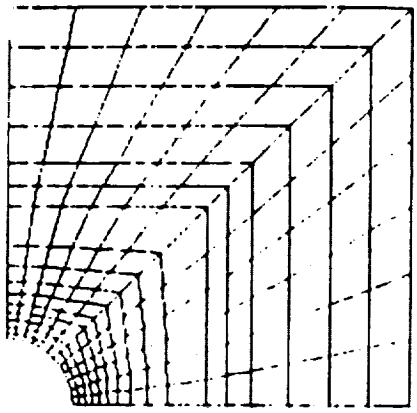

Figure 3.4 One-Quarter Finite Element
For The Case L/W = 1 And D/W = 1/6

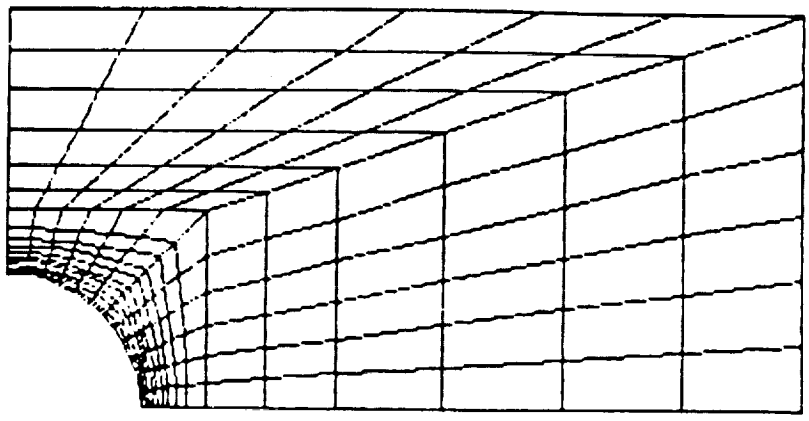

Figure 3.5 One-Quarter Finite Element

For The Case L/W = 2 And D/W = 1/3

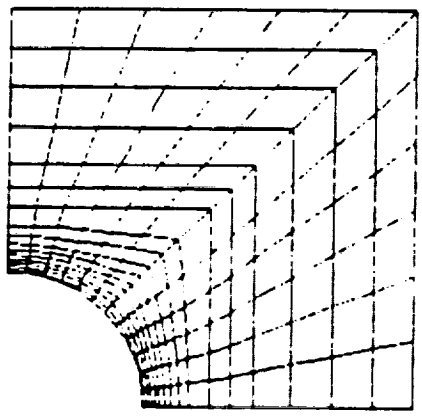

Figure 3.6 One-Quarter Finite Element
For The Case L/W = 1 And D/W = 1/3

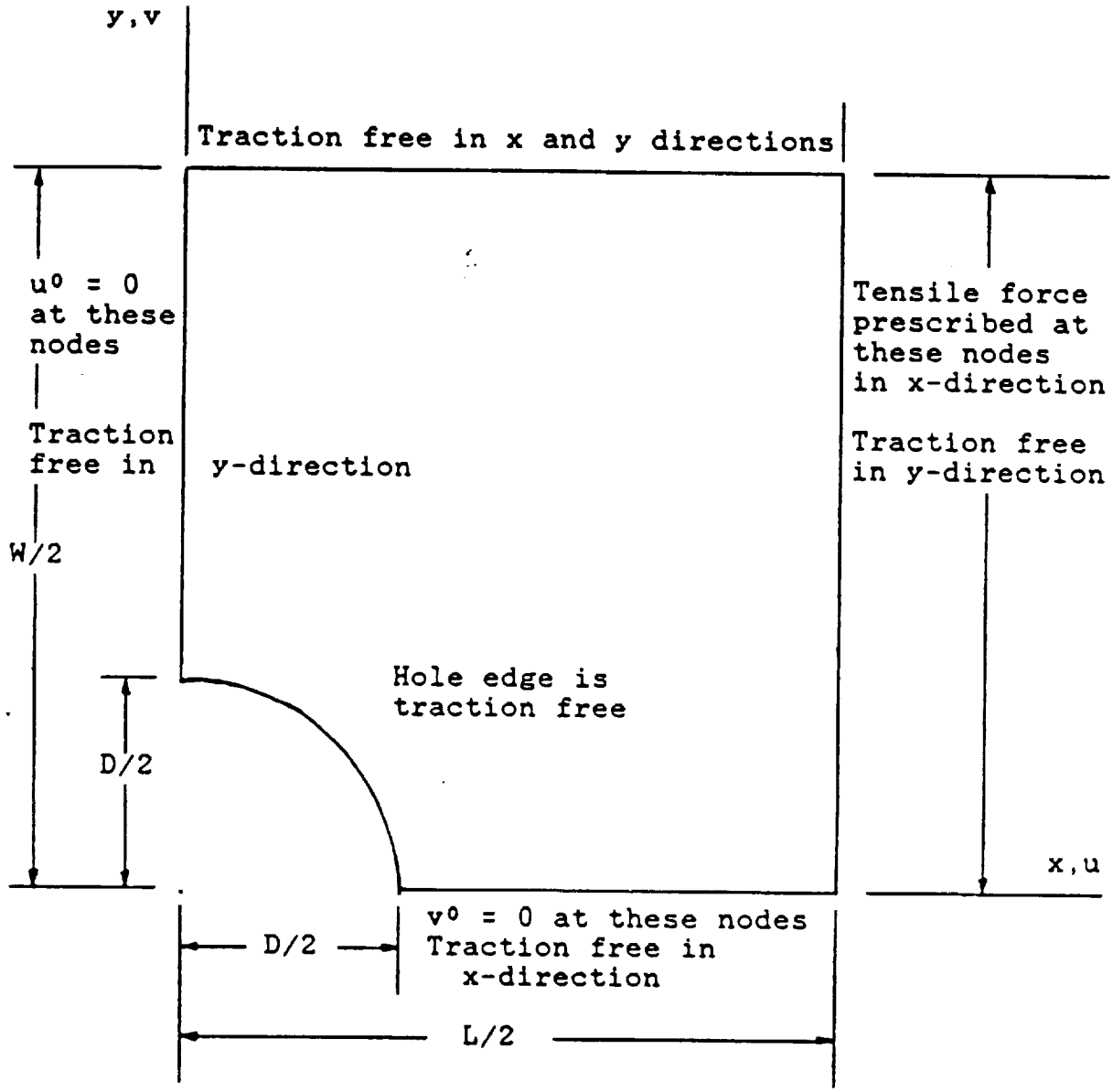

Figure 3.7 Boundary Constraints For

One-Quarter Plate Finite Element Mesh

in the y-direction. The edge which corresponds to $0 \leq x \leq L/2$ and $y = W/2$ is traction free in the x and y directions.

Procedure For Determining Fiber Directions In Curvilinear Fiber Format Layers

As stated previously, the basic idea behind the use of the curvilinear fiber format is to orient the fibers in the principal stress directions. In general, the principal stress directions depend on the stiffness properties. If fibers were introduced into a plate of isotropic material, for instance aluminum, forming in effect a layer, its stiffness properties would be changed. However, its stress state in the thickness direction would not be changed necessarily and a principal stress direction could be determined. In contrast, determining principal stress directions for a laminate is not a meaningful or comparable concept. The response of an entire laminate is dependent on the stiffness properties of each layer which may be different layer by layer. The stress state in each layer of a laminate is different. Thus, principal stress directions may be determined for each layer and those directions will generally vary from layer to layer. An iterative process was used to determine the fiber directions within a group of layers (designated curvilinear layers) such that the fibers were aligned everywhere with the principal stress directions in those curvilinear layers. Other layers (designated to have

a straightline fiber format at a specified angle), which may be included in a laminate design, would not be subject to any required realignment with principal stress directions. The iteration process determines the principal stress directions only for the curvilinear layers. With the procedure, the fiber directions are specified relative to the positive horizontal x-axis.

Due to use of the finite element method, two approximations are inherent to the analysis. First, the fiber directions are assumed to be constant within an element. Second, calculations for principal stress directions, and hence fiber directions, are keyed on the stress computed at just one Gauss point in the element. Gauss point number 8 was chosen in order to use stresses which are as close to the hole edge as possible. Figure 3.8 shows the location of Gauss point 8 as the particular eight-node element was used in this study. Gauss point 8 was chosen rather than Gauss points 7 or 9 because Gauss point 8 is the central point in that group of three and provides a better average value for the stresses.

The iteration process is described in the following as a series of numbered steps in procedure:

1. The iteration process may be initiated with the assumption that the laminate is an isotropic plate of aluminum. Thus, only two independent material properties among the modulus of elasticity E, the shear modulus G, and the

Poisson's ratio μ, are required to compute the reduced stiffnesses Q, using equations 2.9a-d. With the assumption of isotropy, equation 2.8 is equivalent to equation 2.13.

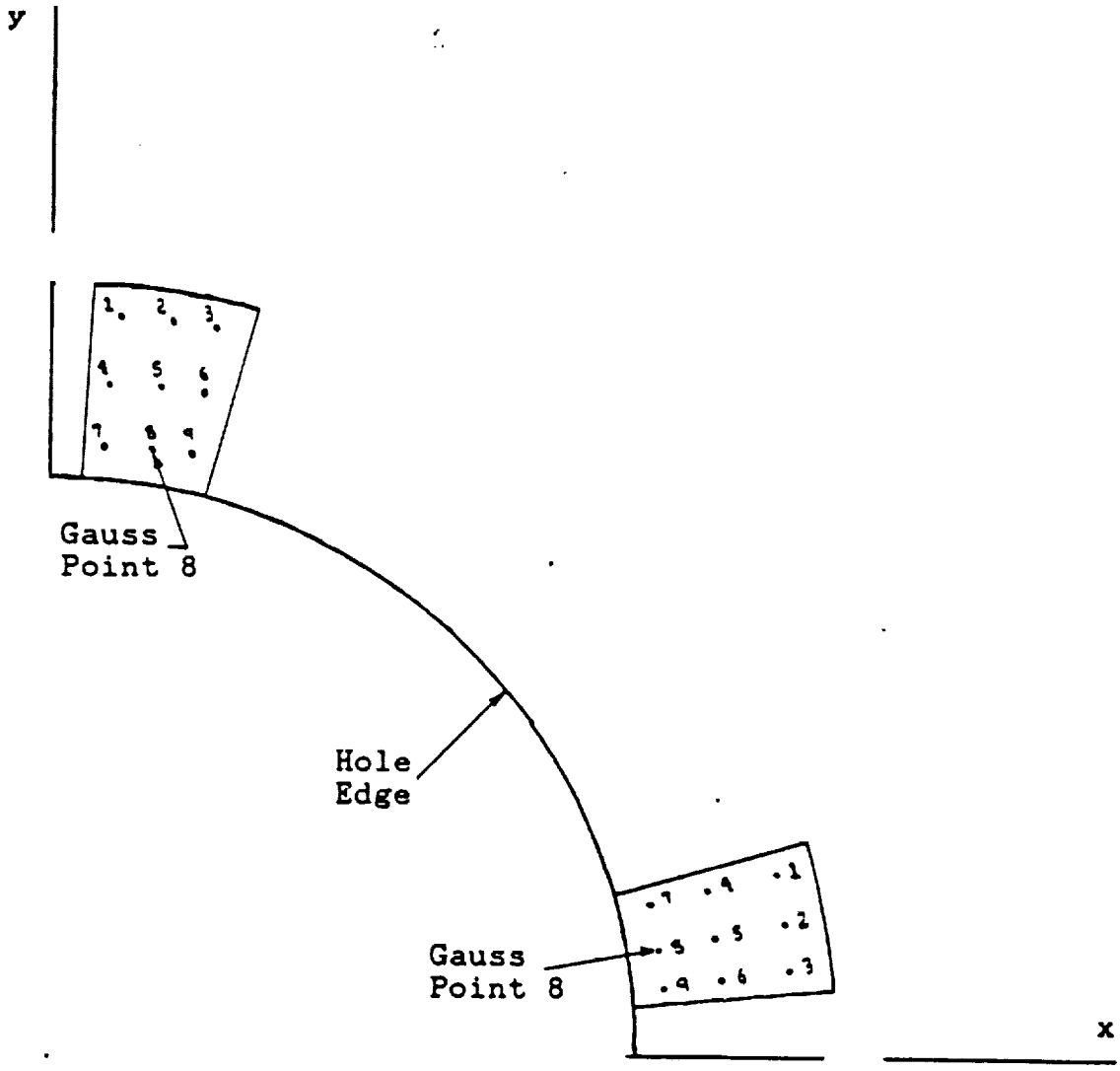

Note: Elements are enlarged in order to show the orientation of Gauss point 8.

Figure 3.8 Orientation Of Gauss Point 8

The isotropic material property values may be used as the required input to the finite element program to provide results for laminate strains ϵ_x, ϵ_y, and Γ_{xy}, and laminate force resultants N_x, N_y, and N_{xy}, at each of the 9 Gauss points in each element of the finite element mesh. As mentioned previously, only the results associated with Gauss point 8 are used to establish the fiber direction character of each element.

2. The iteration process continues with the assumption that the laminate now consists of layers of orthotropic material. Equations 2.9a-d are applied to determine values of the reduced stiffnesses Q, obtained with respect to the 1-2 coordinate system. These values of reduced stiffness are the same for every element in the finite element mesh (as functions only of material properties).

3. At this point, if the fiber directions for the curvilinear layers in the laminate were known, values of the reduced stiffnesses $\bar{Q}$, with respect to the x-y coordinate system, could be computed for each element in the finite element mesh using equation 2.12. These values of reduced stiffness would be different from element to element of the finite element mesh. Initially, however, it is assumed that the fiber directions in all of the elements are equal to zero. Values of reduced stiffness with respect to the x-y coordinate system may be computed on that basis (zero direction). Recall that a laminate may consist of straightline

fiber format layers as well as curvilinear fiber format layers. The stresses for the curvilinear fiber format layers in the x-y coordinate system should be computed separately from those of the straightline fiber format layers in order to determine a new set of element principal stress directions for the curvilinear fiber format layers. Values of stress computed for one curvilinear fiber layer would be the same for every layer in a group of curvilinear fiber format layers within a laminate in the x-y coordinate system. It follows that the element principal stress directions would be the same for each curvilinear layer within a laminate.

4. Having values of laminate strain from step 1. for Gauss point 8 of each element and all fiber layers, and from step 3., values of the reduced stiffness for the curvilinear fiber format layers, equation 2.13 is applied to compute the stresses in each element for the curvilinear fiber format layers within the laminate.

5. The principal stress direction for the curvilinear layers in each element is computed using the equation

$$\theta = 1/2 \tan^{-1} \left[\frac{2 \tau_{xy}}{\sigma_x - \sigma_y} \right] \qquad (3.6)$$

where the principal stress direction for an element is specified by θ, and σ_x , σ_y , and τ_{xy} are the stresses computed in step 4. At this stage in the iteration process, it is convenient to designate these principal stress directions as

the current fiber directions for the curvilinear fiber format layers.

6. Applying equation 2.12, compute with respect to the x-y coordinate system, a set of reduced stiffness values $\bar{Q}$ in each element for the curvilinear fiber format layers, using the values of reduced stiffness Q from step 2. and the principal stress direction values obtained in step 5.

7. Applying equation 2.12, compute with respect to the x-y coordinate system, a set of reduced stiffness values $\bar{Q}$ in each element for the remaining straightline fiber format layers, using the values of reduced stiffness Q from step 2. The fiber direction is specified and characteristic of each layer. For example, the fiber direction of a pair of layers may be specified to have fibers oriented at $+45^0$ and -45^0 relative to the x-axis of the laminate.

8. Applying equation 2.20 to all of the layers in the laminate, compute a set of extensional stiffness values A_{ij} for each element of the finite element mesh using values of the reduced stiffness obtained in step 6. and step 7.

9. Divide the extensional stiffness values A_{ij}, by the value of the thickness of the laminate to obtain laminate stiffness property values for each element of the finite element mesh.

10. Input the laminate stiffness properties for each finite element into the finite element program. The finite

element program produces a new set of results for laminate strains ϵ_x, ϵ_y, and Γ_{xy}, at each of the 9 Gauss points for each element.

11. Using the values designated as current fiber directions for the curvilinear fiber format layers obtained in step 5. and values of the reduced stiffness Q for orthotropic material obtained in step 2., apply equation 2.12 to compute new values for the reduced stiffness $\bar{Q}$.

12. Using the values of reduced stiffness $\bar{Q}$, obtained in step 11. and the values of laminate strain for Gauss point 8 obtained in step 10., apply equation 2.13 to compute values for the stresses σ_x, σ_y, and τ_{xy}, in each element for the curvilinear fiber format layers.

13. Using the values of stress obtained in step 12., apply equation 3.6 to determine the principal stress directions in each finite element for the curvilinear layers. At this stage in the procedure, these principal stress directions are now designated as current fiber directions θ_c, for the curvilinear fiber format layers. The values for the fiber directions obtained in step 5. are now redesignated as previous fiber directions θ_p. With this step, one cycle of the iteration procedure is completed.

The fibers have been aligned with new (current) principal stress directions. The iteration procedure is simple, straightforward, and repetitive, and may be continued until the principal stress directions, and thus the fiber direc-

tions obtained previously, can be compared to current fiber directions within a chosen tolerance. That tolerance level is considered to have converged when the following quantity (relative error in θ_c) is determined to be less than 0.01 for each element.

$$\frac{\theta_p - \theta_c}{\theta_p} < 0.01 \qquad (3.7)$$

where θ_p specifies the fiber direction for an element as a result of a completed previous iteration and θ_c specifies the fiber direction for an element as a result of the completed current iteration.

Additional cycles in the iteration procedure may be accomplished in the following steps.

1. Using values of the current fiber directions θ_c for the curvilinear layers in each finite element, and values of the reduced stiffness Q from application of equations 2.9a-d, apply equation 2.12 to compute values of the reduced stiffness $\bar{Q}$.

2. Using values of the reduced stiffness Q for the straightline fiber format layers which have specified fiber directions, apply equation 2.12 to compute values of the reduced stiffness $\bar{Q}$.

3. Using values of the reduced stiffness $\bar{Q}$ obtained in step 1. and step 2. above, apply equation 2.20 to compute values of the extensional stiffness A_{ij} for each finite element of the laminate.

4. Divide the extensional stiffness values A_{ij} by the thickness of the laminate to obtain values of the laminate stiffness properties for each finite element in the finite element mesh.

5. Input the stiffness properties obtained in step 4. into the finite element program to obtain values of laminate strain ϵ_x, ϵ_y, and Γ_{xy}.

6. Apply equation 2.13 to obtain values of stress σ_x, σ_y, and τ_{xy}, using the values of reduced stiffness $\bar{Q}$ obtained in step 1. and laminate strains obtained in step 5.

7. Apply equation 3.6 to obtain the principal stress directions using the stresses obtained in step 6.

8. Apply equation 3.7 to check if convergence of fiber direction values has been achieved within the chosen level of tolerance of relative error.

The circumferential stress around the hole is tensile at the net-section and compressive at the horizontal centerline of the plate. The circumferential stress changes from tension to compression around the hole edge when proceeding from the net-section to the horizontal centerline of the plate. There is a point on the circumference of the hole where the circumferential stress equals zero. The hole edge is traction free so that all of the stresses equal zero at that point. That point is called the isotropic point at the hole edge. All directions are principal stress directions at the isotropic point so the fiber direction at that point

was chosen to be consistent with the fiber directions of adjacent elements.

Elastic Material Properties

The elastic material properties for a lamina considered in this study were

$E_1 = 19.885 \times 10^6$ psi $E_2 = 1.281 \times 10^6$ psi

$Nu_{12} = 0.298$ $G_{12} = 1.003 \times 10^6$ psi

and the lamina thickness was chosen to be 0.005 in.

These elastic material properties were chosen to represent closely the commercial material AS4/3501. Relations from micromechanics based on the rule-of-mixtures were used to determine the elastic material properties. The relations are given by

$$E_1 = v_f E_{f1} + v_m E_m \qquad (3.8a)$$

$$E_2 = (1 + v_2^*)/(1/E_{f2} + v_2^*/E_m) \qquad (3.8b)$$

$$Nu_{12} = v_f Nu_f + v_m Nu_m \qquad (3.8c)$$

$$G_{12} = (1 + v_{12}^*)/(1/G_f + v_{12}^*/G_m) \qquad (3.8d)$$

where the parameters in equations 3.9a-d are defined as:

$v_f = 0.65$		fiber volume fraction
$v_m = 0.35$		matrix volume fraction
$Nu_f = 0.27$		fiber Poisson's ratio
$Nu_m = 0.35$		matrix Poisson's ratio
$v_2^* = 0.269$		reduced matrix/fiber volume ratio for E_2
$v_{12}^* = 0.162$		reduced matrix/fiber volume ratio for G_{12}

E_{f1}	=	30.32 x 10^5 psi	fiber elastic modulus in fiber direction
E_{f2}	=	2.248 x 10^5 psi	fiber elastic modulus perpendicular to fibers in the plane of the lamina
E_m	=	493 x 10^3 psi	matrix elastic modulus
G_f	=	3.683 x 10^5 psi	fiber elastic shear modulus
G_m	=	182.59 x 10^3 psi	matrix elastic shear modulus

See Tsai [4], pages 11-2 thru 11-11 for a detailed discussion of these relations.

Failure Strength Theories

Two failure strength theories were used in this study to predict the failure load in a laminate. The first is a noninteracting strain-based criterion called the maximum strain failure criterion and the second is an interacting stress-based criterion called the Tsai-Wu tensor polynomial criterion.

Maximum Strain Criterion

According to the maximum strain criterion, five parameters are used to determine how failure occurs in a laminate. These parameters are the failure strains for the material used. The notation is as follows:

ϵ^f_{1T} : Tensile failure in fiber direction

ϵ^f_{1C} : Compression failure in fiber direction

ϵ^f_{2T} : Tensile failure perpendicular to fiber

ϵ^f_{2C} : Compression failure perpendicular to fiber

Γf_{12} : In-plane shear failure

The five strains constitute five failure modes and are assumed to be independent from one another. The strength ratio R is determined by dividing the failure strain by the actual strain due to the applied load. There are five strength ratios, one for each mode of failure.

$$R_{1T} = |\epsilon f_{1T}/\epsilon_1| \quad => \text{Used when } \epsilon_1 > 0 \tag{3.9a}$$

$$R_{1C} = |\epsilon f_{1C}/\epsilon_1| \quad => \text{Used when } \epsilon_1 < 0 \tag{3.9b}$$

$$R_{2T} = |\epsilon f_{2T}/\epsilon_2| \quad => \text{Used when } \epsilon_2 > 0 \tag{3.9c}$$

$$R_{2C} = |\epsilon f_{2C}/\epsilon_2| \quad => \text{Used when } \epsilon_2 < 0 \tag{3.9d}$$

$$R_{12} = |\Gamma f_{12}/\Gamma_{12}| \tag{3.9e}$$

where R_{1T} is the tensile strength ratio in the fiber direction, R_{1C} is the compressive strength ratio in the fiber direction, R_{2T} is the tensile strength ratio perpendicular to the fibers, R_{2C} is the compressive strength ratio perpendicular to the fibers, and R_{12} is the shear strength ratio.

For a given level of applied load, the strength ratio R which has the lowest magnitude among the five possibilities indicates the mode of failure for the layer in the laminate.

Tsai-Wu Criterion

The Tsai-Wu criterion takes into account that modes of failure can be coupled and interact with one another. There are six strength parameters associated with the Tsai-Wu criterion. These are F_{xx}, F_{yy}, F_x, F_y, F_{ss}, and F^*_{xy}. F^*_{xy} is treated as an empirical constant and has a normalized value

of (-0.5).

The strength to stress ratio R is determined from the quadratic equation:

$$R = \frac{-b \pm (b^2 + 4a)^{1/2}}{2a} \tag{3.10}$$

The values of a and b are determined from:

$$a = F_{xx}\sigma_1^2 - 2F^*_{xy}(F_{xx}F_{yy})^{1/2}\sigma_1\sigma_2 + F_{yy}\sigma_2^2 + F_{ss}\tau_{12}^2 \tag{3.11a}$$

$$b = F_x\sigma_1 + F_y\sigma_2 \tag{3.11b}$$

The stress values are stresses due to the applied load and the strength parameters depend upon the material used.

Table 3.1 lists the failure strains for the maximum strain criterion and the failure stresses for the Tsai-Wu criterion.

Table 3.1 Failure Strains And Failure Stresses

Failure Mode	Strain (10^{-3})	Stress (10^3 psi)
Tensile failure in fiber direction	10.49	209.82
Compression failure in fiber direction	10.49	209.82
Tensile failure perpendicular to fiber	5.77	7.54
Compression failure perpendicular to fiber	22.99	29.87
In-Plane shear failure	13.10	13.49

Application of the two failure strength theories to predict the failure load and failure mode of a thin laminated fiber-reinforced plate will be discussed in Chapter V.

CHAPTER IV

PROBLEM FORMULATION AND METHOD OF ANALYSIS FOR BUCKLING RESPONSE

Equations Governing Buckling Response

The equations which govern buckling of a thin flat plate subjected to in-plane loading only ($q(x,y) = 0$) are derived in this chapter. The method used to derive the buckling equations is the adjacent-equilibrium criterion in which the middle surface displacements are given by

$$u^0 = \bar{u}^0 + \epsilon u_1^0 \tag{4.1a}$$

$$v^0 = \bar{v}^0 + \epsilon v_1^0 \tag{4.1b}$$

$$w^0 = \bar{w}^0 + \epsilon w_1^0 \tag{4.1c}$$

where (u^0,v^0,w^0) and $(\bar{u}^0,\bar{v}^0,\bar{w}^0)$ are equilibrium configurations, ϵ is a small parameter, and (u_1^0,v_1^0,w_1^0) are arbitrarily small incremental displacements. The thin flat plate considered here is subjected to in-plane edge loading only so w^0 and its derivatives equal zero. (Brush and Almroth [5], pp. 90-91). With that condition, equations 4.1a-c become

$$u^0 = \bar{u}^0 + \epsilon u_1^0 \tag{4.2a}$$

$$v^0 = \bar{v}^0 + \epsilon v_1^0 \tag{4.2b}$$

$$w^0 = \epsilon w_1^0 \tag{4.2c}$$

The equilibrium equations were derived in Chapter II. These equations, for the case where the normal load distribution $q(x,y)$ equals zero, are

$$[A_{11}\{u^0_{,x} + \tfrac{1}{2}(w^0_{,x})^2\} + A_{12}\{v^0_{,y} + \tfrac{1}{2}(w^0_{,y})^2\} + A_{16}\{u^0_{,y} + v^0_{,x} + w^0_{,x}w^0_{,y}\}]_{,x}$$
$$+ [A_{16}\{u^0_{,x} + \tfrac{1}{2}(w^0_{,x})^2\} + A_{26}\{v^0_{,y} + \tfrac{1}{2}(w^0_{,y})^2\} + A_{66}\{u^0_{,y} + v^0_{,x} + w^0_{,x}w^0_{,y}\}]_{,y} = 0 \quad (4.3)$$

$$[A_{16}\{u^0_{,x} + \tfrac{1}{2}(w^0_{,x})^2\} + A_{26}\{v^0_{,y} + \tfrac{1}{2}(w^0_{,y})^2\} + A_{66}\{u^0_{,y} + v^0_{,x} + w^0_{,x}w^0_{,y}\}]_{,x}$$
$$+ [A_{12}\{u^0_{,x} + \tfrac{1}{2}(w^0_{,x})^2\} + A_{22}\{v^0_{,y} + \tfrac{1}{2}(w^0_{,y})^2\} + A_{26}\{u^0_{,y} + v^0_{,x} + w^0_{,x}w^0_{,y}\}]_{,y} = 0 \quad (4.4)$$

$$[A_{11}\{u^0_{,x} + \tfrac{1}{2}(w^0_{,x})^2\} + A_{12}\{v^0_{,y} + \tfrac{1}{2}(w^0_{,y})^2\} + A_{16}\{u^0_{,y} + v^0_{,x} + w^0_{,x}w^0_{,y}\}]\, w^0_{,xx}$$
$$+ 2\,[A_{16}\{u^0_{,x} + \tfrac{1}{2}(w^0_{,x})^2\} + A_{26}\{v^0_{,y} + \tfrac{1}{2}(w^0_{,y})^2\} + A_{66}\{u^0_{,y} + v^0_{,x} + w^0_{,x}w^0_{,y}\}]\, w^0_{,xy}$$
$$+ [A_{12}\{u^0_{,x} + \tfrac{1}{2}(w^0_{,x})^2\} + A_{22}\{v^0_{,y} + \tfrac{1}{2}(w^0_{,y})^2\} + A_{26}\{u^0_{,y} + v^0_{,x} + w^0_{,x}w^0_{,y}\}]\, w^0_{,yy}$$
$$- [D_{11}w^0_{,xx} + D_{12}w^0_{,yy} + 2\,D_{16}w^0_{,xy}]_{,xx}$$
$$- 2\,[D_{16}w^0_{,xx} + D_{26}w^0_{,yy} + 2\,D_{66}w^0_{,xy}]_{,xy}$$
$$- [D_{12}w^0_{,xx} + D_{22}w^0_{,yy} + 2\,D_{26}w^0_{,xy}]_{,yy} = 0 \quad (4.5)$$

Substituting equations 4.2a-c into equations 4.3, 4.4, and 4.5 results in

$$[A_{11}\{\bar{u}^0_{,x} + \epsilon u^0_{1,x} + \tfrac{1}{2}(\epsilon w^0_{1,x})^2\} + A_{12}\{\bar{v}^0_{,y} + \epsilon v^0_{1,y} + \tfrac{1}{2}(\epsilon w^0_{1,y})^2\} + A_{16}\{\bar{u}^0_{,y} + \epsilon u^0_{1,y} + v^0_{,x} + \epsilon \bar{v}^0_{1,x} + \epsilon^2 w^0_{1,x}w^0_{1,y}\}]_{,x}$$
$$+ [A_{16}\{\bar{u}^0_{,x} + \epsilon u^0_{1,x} + \tfrac{1}{2}(\epsilon w^0_{1,x})^2\} + A_{26}\{\bar{v}^0_{,y} + \epsilon v^0_{1,y} + \tfrac{1}{2}(\epsilon w^0_{1,y})^2\} + A_{66}\{\bar{u}^0_{,y} + \epsilon u^0_{1,y} + v^0_{,x} + \epsilon \bar{v}^0_{1,x} + \epsilon^2 w^0_{1,x}w^0_{1,y}\}]_{,y} = 0 \quad (4.6)$$

$$[A_{16}\{\bar{u}^0_{,x} + \epsilon u^0_{1,x} + \tfrac{1}{2}(\epsilon w^0_{1,x})^2\} + A_{26}\{\bar{v}^0_{,y} + \epsilon v^0_{1,y} + \tfrac{1}{2}(\epsilon w^0_{1,y})^2\}$$
$$+ A_{66}\{\bar{u}^0_{,y} + \epsilon u^0_{1,y} + v^0_{,x} + \epsilon\bar{v}^0_{1,x} + \epsilon^2 w^0_{1,x} w^0_{1,y}\}]_{,x}$$
$$+ [A_{12}\{\bar{u}^0_{,x} + \epsilon u^0_{1,x} + \tfrac{1}{2}(\epsilon w^0_{1,x})^2\} + A_{22}\{\bar{v}^0_{,y} + \epsilon v^0_{1,y} + \tfrac{1}{2}(\epsilon w^0_{1,y})^2\}$$
$$+ A_{26}\{\bar{u}^0_{,y} + \epsilon u^0_{1,y} + v^0_{,x} + \epsilon\bar{v}^0_{1,x} + \epsilon^2 w^0_{1,x} w^0_{1,y}\}]_{,y} = 0 \quad (4.7)$$

$$[A_{11}\{\bar{u}^0_{,x} + \epsilon u^0_{1,x} + \tfrac{1}{2}(\epsilon w^0_{1,x})^2\} + A_{12}\{\bar{v}^0_{,y} + \epsilon v^0_{1,y} + \tfrac{1}{2}(\epsilon w^0_{1,y})^2\}$$
$$+ A_{16}\{\bar{u}^0_{,y} + \epsilon u^0_{1,y} + v^0_{,x} + \epsilon\bar{v}^0_{1,x} + \epsilon^2 w^0_{1,x} w^0_{1,y}\}]\epsilon w^0_{1,xx}$$
$$+ 2[A_{16}\{\bar{u}^0_{,x} + \epsilon u^0_{1,x} + \tfrac{1}{2}(\epsilon w^0_{1,x})^2\} + A_{26}\{\bar{v}^0_{,y} + \epsilon v^0_{1,y} + \tfrac{1}{2}(\epsilon w^0_{1,y})^2\}$$
$$+ A_{66}\{\bar{u}^0_{,y} + \epsilon u^0_{1,y} + v^0_{,x} + \epsilon\bar{v}^0_{1,x} + \epsilon^2 w^0_{1,x} w^0_{1,y}\}]\epsilon w^0_{1,xy}$$
$$+ [A_{12}\{\bar{u}^0_{,x} + \epsilon u^0_{1,x} + \tfrac{1}{2}(\epsilon w^0_{1,x})^2\} + A_{22}\{\bar{v}^0_{,y} + \epsilon v^0_{1,y} + \tfrac{1}{2}(\epsilon w^0_{1,y})^2\}$$
$$+ A_{26}\{\bar{u}^0_{,y} + \epsilon u^0_{1,y} + v^0_{,x} + \epsilon\bar{v}^0_{1,x} + \epsilon^2 w^0_{1,x} w^0_{1,y}\}]\epsilon w^0_{1,yy}$$
$$- [D_{11}\epsilon w^0_{1,xx} + D_{12}\epsilon w^0_{1,yy} + 2 D_{16}\epsilon w^0_{1,xy}]_{,xx}$$
$$- 2[D_{16}\epsilon w^0_{1,xx} + D_{26}\epsilon w^0_{1,yy} + 2 D_{66}\epsilon w^0_{1,xy}]_{,xy}$$
$$- [D_{12}\epsilon w^0_{1,xx} + D_{22}\epsilon w^0_{1,yy} + 2 D_{26}\epsilon w^0_{1,xy}]_{,yy} = 0 \quad (4.8)$$

Grouping equations 4.6, 4.7, and 4.8, by powers of ϵ results in

$$[A_{11}\bar{u}^0_{,x} + A_{12}\bar{v}^0_{,y} + A_{16}(\bar{u}^0_{,y} + \bar{v}^0_{,x})]_{,x}$$
$$+ \epsilon [A_{11}u^0_{1,x} + A_{12}v^0_{1,y} + A_{16}(u^0_{1,y} + v^0_{1,x})]_{,x}$$
$$+ \epsilon^2[A_{11}\tfrac{1}{2}(w^0_{1,x})^2 + A_{12}\tfrac{1}{2}(w^0_{1,y})^2 + A_{16}(w^0_{1,x}w^0_{1,y})]_{,x}$$
$$+ [A_{16}\bar{u}^0_{,x} + A_{26}\bar{v}^0_{,y} + A_{66}(\bar{u}^0_{,y} + \bar{v}^0_{,x})]_{,y}$$
$$+ \epsilon [A_{16}u^0_{1,x} + A_{26}v^0_{1,y} + A_{66}(u^0_{1,y} + v^0_{1,x})]_{,y}$$
$$+ \epsilon^2[A_{16}\tfrac{1}{2}(w^0_{1,x})^2 + A_{26}\tfrac{1}{2}(w^0_{1,y})^2 + A_{66}(w^0_{1,x}w^0_{1,y})]_{,y} = 0 \quad (4.9)$$

$$[A_{16}\bar{u}^0_{,x} + A_{26}\bar{v}^0_{,y} + A_{66}(\bar{u}^0_{,y} + \bar{v}^0_{,x})]_{,x}$$
$$+ \epsilon [A_{16}u^0_{1,x} + A_{26}v^0_{1,y} + A_{66}(u^0_{1,y} + v^0_{1,x})]_{,x}$$
$$+ \epsilon^2[A_{16}\tfrac{1}{2}(w^0_{1,x})^2 + A_{26}\tfrac{1}{2}(w^0_{1,y})^2 + A_{66}(w^0_{1,x}w^0_{1,y})]_{,x}$$

$$+ \left[A_{12}\bar{u}^0_{,x} + A_{22}\bar{v}^0_{,y} + A_{26}(\bar{u}^0_{,y} + \bar{v}^0_{,x})\right]_{,y}$$
$$+ \epsilon \left[A_{12}u^0_{1,x} + A_{22}v^0_{1,y} + A_{26}(u^0_{1,y} + v^0_{1,x})\right]_{,y}$$
$$+ \epsilon^2\left[A_{12}\tfrac{1}{2}(w^0_{1,x})^2 + A_{22}\tfrac{1}{2}(w^0_{1,y})^2 + A_{26}(w^0_{1,x}w^0_{1,y})\right]_{,y} = 0 \quad (4.10)$$

$$\epsilon \left[A_{11}\bar{u}^0_{,x} + A_{12}\bar{v}^0_{,y} + A_{16}(\bar{u}^0_{,y} + \bar{v}^0_{,x})\right]w^0_{1,xx}$$
$$+ \epsilon^2\left[A_{11}u^0_{1,x} + A_{12}v^0_{1,y} + A_{16}(u^0_{1,y} + v^0_{1,x})\right]w^0_{1,xx}$$
$$+ \epsilon^3\left[A_{11}\tfrac{1}{2}(w^0_{1,x})^2 + A_{12}\tfrac{1}{2}(w^0_{1,y})^2 + A_{16}(w^0_{1,x}w^0_{1,y})\right]w^0_{1,xx}$$
$$+ 2\epsilon \left[A_{16}\bar{u}^0_{,x} + A_{26}\bar{v}^0_{,y} + A_{66}(\bar{u}^0_{,y} + \bar{v}^0_{,x})\right]w^0_{1,xy}$$
$$+ 2\epsilon^2\left[A_{16}u^0_{1,x} + A_{26}v^0_{1,y} + A_{66}(u^0_{1,y} + v^0_{1,x})\right]w^0_{1,xy}$$
$$+ 2\epsilon^3\left[A_{16}\tfrac{1}{2}(w^0_{1,x})^2 + A_{26}\tfrac{1}{2}(w^0_{1,y})^2 + A_{66}(w^0_{1,x}w^0_{1,y})\right]w^0_{1,xy}$$
$$+ \epsilon \left[A_{12}\bar{u}^0_{,x} + A_{22}\bar{v}^0_{,y} + A_{26}(\bar{u}^0_{,y} + \bar{v}^0_{,x})\right]w^0_{1,yy}$$
$$+ \epsilon^2\left[A_{12}u^0_{1,x} + A_{22}v^0_{1,y} + A_{26}(u^0_{1,y} + v^0_{1,x})\right]w^0_{1,yy}$$
$$+ \epsilon^3\left[A_{12}\tfrac{1}{2}(w^0_{1,x})^2 + A_{22}\tfrac{1}{2}(w^0_{1,y})^2 + A_{26}(w^0_{1,x}w^0_{1,y})\right]w^0_{1,yy}$$
$$- \epsilon \left[D_{11}w^0_{1,xx} + D_{12}w^0_{1,yy} + 2\,D_{16}w^0_{1,xy}\right]_{,xx}$$
$$- 2\epsilon \left[D_{16}w^0_{1,xx} + D_{26}w^0_{1,yy} + 2\,D_{66}w^0_{1,xy}\right]_{,xy}$$
$$- \epsilon \left[D_{12}w^0_{1,xx} + D_{22}w^0_{1,yy} + 2\,D_{26}w^0_{1,xy}\right]_{,yy} = 0 \quad (4.11)$$

Referring to equations 4.9, 4.10, and 4.11, the pre-buckling force resultants for the equilibrium configuration are

$$\bar{N}_x = A_{11}\bar{u}^0_{,x} + A_{12}\bar{v}^0_{,y} + A_{16}(\bar{u}^0_{,y} + \bar{v}^0_{,x}) \quad (4.12a)$$

$$\bar{N}_y = A_{12}\bar{u}^0_{,x} + A_{22}\bar{v}^0_{,y} + A_{26}(\bar{u}^0_{,y} + \bar{v}^0_{,x}) \quad (4.12b)$$

$$\bar{N}_{xy} = A_{16}\bar{u}^0_{,x} + A_{26}\bar{v}^0_{,y} + A_{66}(\bar{u}^0_{,y} + \bar{v}^0_{,x}) \quad (4.12c)$$

Referring again to equations 4.9, 4.10, and 4.11, the buckling force and moment resultants are

$$N_{x1} = A_{11}u^0_{1,x} + A_{12}v^0_{1,y} + A_{16}(u^0_{1,y} + v^0_{1,x}) \quad (4.13a)$$

$$N_{y1} = A_{12}u^0_{1,x} + A_{22}v^0_{1,y} + A_{26}(u^0_{1,y} + v^0_{1,x}) \quad (4.13b)$$

$$N_{xy1} = A_{16}u^0_{1,x} + A_{26}v^0_{1,y} + A_{66}(u^0_{1,y} + v^0_{1,x}) \quad (4.13c)$$

$$M_{x1} = -\left[D_{11}w^0_{1,xx} + D_{12}w^0_{1,yy} + 2\,D_{16}w^0_{1,xy}\right] \qquad (4.14a)$$

$$M_{y1} = -\left[D_{12}w^0_{1,xx} + D_{22}w^0_{1,yy} + 2\,D_{26}w^0_{1,xy}\right] \qquad (4.14b)$$

$$M_{xy1} = -\left[D_{16}w^0_{1,xx} + D_{26}w^0_{1,yy} + 2\,D_{66}w^0_{1,xy}\right] \qquad (4.14c)$$

The terms which involve $\bar{u}^0$ and $\bar{v}^0$ in equations 4.9 and 4.10 sum to zero in view of equations 2.86 and 2.87, equations 2.96 and 2.97, and equations 3.1 and 3.2, all of which refer to the equilibrium configuration. Therefore, those terms may be eliminated from equations 4.9 and 4.10. The terms which involve the incremental displacements in equations 4.9, 4.10, and 4.11 contain terms which are linear, quadratic, and cubic in the small parameter ϵ. Since ϵ is small, terms associated with quadratic and cubic values of ϵ may be neglected. The terms which remain comprise the buckling equations (having omitted the small parameter ϵ).

$$\left[A_{11}u^0_{1,x} + A_{12}v^0_{1,y} + A_{16}(u^0_{1,y} + v^0_{1,x})\right]_{,x} + \left[A_{16}u^0_{1,x} + A_{26}v^0_{1,y} + A_{66}(u^0_{1,y} + v^0_{1,x})\right]_{,y} = 0 \qquad (4.15)$$

$$\left[A_{16}u^0_{1,x} + A_{26}v^0_{1,y} + A_{66}(u^0_{1,y} + v^0_{1,x})\right]_{,x} + \left[A_{12}u^0_{1,x} + A_{22}v^0_{1,y} + A_{26}(u^0_{1,y} + v^0_{1,x})\right]_{,y} = 0 \qquad (4.16)$$

$$\begin{aligned}&\left[A_{11}\bar{u}^0_{,x} + A_{12}\bar{v}^0_{,y} + A_{16}(\bar{u}^0_{,y} + \bar{v}^0_{,x})\right]w^0_{1,xx} \\ &+ 2\left[A_{16}\bar{u}^0_{,x} + A_{26}\bar{v}^0_{,y} + A_{66}(\bar{u}^0_{,y} + \bar{v}^0_{,x})\right]w^0_{1,xy} \\ &\quad + \left[A_{12}\bar{u}^0_{,x} + A_{22}\bar{v}^0_{,y} + A_{26}(\bar{u}^0_{,y} + \bar{v}^0_{,x})\right]w^0_{1,yy} \\ &- \left[D_{11}w^0_{1,xx} + D_{12}w^0_{1,yy} + 2\,D_{16}w^0_{1,xy}\right]_{,xx} \\ &\quad - 2\left[D_{16}w^0_{1,xx} + D_{26}w^0_{1,yy} + 2\,D_{66}w^0_{1,xy}\right]_{,xy} \\ &\qquad - \left[D_{12}w^0_{1,xx} + D_{22}w^0_{1,yy} + 2\,D_{26}w^0_{1,xy}\right]_{,yy} = 0 \qquad (4.17)\end{aligned}$$

C-2

Substituting equations 4.12 to 4.14 into equations 4.15 to 4.17 results in

$$N_{x1,x} + N_{xy1,y} = 0 \qquad (4.18)$$

$$N_{xy1,x} + N_{y1,y} = 0 \qquad (4.19)$$

$$M_{x1,xx} + 2\,M_{xy1,xy} + M_{y1,yy} + \bar{N}_x w^0_{1,xx} + 2\,\bar{N}_{xy} w^0_{1,xy} + \bar{N}_y w^0_{1,yy} = 0 \qquad (4.20)$$

Equation 4.20 is uncoupled from equations 4.18 and 4.19. Equations 4.18 and 4.19 are independent of the pre-buckling state or equilibrium configuration and are partial differential equations. Their only solutions are $u^0_1 = 0$ and $v^0_1 = 0$. Equation 4.20 is the governing partial differential equation for buckling analysis and in terms of displacements has been written previously as equation 4.17. Values of w^0_1, when determined, provide a measure of the amount of buckling. The laminate extentional stiffness properties A_{ij} and the laminate bending stiffness properties D_{ij} are functions of position in x and y in the plane of the plate. Equation 4.17 may not be solved exactly. A finite element code using the Engineering Analysis Language (EAL) [6] was used to obtain approximate solutions and numerical results.

Finite Element Model Used In The Engineering Analysis Language (EAL)

The finite element model used in EAL is formulated using the assumed stress field - minimum complementary energy method developed by T. H. H. Pian [7]. The element used is

a four-node combined plate membrane and plate bending element having five degrees of freedom per node as shown in Figure 4.1.

The strain energy of an element for linear elastic behavior in terms of the generalized displacements {q} is

$$U = 1/2 \lfloor q \rfloor [\ k\ ] \{q\} \tag{4.21}$$

where [k] is the element stiffness matrix.

The minimum complementary energy is

$$\pi_c = U - \iint u_i\ S_i\ dA = \text{minimum} \tag{4.22}$$

where U is the strain energy in terms of the stress components, u_i are the prescribed boundary displacements, and S_i are components of forces on the boundary. These force components are related to stresses directly next to the boundary through Cauchy's formula

$$S_i = \sigma_{ji}\ n_j \tag{4.23}$$

where n_j is the direction cosine of the boundary normal.

The stress distribution is expressed in terms of undetermined stress coefficients {ß} such that

$$\{\sigma\}^T = \lfloor \sigma_{11} \quad \sigma_{22} \quad \sigma_{33} \quad \cdots \quad \rfloor$$

$$\{ß\}^T = \lfloor ß_1 \quad ß_2 \quad ß_3 \quad \cdots \quad \rfloor$$

$$\{\sigma\} = [\ P\ ]\ \{ß\} \tag{4.24}$$

The elements of the matrix [P] are functions of position.

The stress-strain relations are

$$\{\epsilon\} = [\ N\ ]\ \{\sigma\} \tag{4.25}$$

Using equation 4.25, the internal strain energy is

$$U = 1/2 \iiint_V \lfloor \sigma \rfloor\ [\ N\ ]\ \{\sigma\}\ dV \tag{4.26}$$

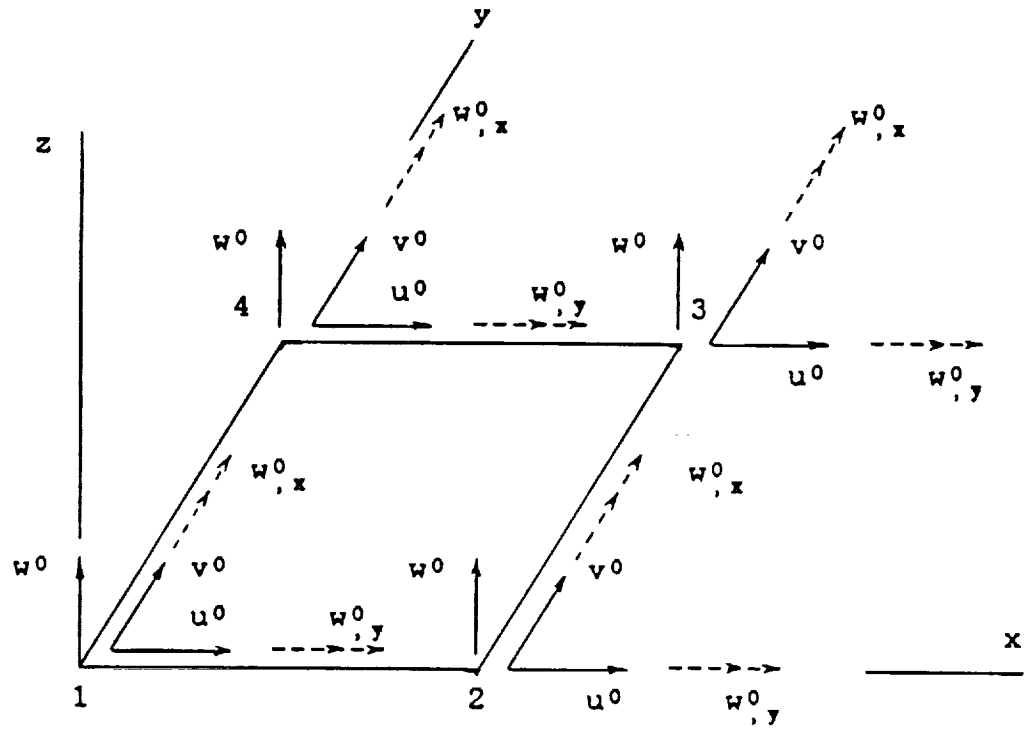

Figure 4.1 Four-Node Quadrilateral
Combined Membrane And Bending Element

Using equation 4.24, equation 4.26 may be expressed as

$$U = 1/2 \lfloor \beta \rfloor [H] \{\beta\} \qquad (4.27)$$

where the matrix [H] is

$$[H] = \iiint_{\underline{V}} [P]^T [N] [P] \, d\underline{V} \qquad (4.28)$$

The prescribed boundary displacements are

$$\{u\} = [L] \{q\} \qquad (4.29)$$

where the terms in the matrix [L] are functions of position on the boundary and the terms in the vector {q} are the generalized displacements at the nodes. Since the forces {S} on the boundary may be expressed in terms of the stresses {σ} as in equation 4.23, these forces may be related to the undetermined stress coefficients {β} through equation 4.24 such that

$$\{S\} = [R] \{\beta\} \qquad (4.30)$$

where the terms in the matrix [R] are functions of position on the boundary.

The total complementary energy given in equation 4.22 may be written as

$$\pi_c = 1/2 \lfloor \beta \rfloor [H] \{\beta\} - \lfloor \beta \rfloor [T] \{q\} \qquad (4.31)$$

where: $$[T] = \iint [R] [L] \, dA \qquad (4.32)$$

The condition to be satisfied in order for the total complementary energy to be a minimum is that the partial derivative of the complementary energy with respect to each of the undetermined stress coefficients β_i, ($i = 1,2,3,\ldots$) should be equal to zero. Using equation 4.31 and taking partial derivatives produces the following result

$$[H] \{\beta\} = [T] \{q\} \quad (4.33)$$

The undetermined stress coefficients $\{\beta\}$ may be obtained by pre-multiplying equation 4.33 by the inverse of $[H]$ which produces the result

$$\{\beta\} = [H]^{-1}[T] \{q\} \quad (4.34)$$

Substituting equation 4.34 into equation 4.27 results in

$$U = 1/2 \{q\}^T [T]^T[H]^{-1}[T] \{q\} \quad (4.35)$$

Comparing equation 4.35 to equation 4.21 provides a relation with which to determine the stiffness matrix $[k]$.

$$[k] = [T]^T[H]^{-1}[T] \quad (4.36)$$

Increasing the number of assumed stress coefficients in effect decreases the excess strain energy and provides a more accurate solution. Increasing the number of elements, which increases the size and number of stiffness matrices, also leads to an increase in accuracy of the results.

Finite Element Meshes And Boundary Conditions

The finite element meshes for the four geometries considered in the buckling analysis are depicted in Figures 4.2 through 4.5. Each upper right quadrant in these meshes is identical to the one-quarter plate meshes considered in Chapter III. In other words, the mesh configurations are the same in each chapter. There are 192 elements in each quadrant with 12 elements placed around the edge of the hole or 768 elements for the entire plate with 48 elements placed around the entire edge of the hole. The complete plate con-

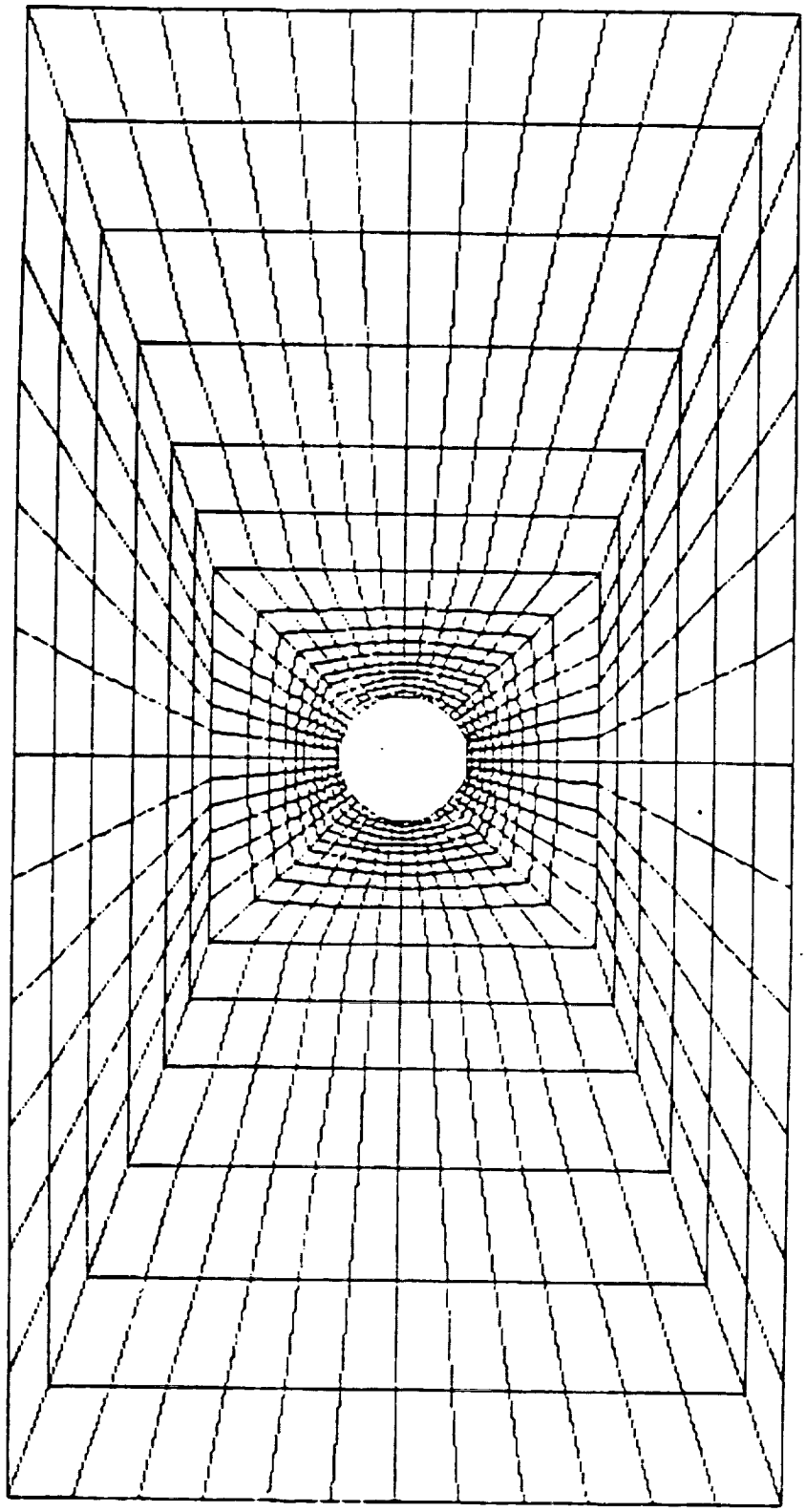

Figure 4.2 Finite Element Mesh For Case

L/W = 2, D/W = 1/6

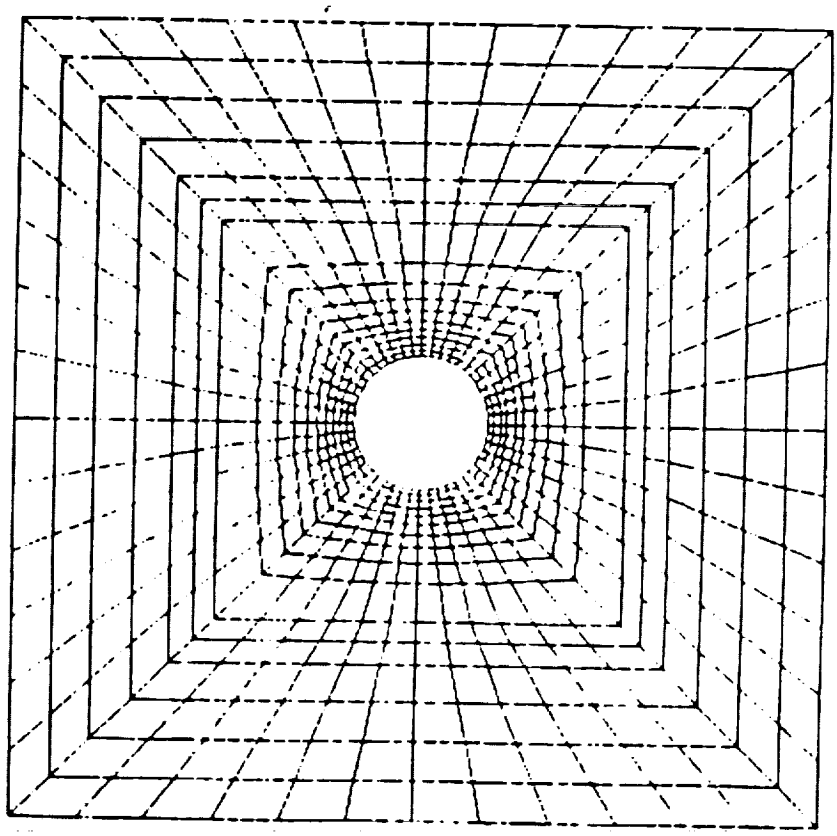

Figure 4.3 Finite Element Mesh For Case

L/W = 1, D/W = 1/6

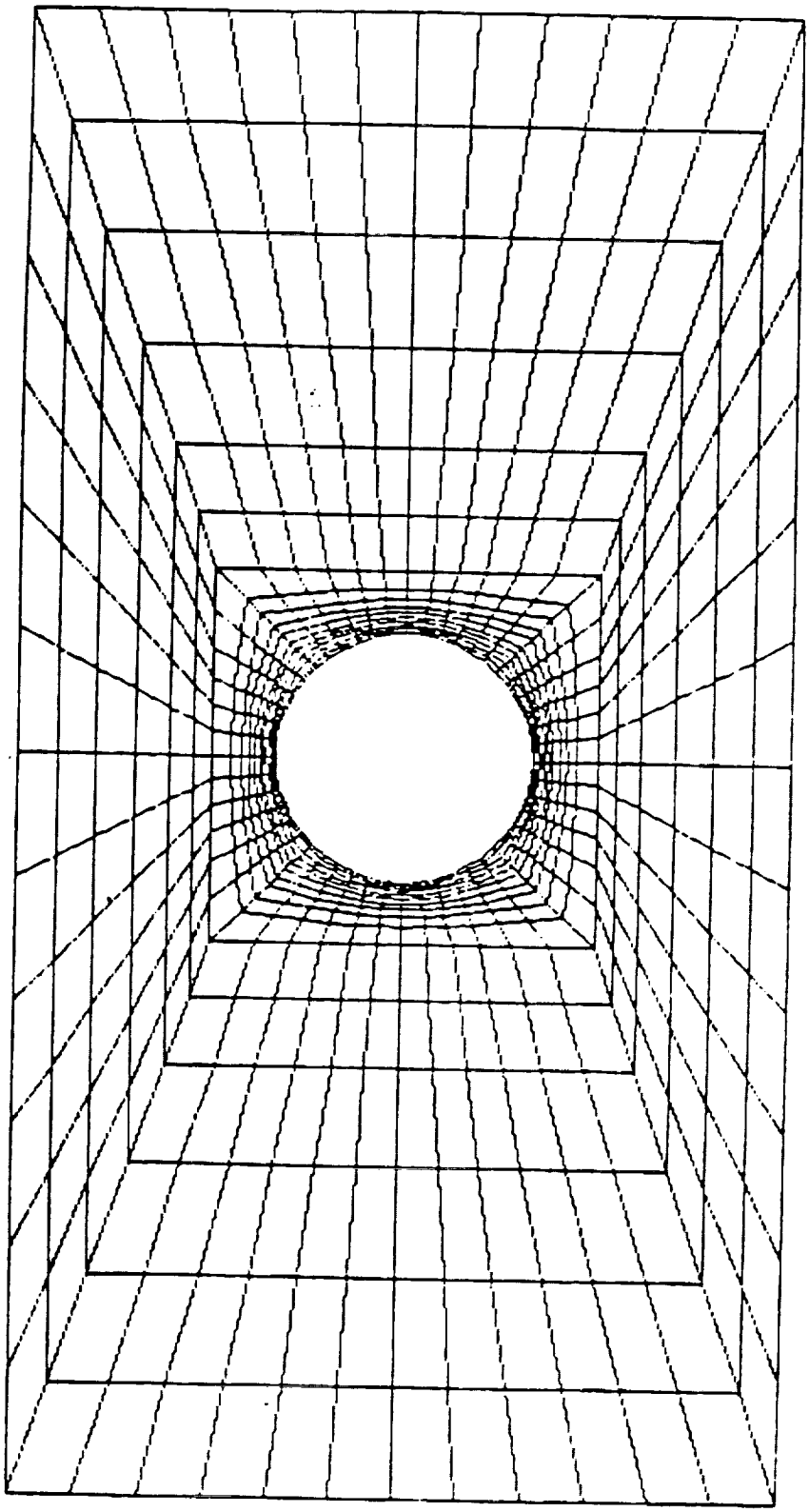

Figure 4.4 Finite Element Mesh For Case L/W = 2, D/W = 1/3

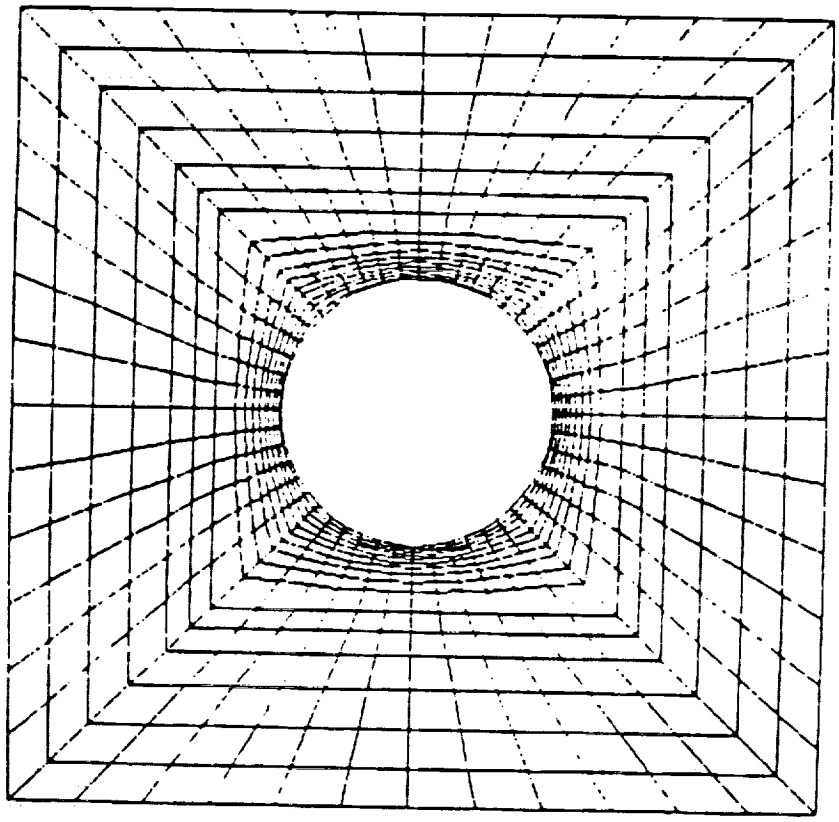

Figure 4.5 Finite Element Mesh For Case L/W = 1, D/W = 1/3

figuration of 768 elements is used in the buckling analysis instead of only a one-quarter plate configuration because only one buckling analysis per design is required. Four buckling analyses per design would be required with the one-quarter plate configuration (one analysis per quadrant). Four sets of boundary conditions would be required in a one-quarter plate analysis in order to obtain results for all of the possible buckling modes. The four sets of boundary conditions for the one-quarter plate configuration are symmetric-symmetric, symmetric-antisymmetric, antisymmetric-symmetric, and antisymmetric-antisymmetric. The choice was made to use one set of boundary conditions applicable to the complete plate in order to obtain results for all of the possible buckling modes. The boundary conditions imposed are those for a simply supported plate.

The following two chapters contain the results of the tensile and buckling analyses.

CHAPTER V

TENSILE STRENGTH OF THE PLATE DESIGNS

Numerical Results

This chapter presents the results for the uniaxial tensile loading problem. The failure loads and failure modes of four plate geometries are considered. Each geometry is used in conjunction with four straightline composite layups and five curvilinear composite layups to form sixteen-layer laminate designs. Tables 5.1 through 5.4 show the predicted tensile failure loads for the 36 designs considered. These tables are arranged according to the plate geometries. The failure loads shown in Tables 5.1 through 5.4 are based on the maximum strain criterion and the Tsai-Wu criterion. The maximum strain criterion is a strain-based noninteracting criterion and, as such, does not differentiate or account for possible interactions which may occur between failure modes. The Tsai-Wu criterion, on the other hand, can account for interactions among the possible failure modes, such as an interaction between fiber failure and shear failure. The maximum strain criterion is used as the primary criterion to determine the failure mode, and the Tsai-Wu criterion is used to verify the accuracy of the maximum strain criterion and to provide additional insight on possible interactions among failure modes. The legend at the top of each table defines the notation associated with each

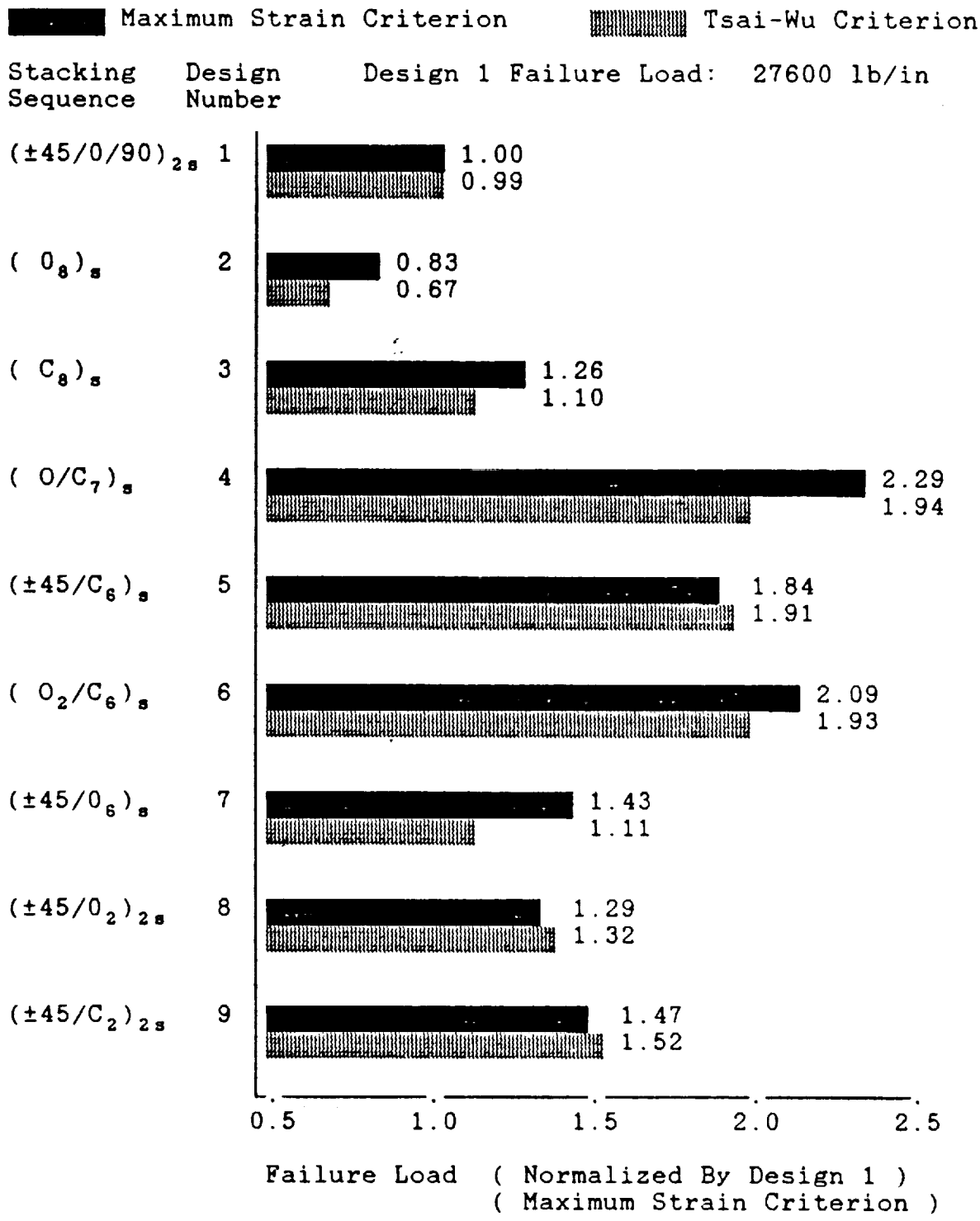

Table 5.1 Normalized Tensile Failure Load

Case: L = 20 in., W = 10 in., D/W = 1/6

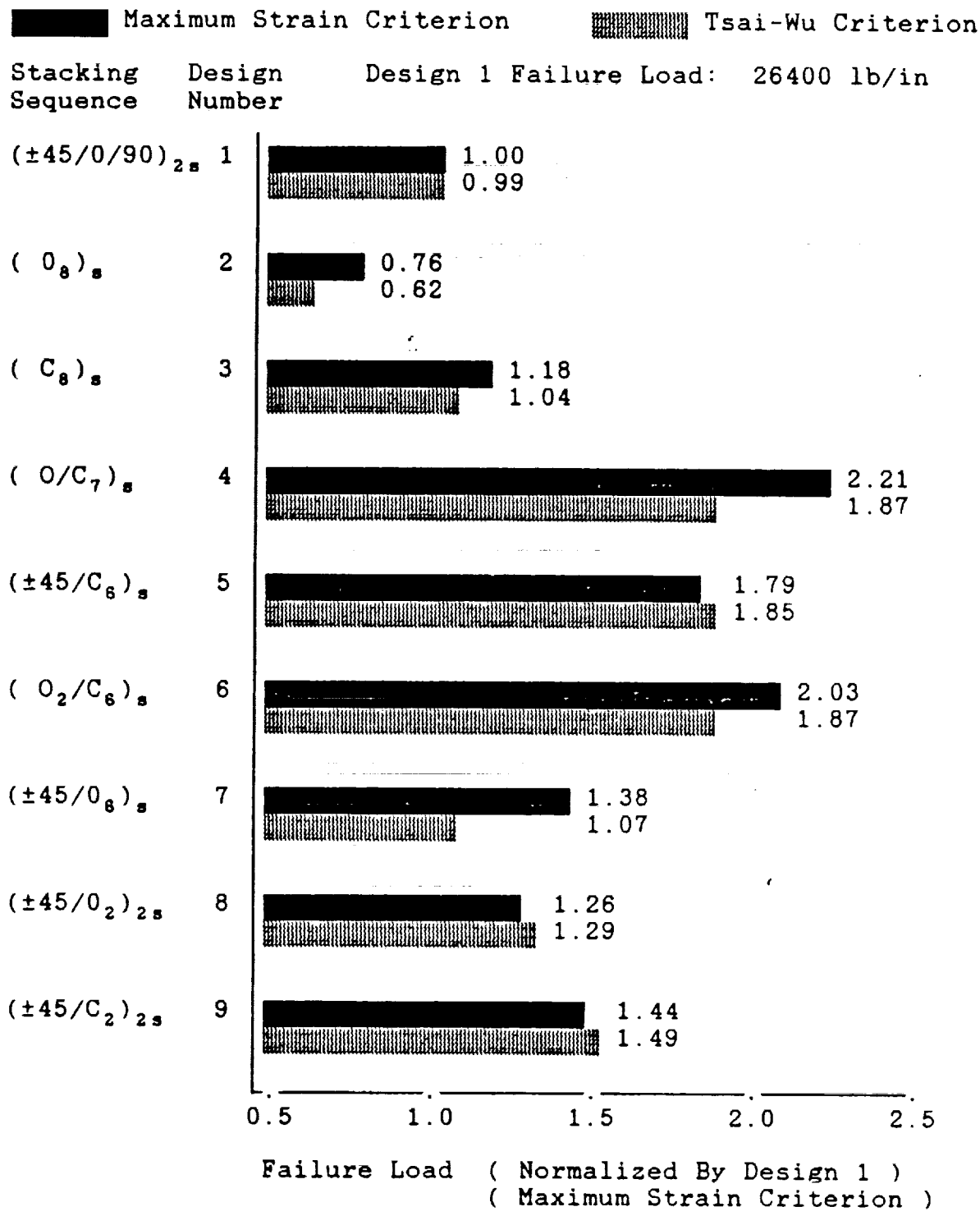

Table 5.2 Normalized Tensile Failure Load

Case: L = 10 in., W = 10 in., D/W = 1/6

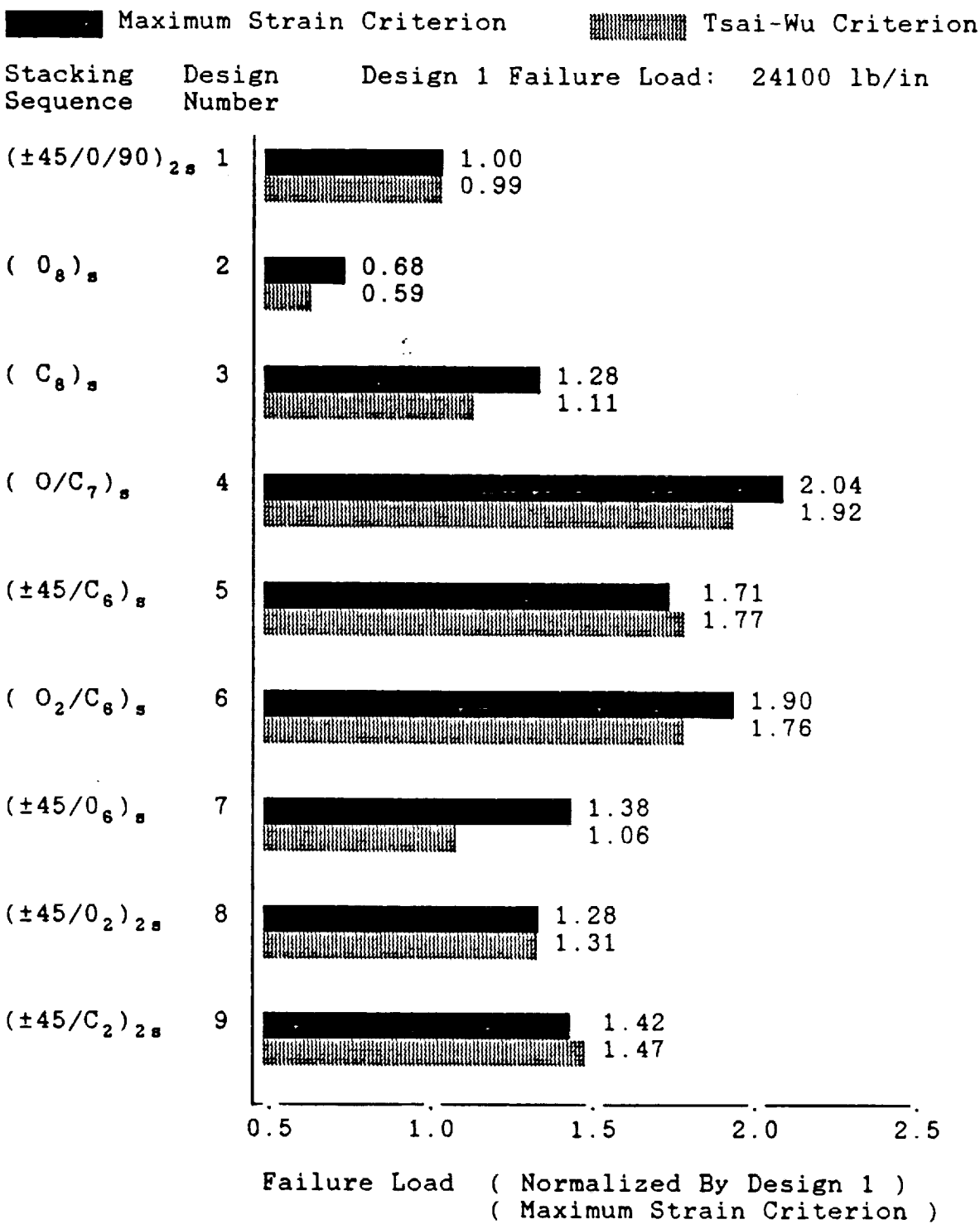

Table 5.3 Normalized Tensile Failure Load

Case: L = 20 in., W = 10 in., D/W = 1/3

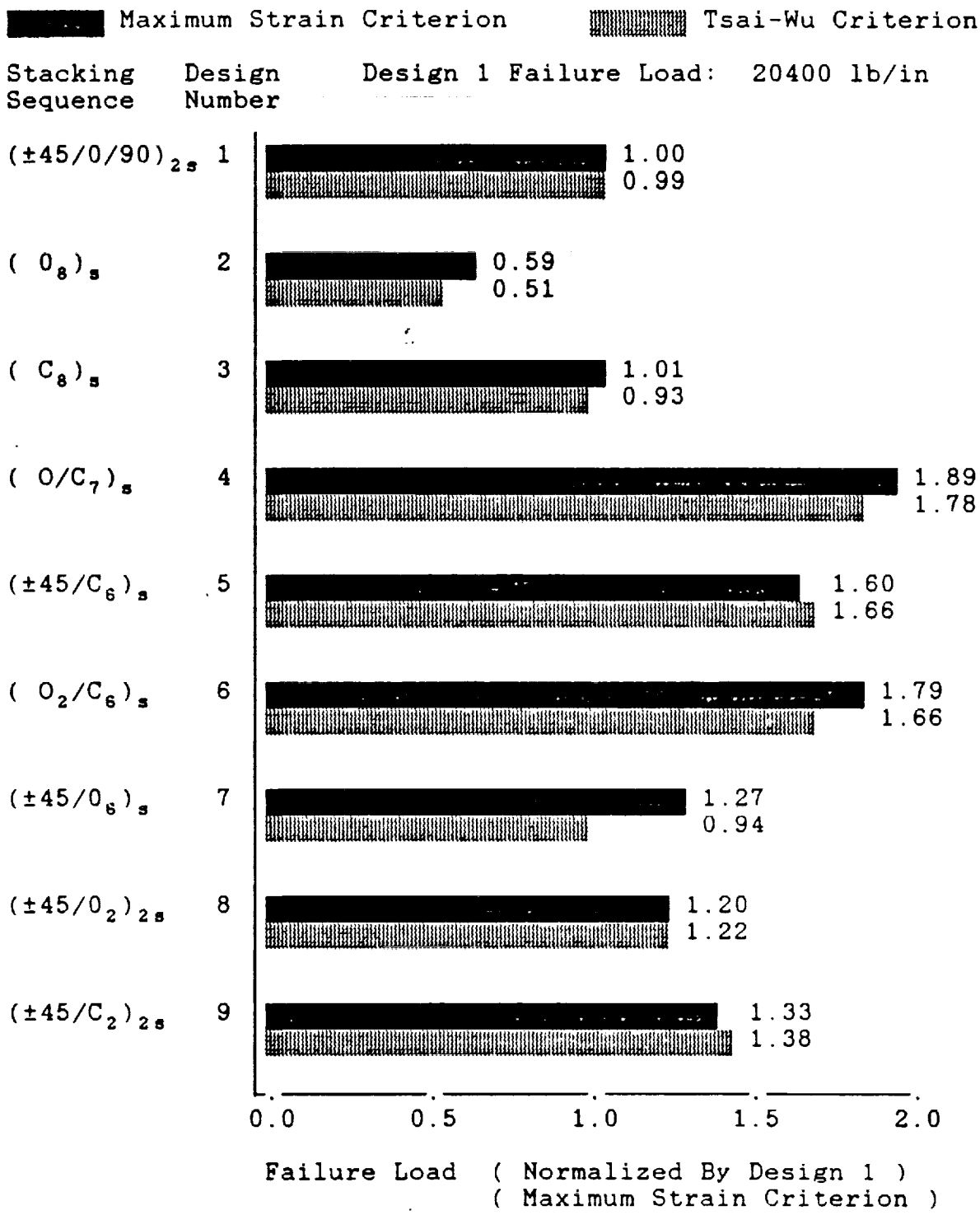

Table 5.4 Normalized Tensile Failure Load

Case: L = 10 in., W = 10 in., D/W = 1/3

table. In each table, the failure loads of each design (stacking sequence) are normalized by the failure load of the straightline quasi-isotropic design (Design 1) for that particular geometry based on the maximum strain criterion. Quasi-isotropic laminates represent a conventional, conservative, current day design philosophy. For each geometry, if the normalized failure load for a particular design is less than 1.00, that design is not as capable of supporting a load as the quasi-isotropic design. Conversely, if the normalized failure load is greater than 1.00, that particular design is predicted to support a higher load at failure than the quasi-isotropic design.

Table 5.1 shows the results for plates with parameters L/W = 2 and D/W = 1/6. These plates are rectangular and the actual plate dimensions are L = 20 in., W = 10 in., and D = 1.667 in. (length, width, and hole diameter). The maximum strain criterion predicts that the Design 1 laminate will experience fiber failure in the 0^0 layers at the net-section hole edge at a load of 27600 lb/in. The Tsai-Wu criterion predicts the same result at virtually the same failure load.

Considering Design 2 next, the unidirectional fiber format laminate $(0_8)_s$ is one that comes to mind when thinking about using fibers most effectively, i.e.,aligned with the load direction. However, Design 2 experiences shear failure in the matrix, at the hole, near the net-section, at a load 17% below that of quasi-isotropic Design 1. This

failure results in a crack which runs parallel to the fibers from the net-section hole edge to the ends of the plate. Shear occurs because of the rapid change in the direction of stress as the load is transmitted around the hole. In order to accomodate the hole, the uniform load on the ends of the plate necessarily must become nonuniform as the hole is approached. This generates gradients in one stress component that in turn produces gradients in the other stress components. Since there are no shear stresses at the ends of the plate, shear stresses are generated when approaching the hole. Since a unidirectional fiber format is very weak in shear, this laminate is design-limited in shear. The Tsai-Wu criterion predicts the same result at a failure load 33% lower than that of Design 1.

The choice of a curvilinear fiber format and the stacking sequence $(C_{\theta})_s$ for Design 3, where the fibers are aligned with the principal stress directions at every point in the plate, is a logical progression to overcome the inherent problems of Design 2 which led to shear failure. Herein "C" is used to denote curvilinear layers. As a result, no shear stress can occur in the principal material directions. The maximum strain criterion predicts that Design 3 is 26% stronger than Design 1 (quasi-isotropic) and 43% stronger than Design 2 (unidirectional). Failure of the laminate of Design 3 is traced to the relative weakness of the matrix in the direction transverse to the fibers. Design 3 fails due

to strain elongation in the fiber direction generating contraction strains in the transverse direction at the net-section near the hole edge (Poisson ratio effect). The material simply separates perpendicular to the fiber direction. The Tsai-Wu failure criterion predicts the same result at a failure load 10% greater than that of Design 1.

Again, a logical progression in choice of stacking sequence, to overcome the inherent problems encountered with Design 3, is that of Design 4, a $(0/C_7)_s$ laminate, and Design 6, a $(0_2/C_8)_s$ laminate, where the "0" denotes orthogonal. In Design 4, the fibers in the two "0" layers are aligned orthogonally everywhere to the 14 load-bearing curvilinear layers to prevent failure of the material perpendicular to the fiber direction. Similarly, in Design 6 the fibers in the four "0" layers are aligned orthogonally everywhere to the 12 load-bearing curvilinear layers to alleviate failure of the material perpendicular to the fibers at the net-section away from the hole edge. The failure mechanism for Design 4 and Design 6 is fiber failure in the curvilinear layers at the net-section near the hole edge. Design 4 supports the highest fiber direction tensile stress in the curvilinear layers among the designs considered, and shows that two orthogonal layers are all that is necessary to eliminate failure of the material perpendicular to the fibers. The maximum strain criterion predicts that Design 4 is 129% stronger and Design 6 is 109% stronger than Design

1. This is a dramatic increase in strength. The Tsai-Wu criterion also predicts about a factor of 2 strength increase relative to Design 1. Unfortunately, any attempt to fabricate an orthogonal grid of fibers would probably result in less than perfect orthogonal alignment relative to the curvilinear fibers. If the alignment was less than perfect shear stresses would be introduced which would lead to matrix failure. Even if the orthogonal alignment was perfect, if the load was other than pure axial loading (i.e., a shear component was present), shear stresses would be generated within the laminate and this would lead to laminate failure due to shear. Otherwise, Design 4 and Design 6 are excellent designs for the case of pure axial load.

The choice of a more practical design, especially for easier fabrication and to anticipate inadvertent introduction of shear, is that of Design 5, a $(\pm 45/C_6)_s$ laminate, which includes 12 load-bearing curvilinear fiber layers. Design 7, a $(\pm 45/0_6)_s$ laminate, is a comparable laminate which includes 12 load-bearing straightline fiber layers instead of 12 curvilinear layers. Both designs include 4 straightline fiber layers at $\pm 45^0$ (two positive and two negative to maintain symmetry) which provide the desired resistance to shear. These layers also help carry axial load. Use of the $\pm 45^0$ layers effectively eliminates the problem of shear failure in the matrix. The iteration scheme, discussed in Chapter III, is used to determine the necessary fiber

orientation of the curvilinear layers to maintain fiber alignment in the principal stress direction. It is important to note that the directions of the curvilinear fibers at a given point in the $(\pm 45/C_8)_s$ laminate are not the same as the directions of the curvilinear fibers in the $(C_8)_s$ laminate, even though the notation "C" is used in both cases.

The maximum strain criterion predicts that Design 5 is 84% stronger than Design 1, that Design 7 is 43% stronger than Design 1, and that Design 5 with its curvilinear fiber format has a distinct margin of strength over Design 7 with its straightline fiber format. Failure for Design 5 occurs in the curvilinear layers, and for Design 7 occurs in the 0^0 layers, with fiber failure at the net-section near the hole edge as the mechanism for both designs. The Tsai-Wu criterion predicts the same failure mode for both designs, and predicts a 91% strength increase for Design 5, and an 11% strength increase for Design 7, both relative to Design 1. Moreover, for Design 7, the Tsai-Wu criterion indicates interaction between shear failure and fiber failure, with fiber failure controlling the response at the hole near the net-section. This interaction may account for the increased difference in strength (91% versus 11%) between Design 5 (curvilinear) and Design 7 (straightline). Also, a possible difference is that the transmission of the load around the hole through the net-section is accomplished differently

with the curvilinear fiber format than with the straightline fiber format. This will be discussed in more detail later in this chapter.

Care should be exercised not to make comparisons among the various designs based on factors which may be too narrow and restrictive. All of the designs were kept constant with respect to weight by maintaining each design as 16 layer laminates. Strength as the only factor to be considered in making a best design choice would be too narrow. Based on the maximum strain criterion, if Design 6 was to be chosen over Design 5 because of its 25% strength margin, the disadvantages associated with possible shear load introduction would have been ignored. As can be seen from Table 5.1, comparisons based on the Tsai-Wu criterion would lead to the same conclusions. However, according to the Tsai-Wu criterion, possible interactions between fiber failure and shear failure favors Design 5.

Finally, considering Design 8, a $(\pm 45/0_2)_{2s}$ laminate, and Design 9, a $(\pm 45/C_2)_{2s}$ laminate, both criteria predict that the curvilinear fiber format will have a greater load capacity than the straightline fiber format. Design 8 and Design 9 have more $\pm 45^0$ layers, at the expense of less 0^0 or less curvilinear load-bearing layers than Designs 4-7. For Design 8, the failure mode is predicted to be fiber failure at the net-section near the hole edge in the 0^0 layers. According to the maximum strain criterion, Design 8, with

less 0^0 load-bearing layers, has a lower failure load margin than Design 7, 29% versus 43%, relative to Design 1, the baseline quasi-isotropic laminate. However, the Tsai-Wu criterion indicates interaction between fiber failure and shear failure and predicts that Design 8 will have a higher failure load margin than Design 7 (32% versus 11%). Any indication of possible interaction should not be dismissed lightly.

For Design 9, the failure mode is predicted to be fiber failure at the net-section, near the hole edge, in the curvilinear layers. The maximum strain criterion predicts a strength increase of 47% for Design 9 relative to Design 1, and a failure load margin of 18% over Design 8, a straightline design. The Tsai-Wu criterion predicts that Design 9 is 52% stronger than Design 1 and 20% stronger than Design 8. This agrees with the comparison and trend established for Design 5 and Design 7, where the curvilinear fiber format has superior load capacity over the similar design straightline fiber format. As is the case for Design 5 and Design 7, with Design 8 and Design 9, at the net-section near the hole edge, the failure mechanism (fiber failure), layer orientation, and fiber alignment are virtually identical. However, as mentioned above, the curvilinear fiber format seems to be able to transmit a higher load around the hole and through the net-section than the straightline fiber format can.

Table 5.2 shows the results for plates with parameters L/W = 1 and D/W = 1/6, namely, square plates. The actual plate dimensions are L = 10 in., W = 10 in., and D = 1.667 in. (length, width, and hole diameter). For this geometry, the quasi-isotropic design (Design 1) failure load determined by the maximum strain criterion is used as a baseline value with which to normalize and compare the failure loads of the other designs, including the failure loads predicted by the Tsai-Wu failure criterion. As shown in Table 5.1 for the rectangular plate, the same favorable results for the curvilinear designs relative to the straightline designs were obtained for the square plate geometry. For example, as seen in Table 5.2, the Design 5 square laminate, a $(\pm 45/C_6)_s$, has a normalized failure load of 1.79 relative to the Design 1 laminate, compared to 1.84 for the rectangular laminate, and fiber failure is predicted to occur in the curvilinear layers at the net-section near the hole edge, the problem of shear failure in the matrix being eliminated. The square straightline laminate Design 7, a $(\pm 45/0_6)_s$, has a normalized failure load of 1.38, compared to 1.43 for the rectangular laminate, and fiber failure is predicted to occur in the 0^0 layers at the net-section near the hole edge. Interaction between shear failure and fiber failure causes fiber failure in this laminate at a load 41% below that of the curvilinear laminate Design 5.

Tables 5.3 and 5.4, which consider rectangular and

square plates with holes twice as large as the other two cases, continue the pattern established in Tables 5.1 and 5.2. The results show clearly that the curvilinear designs are stronger, having higher tensile load capacities relative to the straightline designs. Like the other plate geometries, each curvilinear design exhibits the same relative improvement over its straightline counterpart. Table 5.3 shows the results for plates with parameters L/W = 2 and D/W = 1/3. The actual plate dimensions are L = 20 in., W = 10 in., and D = 3.333 in. (length, width, and hole diameter). Failure loads are normalized by that of the quasi-isotropic Design 1 laminate. Table 5.4 shows the results for plates with parameters L/W = 1 and D/W = 1/3. The actual plate dimensions are L = 10 in., W = 10 in., and D = 3.333 in. (length, width, and hole diameter). Failure loads are normalized by that of the quasi-isotropic Design 1 laminate. An increase in failure load for the curvilinear designs over the straightline designs is realized for all plate geometric configurations.

It is important to note that even though the strengths of the curvilinear designs relative to the straightline designs were basically the same for all four plate geometries considered, the absolute strengths of the various geometries, both straightline and curvilinear, are a function of plate geometry. Table 5.5 shows the failure load of all designs normalized by a single failure load, namely the fail-

Table 5.5

Normalized Tensile Failure Load (Geometry Comparison)[1]

Stacking Sequence	Design Number	L/W = 2 D/W = 1/6	L/W = 1 D/W = 1/6	L/W = 2 D/W = 1/3	L/W = 1 D/W = 1/3
$(\pm 45/0/90)_{2s}$	1	1.00 (0.99)	0.96 (0.95)	0.88 (0.87)	0.74 (0.73)
$(0_8)_s$	2	0.83 (0.67)	0.72 (0.59)	0.59 (0.52)	0.43 (0.38)
$(C_8)_s$	3	1.26 (1.10)	1.13 (1.00)	1.13 (0.98)	0.75 (0.69)
$(O/C_7)_s$	4	2.29 (1.94)	2.11 (1.79)	1.79 (1.68)	1.40 (1.32)
$(\pm 45/C_6)_s$	5	1.84 (1.91)	1.71 (1.77)	1.50 (1.55)	1.18 (1.23)
$(O_2/C_6)_s$	6	2.09 (1.93)	1.94 (1.79)	1.67 (1.54)	1.32 (1.23)
$(\pm 45/0_6)_s$	7	1.43 (1.11)	1.32 (1.03)	1.21 (0.93)	0.94 (0.70)
$(\pm 45/0_2)_{2s}$	8	1.29 (1.32)	1.21 (1.24)	1.12 (1.15)	0.89 (0.90)
$(\pm 45/C_2)_{2s}$	9	1.47 (1.52)	1.38 (1.43)	1.25 (1.29)	0.99 (1.02)

[1] Normalized by Design 1 failure load (maximum strain criterion), L/W = 2, D/W = 1/6. Failure loads determined by the Tsai-Wu failure criterion are specified in parentheses.

ure load of the quasi-isotropic rectangular plate with a small hole (L/W = 2, D/W = 1/6, Design 1, Table 5.1) as predicted by the maximum strain criterion. As can be seen, the failure loads going from Tables 5.1 to 5.4 decrease for any given design. For example, if the normalized values of failure loads for Design 5 (curvilinear fiber format) and Design 7 (straightline fiber format) are compared progressively from Table 5.1 through 5.4, this statement is seen to be true. All of the data shown for each geometric configuration in Tables 5.1 through 5.4 is combined in Table 5.5 to illustrate the influence of geometry on failure load. The normalized values of the failure loads predicted by application of the Tsai-Wu criterion are enclosed in parentheses. Designs which have the largest tensile load capacities are realized by laminates with the geometric parameters L/W = 2 and D/W = 1/6. The geometries in order of decreasing tensile load capacity are: L/W = 1 and D/W = 1/6; L/W = 2 and D/W = 1/3; L/W = 1 and D/W = 1/3.

Iteration Procedure And Convergence Of Fiber Directions

The iteration procedure used to determine the direction of the fibers in the curvilinear layers for fiber alignment with the principal stress directions was described in some detail in Chapter III. In Table 5.6, the fiber directions in four representative elements for a laminate with a stacking sequence of $(\pm 45/C_6)_s$ and geometric parameters L/W = 1

Table 5.6

Convergence Of Fiber Directions[1]

Iteration	Element 28	Element 81	Element 154	Element 177
1	- 3.74	-12.60	0.15	- 0.49
2	-12.36	-41.15	1.17	- 1.69
3	-15.65	-42.30	1.95	- 2.34
4	-16.91	-42.93	2.48	- 2.70
5	-17.34	-42.96	2.82	- 2.89
6	-17.44	-42.96	3.04	- 2.99
7	-17.41	-42.96	3.19	- 3.05
8	-17.35	-42.99	3.29	- 3.08
9	-17.29	-43.01	3.36	- 3.09
10	-17.23	-43.04	3.40	- 3.10
11	-17.19	-43.04	3.44	- 3.10
12	-17.17	-43.06	3.46	- 3.11

[1] Fiber directions are in units of degrees

and D/W = 1/3 are listed as a function of iteration number. Location of the four elements in the quarter plate is shown in Figure 5.1. Equation 3.7, page 75, is used as the condition to be satisfied for convergence of the fiber alignment angle. An application of equation 3.7 provides results as shown in Table 5.7 where data from Table 5.6 and iterations 11 and 12 are used to check for convergence. As can

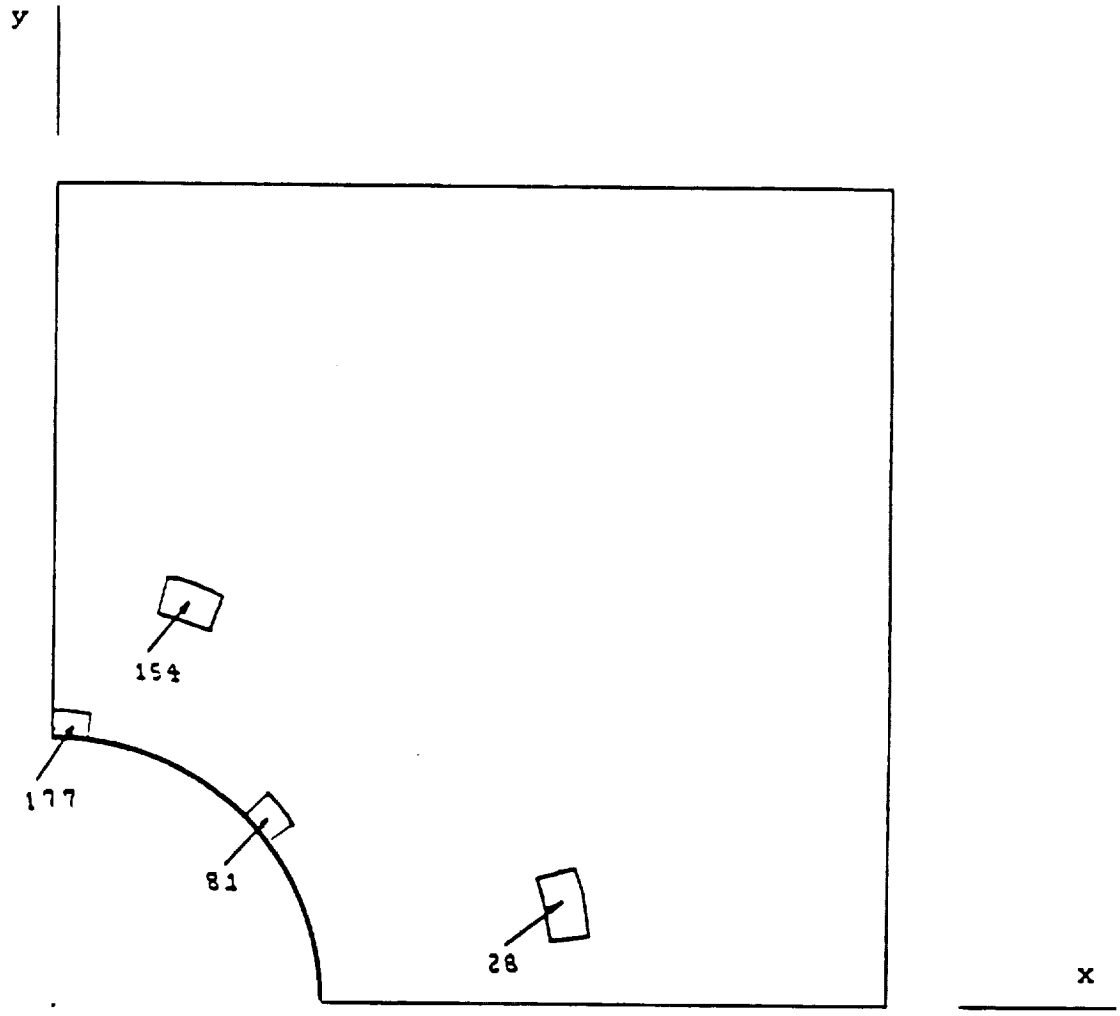

Figure 5.1 Location Of Four Elements

be seen from the table, convergence is quite rapid, and can actually be achieved within 6 or 7 iterations.

Table 5.7

Relative Error In Current Principal Stress Direction[1]

Element 28	Element 81	Element 154	Element 177
0.0012	0.0005	0.0058	0.0032

[1] Tabular values obtained using data of previous iteration 11 and current iteration 12 from Table 5.6 and applying equation 3.7, p. 75. Convergence is assumed as achieved when the relation given by equation 3.7 is less than 0.01.

Stress Continuity Across Element Boundaries

The question of the accuracy of the method of analysis could be a matter of concern. Finite element methods are well established methods for providing numerical results. The effectiveness of the eight-node isoparametric element in general applications to satisfy convergence requirements, compatability, and stress continuity is well established in the literature. Related discussions will not be included. However, in this problem, because of the idealization, the fiber orientation varies from element to element, causing possible discontinuities in the stress field. It is there-

fore logical to ask about the convergence of the results. The standard approach is to compute results using a finer mesh and compare the results with those of the established mesh. If the results from the finer mesh compare well with the results of the established mesh, the answers are assumed to have converged. Here a finer mesh results in less of a jump in fiber orientation from element to element, and thereby, perhaps less problems for convergence of the stress field. To investigate this point, the standard mesh size density was doubled, from 192 elements to 384 elements in a quarter plate analysis. The circumferential force resultant N_s around the hole edge was used as a measure of stress field continuity. The 192 element mesh resulted in 12 elements around the quarter hole, while the 384 element mesh resulted in 24 elements around the quarter hole. Data for the laminate design case $(\pm 45/C_6)_s$, L/W = 1, D/W = 1/3, were used for the comparison. In Figure 5.2 the force resultants for the two meshes are plotted against element position around the hole given by the angle relative to the x-axis. The results for the two meshes are virtually superimposed and show neglible difference in results. The jump in the force resultant from element to element is evidenced by the fact that the results are smooth and continuous and is negligible. Data used to plot the curves of Figure 5.2 are shown in Table 5.8.

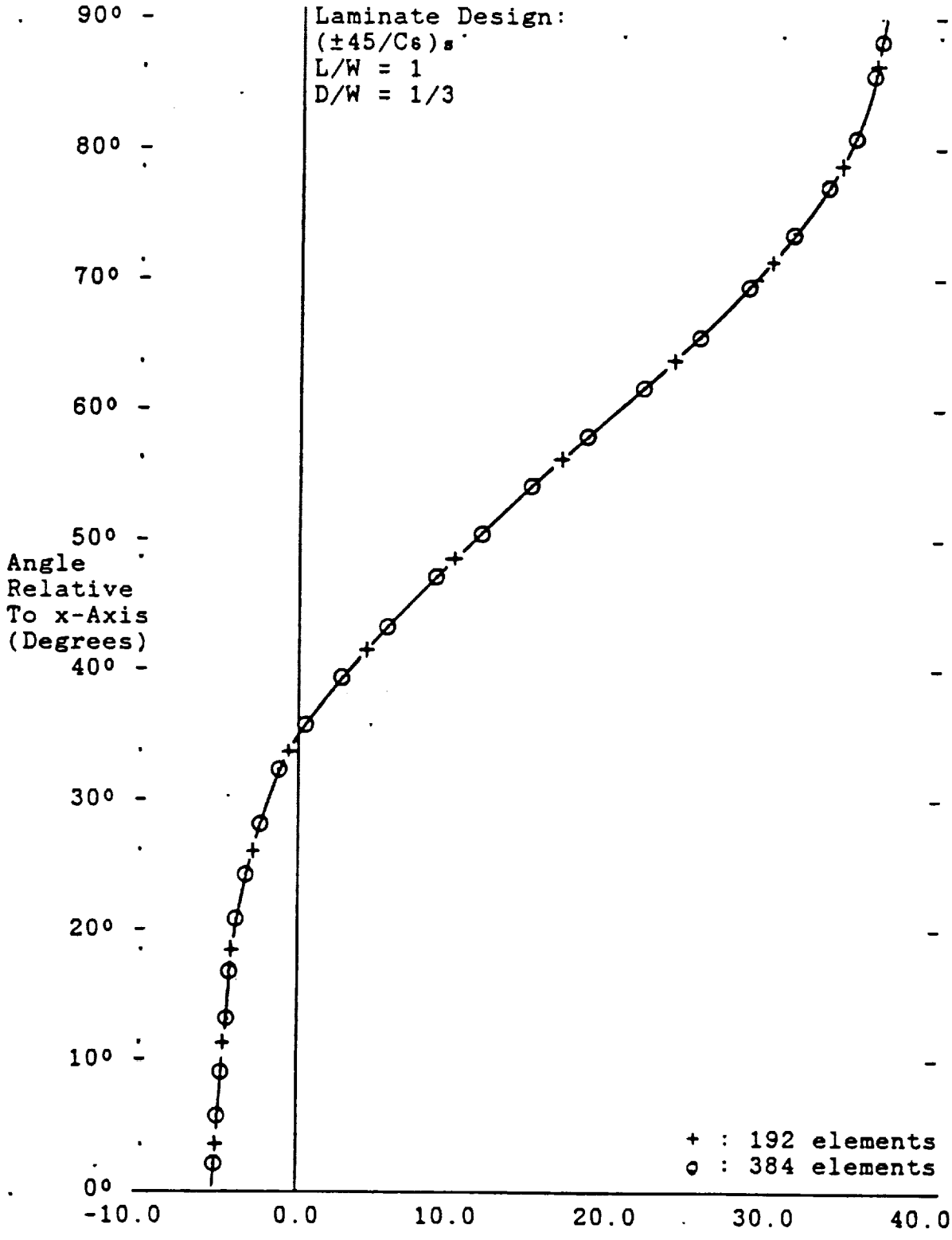

Figure 5.2 Influence Of Mesh Size On Results

Table 5.8

Circumferential Force Resultant Data

Laminate Design Case: $(\pm 45/C_6)_s$ L/W = 1 D/W = 1/3

192 Element Mesh[1]		384 Element Mesh[1]		
Element Number	N_s (lb/in)	Element Number	N_s (lb/in)	Angle: θ (Degrees)
		1	- 514.96	1.875
1	- 512.32			3.75
		17	- 507.70	5.625
		33	- 492.50	9.375
17	- 482.16			11.25
		49	- 467.94	13.125
		65	- 432.21	16.875
33	- 410.63			18.75
		81	- 382.92	20.625
		97	- 317.33	24.375
49	- 280.20			26.25
		113	- 233.10	28.125
		129	- 123.39	31.875
65	- 54.29			33.75
		145	50.16	35.625
		161	278.15	39.375
81	417.13			41.25
		177	546.82	43.125
		193	829.37	46.875
97	975.91			48.75
		209	1126.82	50.625
		225	1463.28	54.375
113	1643.00			56.25
		241	1813.34	58.125
		257	2164.73	61.875
129	2336.73			63.75
		273	2502.58	65.625
		289	2811.98	69.375
145	2946.92			71.25
		305	3081.38	73.125
		321	3301.78	76.875
161	3383.61			78.75
		337	3468.43	80.625
		353	3579.12	84.375
177	3605.42			86.25
		369	3634.28	88.125

[1] Data for each element taken at Gauss point 5.

A further comparison was made by simply examining the circumferential force resultant for the three sets of elements bordering the edge of the hole (12 elements on the boundary, 12 elements next to those boundary elements, and a third set of 12 elements next to the second set). Essentially these elements form three concentric rings of elements around a quarter of the hole. Data for the laminate design case $(\pm 45/C_6)_s$, L/W = 1, D/W = 1/3, were also used for the comparison. In Figure 5.3 these results for the three sets of elements are plotted against element position around the hole given as the angle relative to the x-axis. The jump in the circumferential force from element to element, both circumferentially and radially as shown by the curves, is minimal, as evidenced by the smoothness of each curve, and the order among the three curves. Data used to plot the curves of Figure 5.3 is shown in Table 5.9. It is clear from the results of using two mesh densities, and from the smoothness both radially and circumferentially, that the original 192 element mesh for the quarter plate is sufficient.

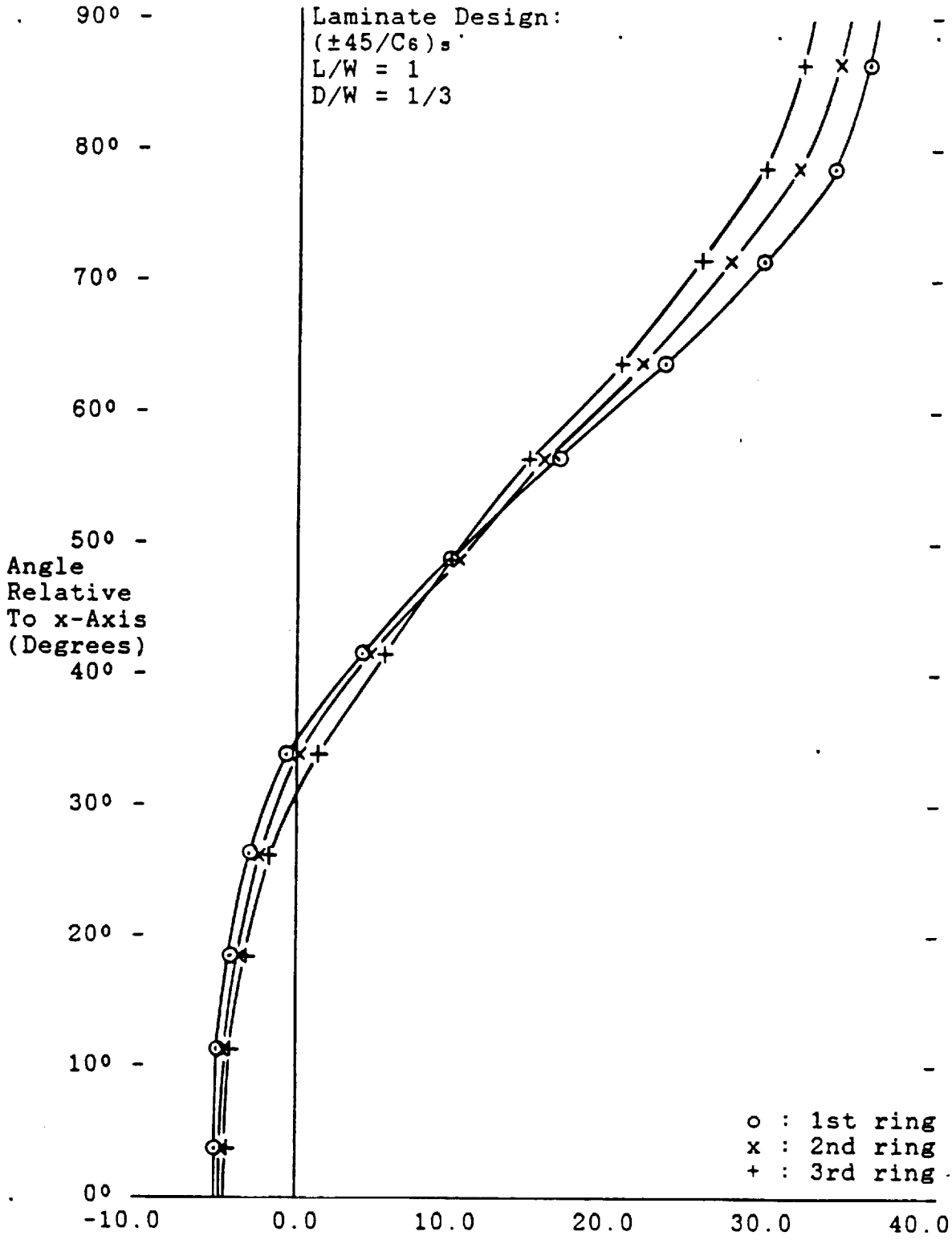

Figure 5.3 Change In Force Element To Element

Table 5.9

Circumferential Force Resultant Data[1]

Laminate Design Case: $(\pm 45/C_6)_s$ L/W = 1 D/W = 1/3

Element Number	N_s (lb/in)	Element Number	N_s (lb/in)	Element Number	N_s (lb/in)
1	- 512.32	2	- 483.86	3	- 454.18
17	- 482.16	18	- 449.19	19	- 415.53
33	- 410.63	34	- 368.89	35	- 328.00
49	- 280.20	50	- 226.64	51	- 172.00
65	- 54.29	66	15.93	67	123.96
81	417.13	82	463.80	83	546.98
97	975.91	98	1025.66	99	980.21
113	1643.00	114	1569.01	115	1475.45
129	2336.73	130	2174.00	131	2023.99
145	2946.92	146	2735.79	147	2544.69
161	3383.61	162	3164.88	163	2956.41
177	3605.42	178	3393.46	179	3183.57

[1] Data for each element taken at Gauss point 5.

Influence Of The Curvilinear Fiber Format On The Load Carrying Capacity

The curvilinear design $(\pm 45/C_6)_s$ and the straightline design $(\pm 45/0_6)_s$ look very similar near the net-section hole edge. The fibers in the curvilinear layers of the curvilinear design pass by the net-section perpendicular to a line from the hole edge to the plate edge. For the straightline design, the fibers in the 0^0 layers are also perpendicular to a line from the hole edge to the plate edge. Both designs have $\pm 45^0$ layers with identical orientation at the net-section hole edge. Locally, near the net-section hole edge both designs are predicted to have fiber failure at this point. However, the curvilinear design is able to carry a much higher tensile load than the straightline design. Why is this so?

Figures 5.4 and 5.5 are presented in order to provide insight as to why the curvilinear design has a larger tensile load capacity than the straightline design. Contour lines of stress in the x-direction are shown in Figure 5.4 for the curvilinear layers in the design $(\pm 45/C_6)_s$. Contour lines of stress in the x-direction are shown in Figure 5.5 for the 0^0 layers in the design $(\pm 45/0_6)_s$. The curvilinear design has fewer contour lines grouped near the net-section hole edge, and the contour lines are generally spread farther apart. This behavior indicates a more gradual change in the stress gradients at the net-section. This can be

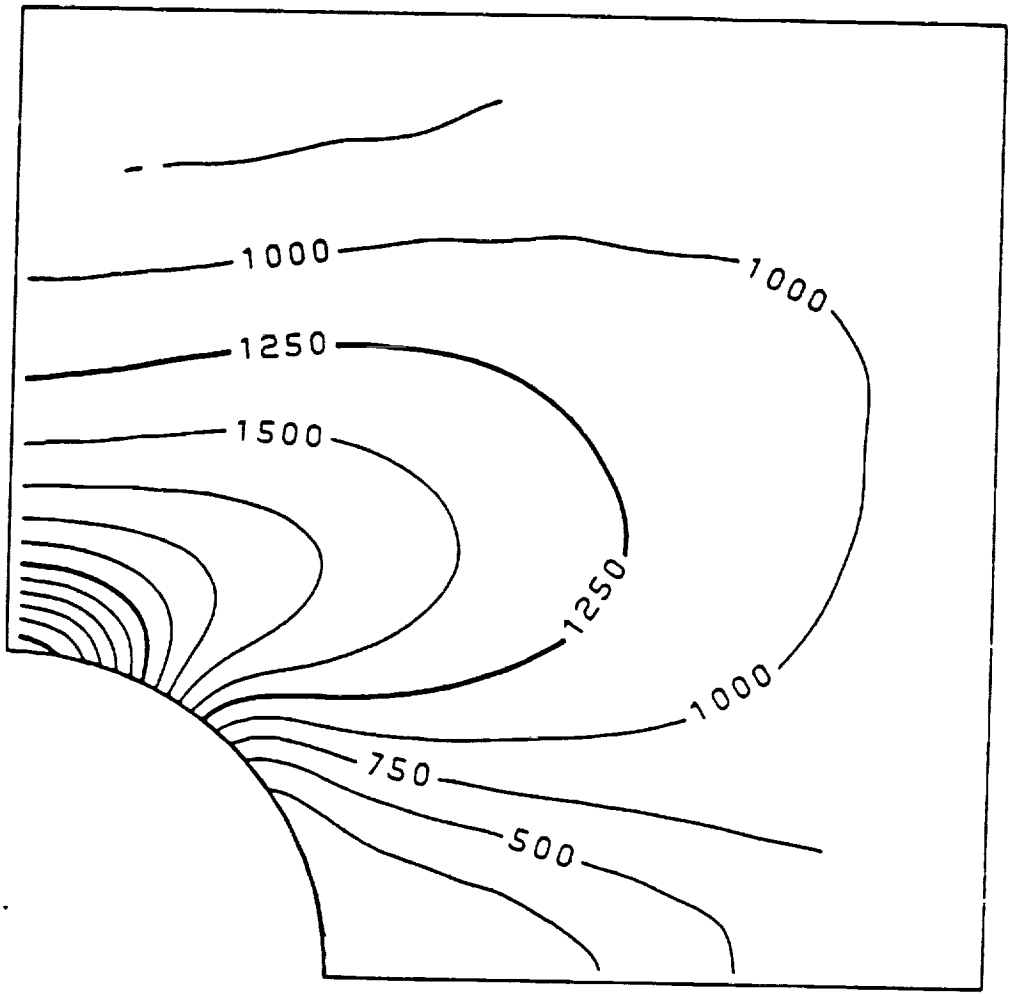

Figure 5.4 Plot Of Contour Lines Of Stress σ_x
For Curvilinear Layers
Case: $(\pm 45/C_6)_s$ L/W = 1 D/W = 1/3

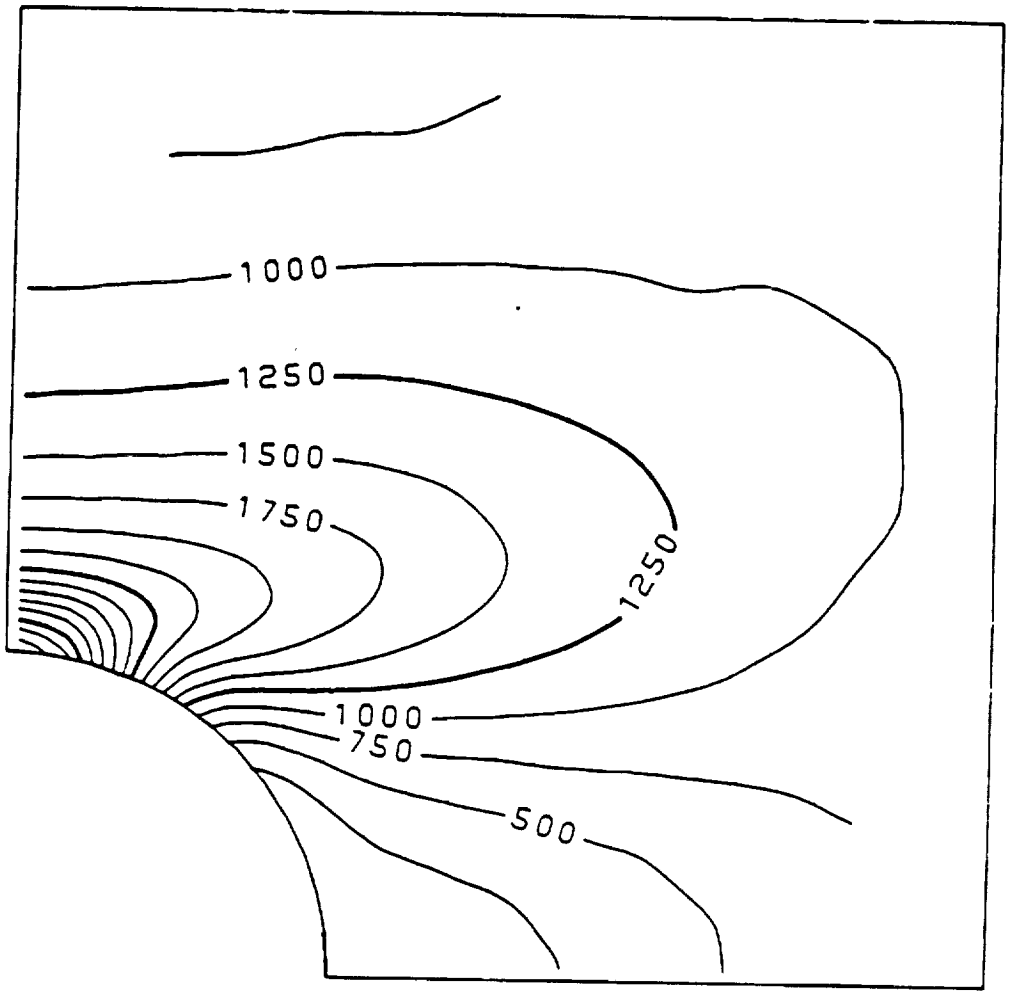

Figure 5.5 Plot Of Contour Lines Of Stress σ_x

For 0° Layers

Case: $(\pm 45/0_6)_s$ L/W = 1 D/W = 1/3

interpreted to mean that the stress concentration is lower near the net-section hole edge for the curvilinear design than it is for the straightline design. Figure 5.4 shows that the stress near the net-section hole edge is approximately 3750 psi due to a tensile load of 7200 lb for the curvilinear design. Figure 5.5 shows that the stress near the net-section hole edge is approximately 4250 psi due to a load of 7200 lb for the straightline design. The plot of contour lines in Figure 5.4 indicates that the curvilinear design carries the load along stress trajectories in a streamline pattern which flow around the hole.

An even better example of this is shown in the following two figures. Figures 5.6 and 5.7 show plots of contour lines of stress in the x-direction in the curvilinear layers for the orthogonal curvilinear designs $(O_2/C_6)_s$ and $(O/C_7)_s$. Here it is clear the orthogonal layers help to move the stress away from the hole edge, reducing the gradients around the hole and allowing the load to be transmitted more smoothly around the hole. Though it is not needed, because the $(O/C_7)_s$ laminate is sufficient, the value of doubling the orthogonal layers is clear. Those layers help move the load away from the hole.

This concludes the chapter on tensile loading. It is clear that the variable fiber orientation is beneficial. The next chapter addresses the influence of these designs on the buckling loads.

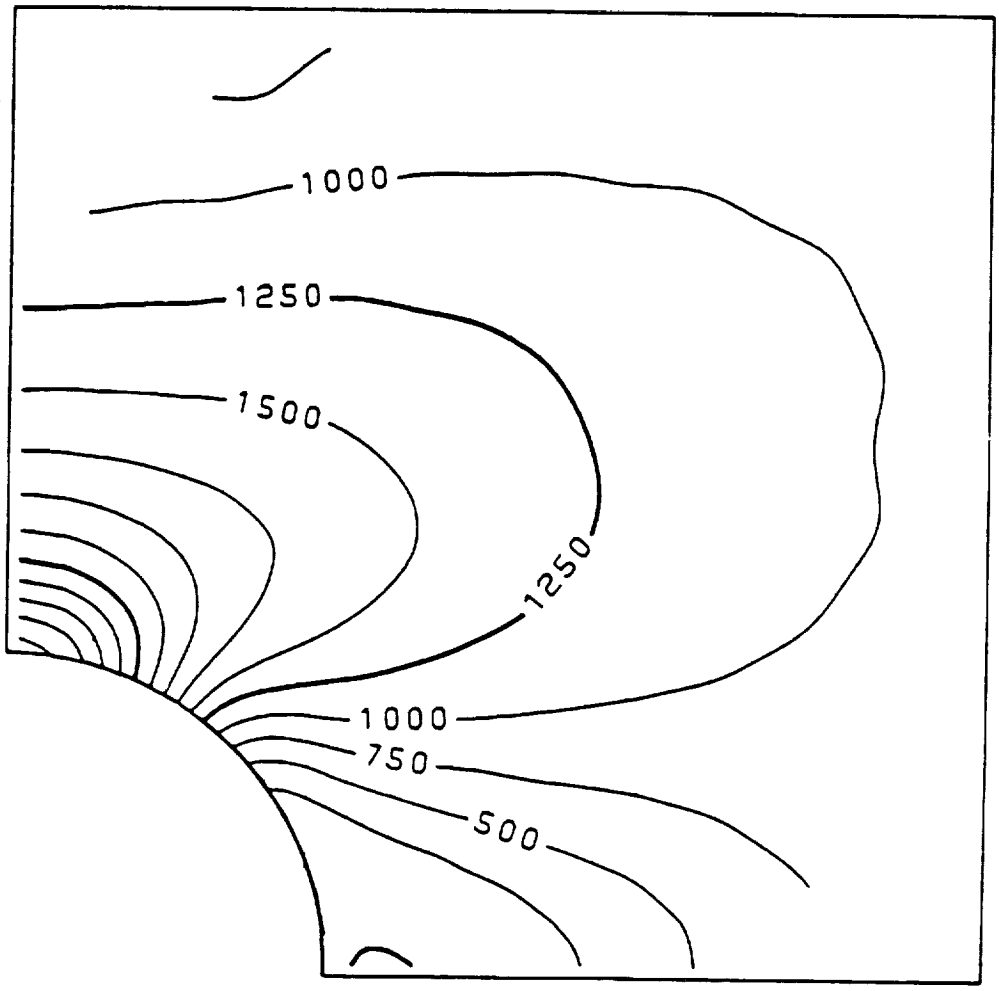

Figure 5.6 Plot Of Contour Lines Of Stress σ_x

For Curvilinear Layers

Case: $(O_2/C_6)_s$. L/W = 1 D/W = 1/3

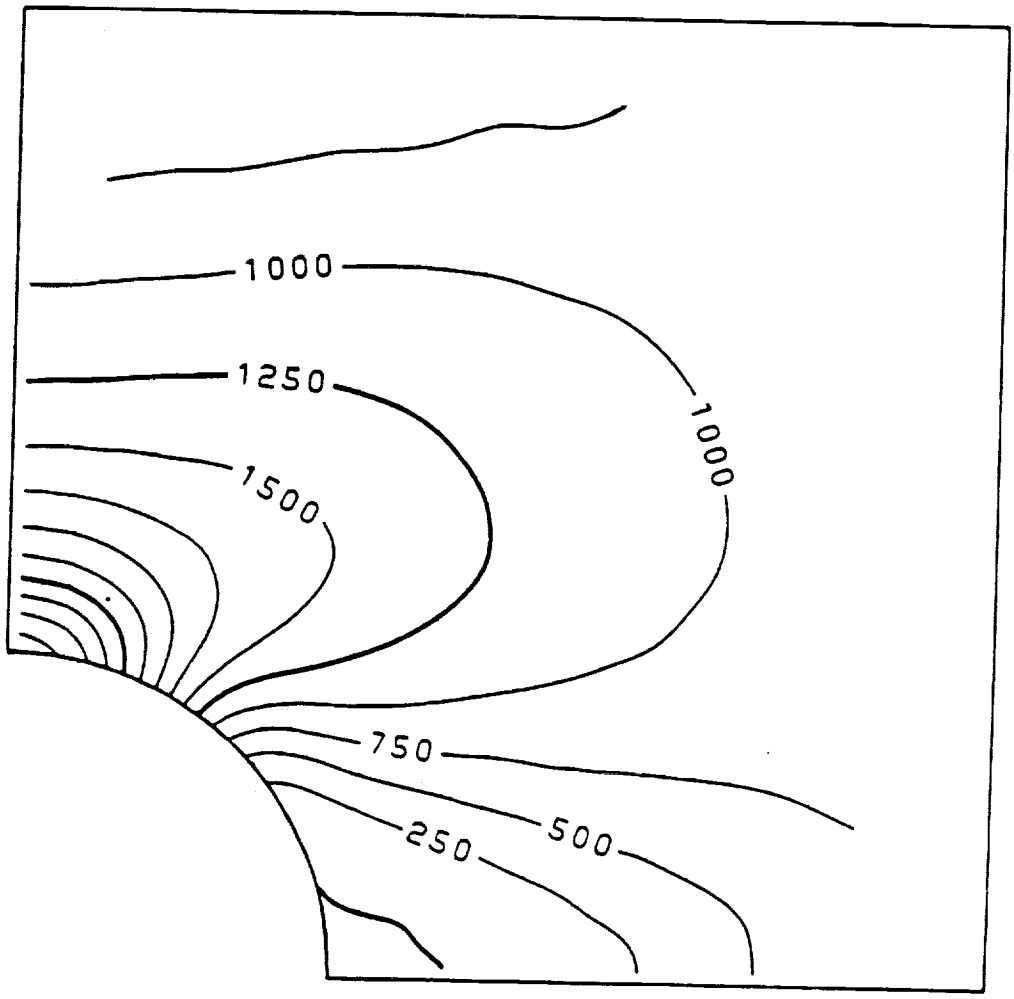

Figure 5.7 Plot Of Contour Lines Of Stress σ_x

For Curvilinear Layers

Case: $(0/C_7)_s$ L/W = 1 D/W = 1/3

CHAPTER VI

BUCKLING RESISTANCE OF THE PLATE DESIGNS

Establishment of criteria applicable to the design and analysis of plates subjected to tensile loads was of primary concern in the previous chapter. Having considered and compared plate designs which carry tensile loads, it is of interest to determine the buckling resistance of these designs. While it may be possible to design the curvilinear fiber format to best resist buckling, that is not the intent here. Here, simply, the tensile load designs were checked for their resistance to buckling. The buckling analysis was conducted to determine the extent to which the tensile-load-designed curvilinear fiber format could influence and perhaps improve the capacity of the plate to resist buckling.

The plates were subjected to in-plane compression loads and the critical compression load was determined. The critical compression load of each plate was defined to be that load which would cause the plate to buckle into its first buckling mode shape. Figure 6.1 shows a typical first buckling mode for square plates, and Figure 6.2 shows a typical first buckling mode for rectangular plates with length to width ratios of 2.0. For the square plate the buckling mode is a single half-wave in both directions, while for the rectangular plate there are two half-waves in the lengthwise direction.

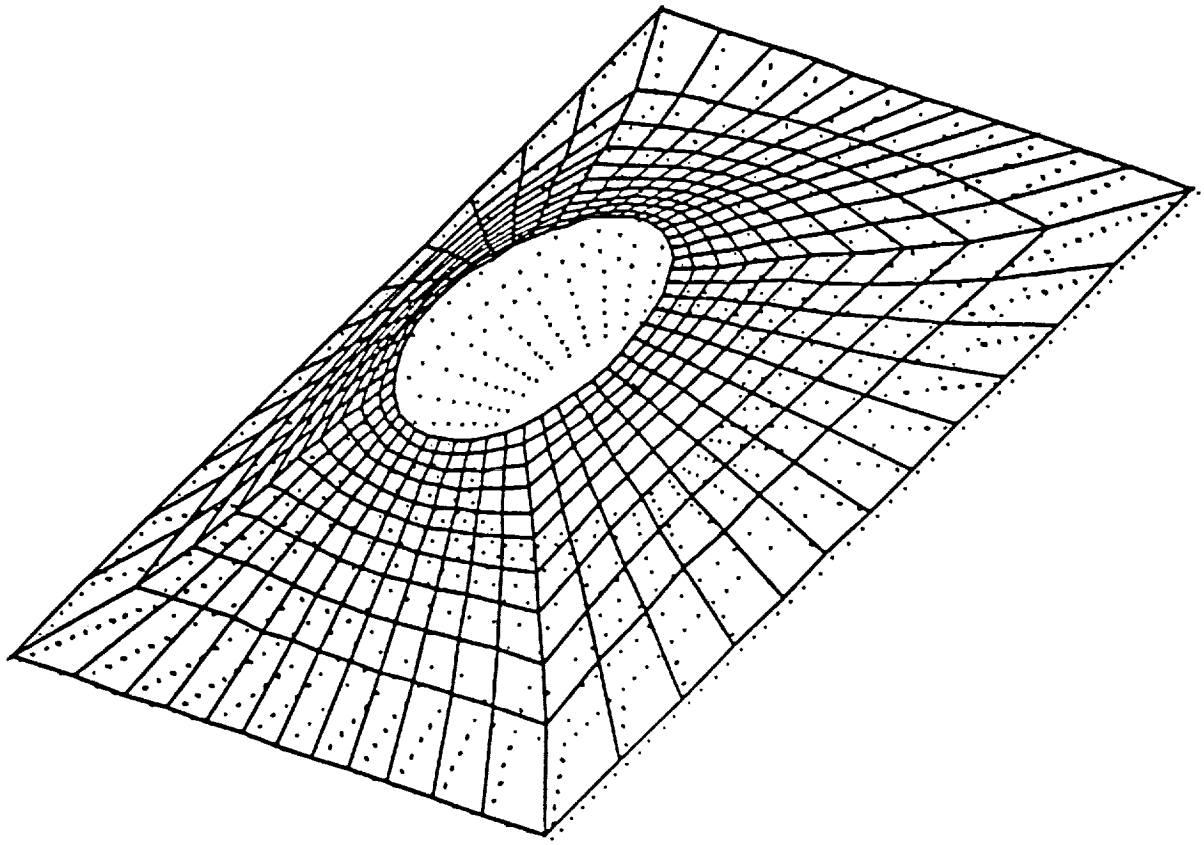

Figure 6.1 First Buckling Mode Shape

Square Plate

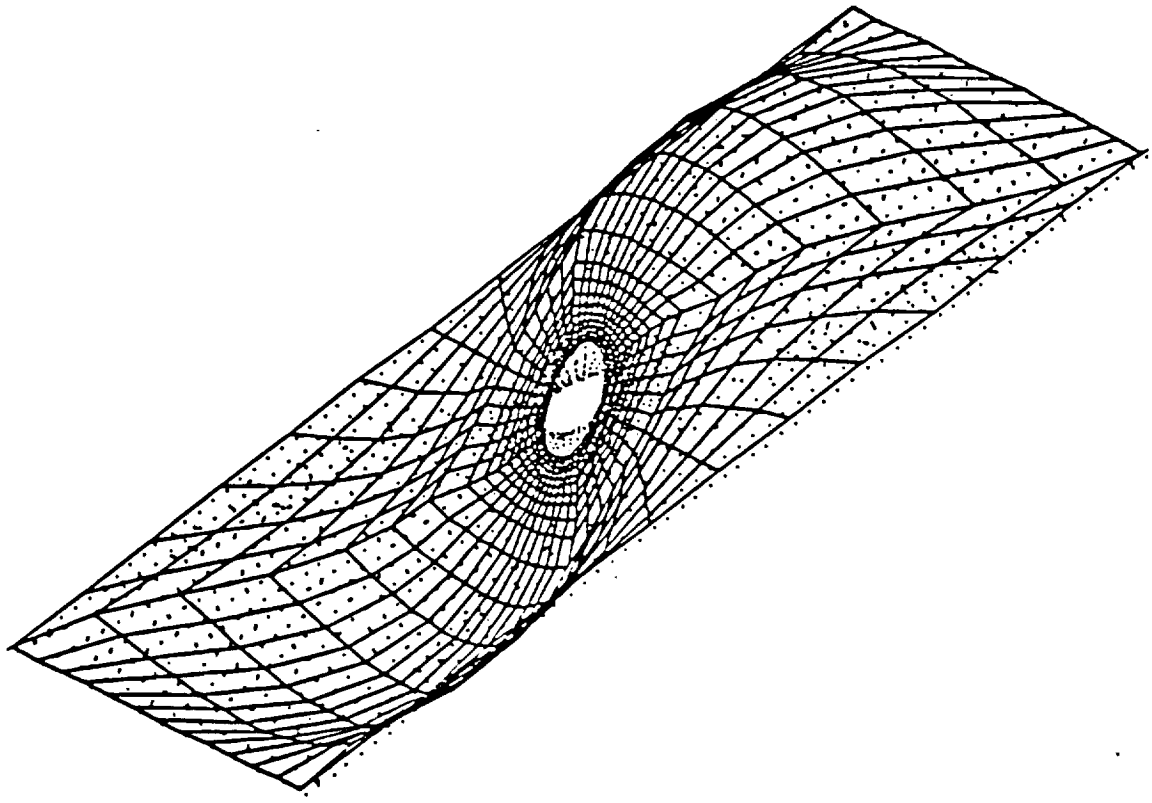

Figure 6.2 First Buckling Mode Shape

Rectangular Plate: L/W = 2.0

Tables 6.1 through 6.4 present the critical buckling loads of 36 different plate designs. There are four different geometries, each having the nine stacking sequences considered in Chapter V. The critical buckling loads of the nine stacking sequences for each geometry are normalized by the critical buckling load of the quasi-isotropic design of each geometry. The buckling analysis results for the square plates were verified by comparing the results of the $(0_8)_s$ laminates in Tables 6.2 and 6.4 with the results obtained by Nemeth [8]. The buckling analysis results for the rectangular plates in Tables 6.1 and 6.3 were verified by running a test case on a rectangular plate with a hole diameter to plate width ratio equal to 0.4 with a stacking sequence of $(\pm 45_8)_s$ and then comparing those results with the results obtained by Nemeth [8]. In both cases the results obtained in this study agreed very well with the results given in Reference 8.

The results given in Tables 6.1 through 6.4 show that the curvilinear fiber format is as good as a straightline format as regards buckling resistance. Interestingly enough, none of the designs considered, straightline or curvilinear, is better than the quasi-isotropic design in resisting buckling. For example, considering the data of Table 6.1, the $(0_8)_s$ design resists only 38% of the buckling load of the quasi-isotropic design. Allowing the straight fibers to become curvilinear does little to improve the

Design 1 Buckling Load: 1615.22 lb.

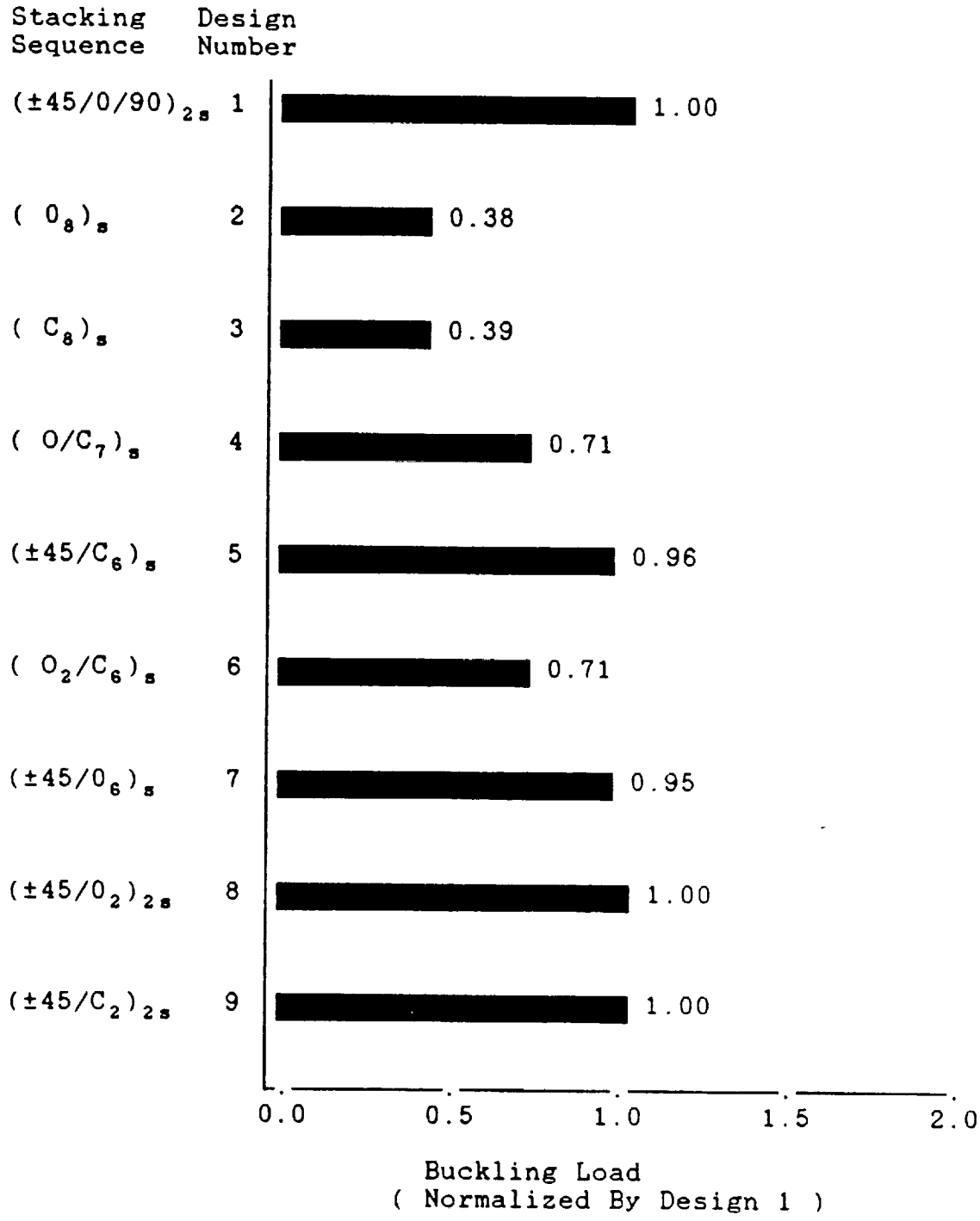

Table 6.1 Critical Buckling Load

Case: L = 20 in., W = 10 in., D/W = 1/6

Design 1 Buckling Load: 1443.33 lb.

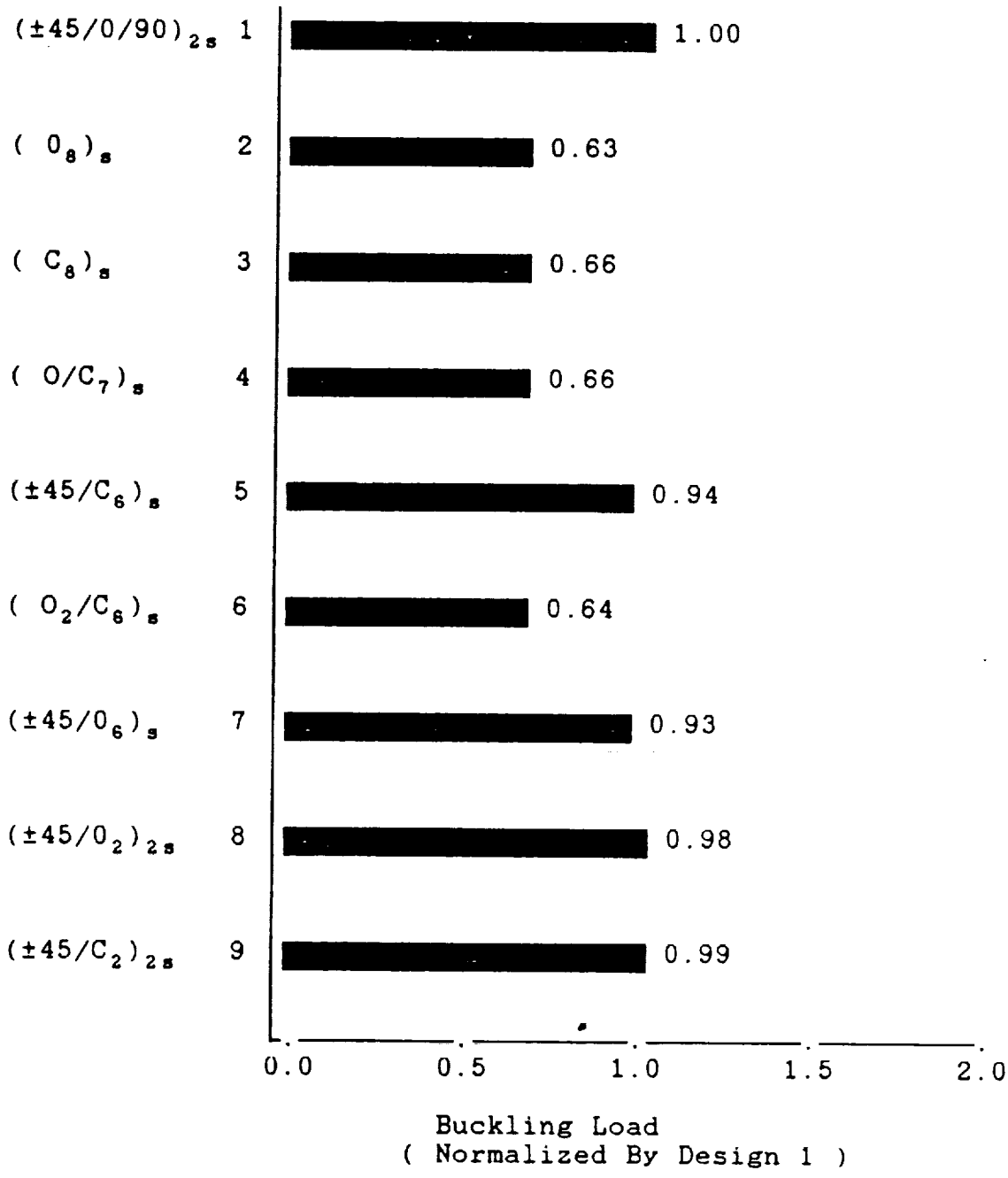

Table 6.2 Critical Buckling Load

Case: L = 10 in., W = 10 in., D/W = 1/6

Design 1 Buckling Load: 1727.94 lb.

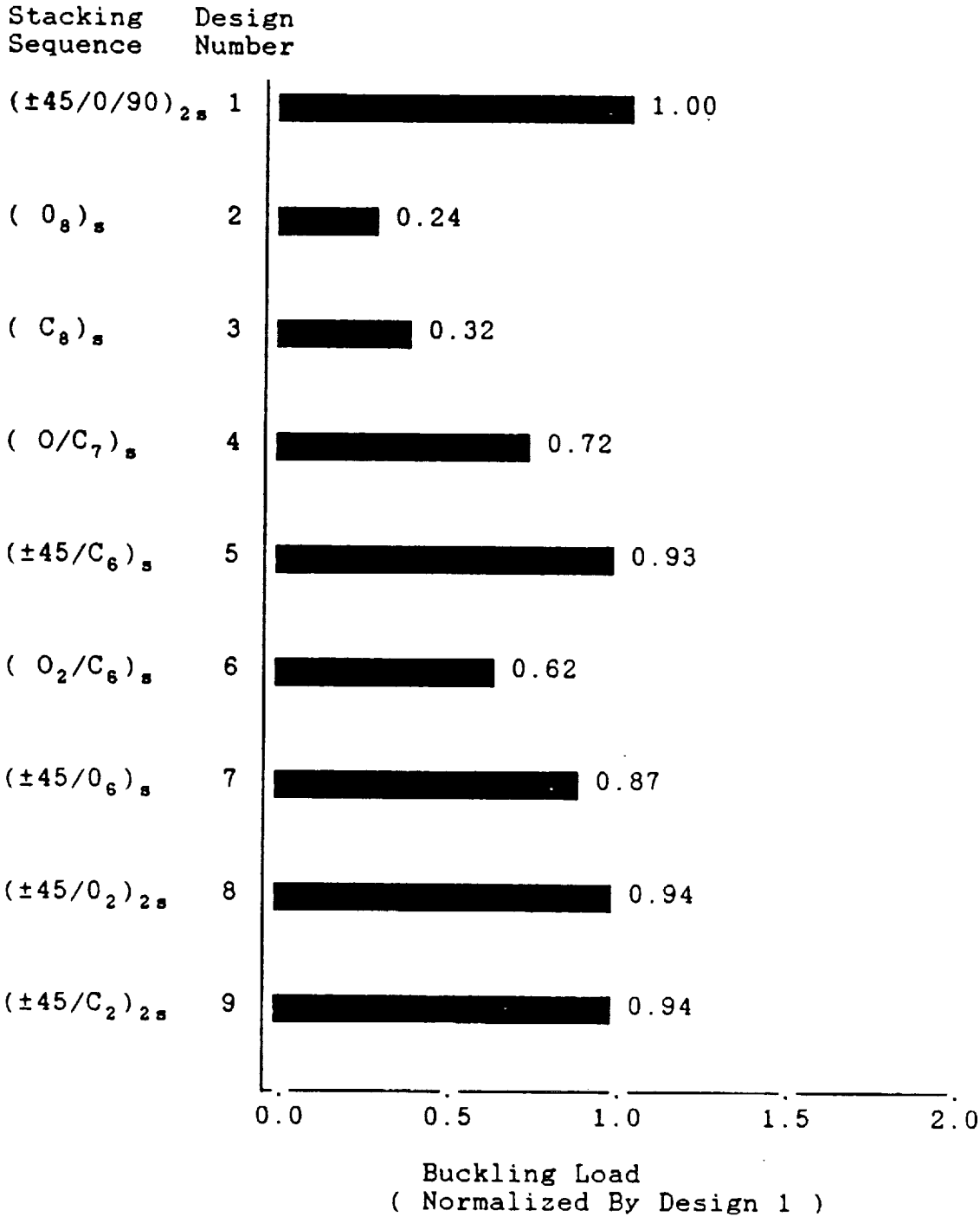

Table 6.3 Critical Buckling Load

Case: L = 20 in., W = 10 in., D/W = 1/3

Design 1 Buckling Load: 1267.71 lb.

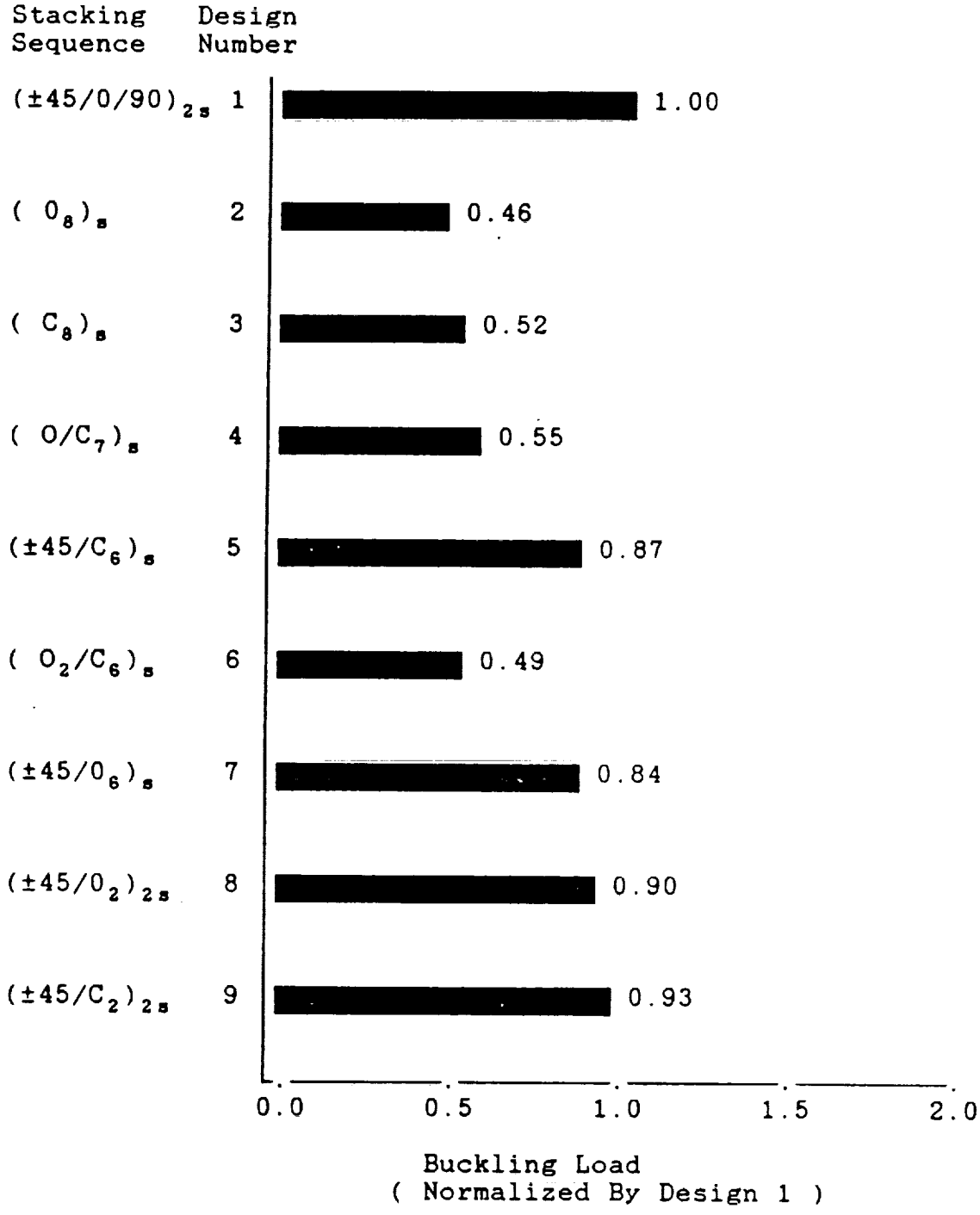

Table 6.4 Critical Buckling Load

Case: L = 10 in., W = 10 in., D/W = 1/3

load. Adding orthogonal layers to make a $(0/C_7)_s$ laminate greatly improves the buckling capacity relative to the $(0_8)_s$ and the $(C_8)_s$ designs, but it is not as good as the quasi-isotropic laminate. Adding the $\pm 45^0$ layers to form the $(\pm 45/C_6)_s$ laminate dramatically improves the buckling resistance, with the $\pm 45^0$ layers having a substantial influence. The $(0_2/C_6)_s$ laminate is very similar to the $(0/C_7)_s$ laminate. As a comparison with the $(\pm 45/C_6)_s$ laminate, the $(\pm 45/0_6)_s$ laminate shows very similar buckling capacity. Finally, the $(\pm 45/0_2)_{2s}$ laminate and the $(\pm 45/C_2)_{2s}$ laminate show similar characteristics and are both as good as the quasi-isotropic designs. Aside from understanding the influence of the curvilinear layers, the results in Table 6.1, and similarly, the other three tables, indicate that the $\pm 45^0$ layers strongly influence buckling resistance.

By examining the four tables it is also clear that there is a geometric influence on the normalized results. For example, for the rectangular plate with the small hole (Table 6.1), the $(C_8)_s$ laminate has only 39% of the buckling capacity of its quasi-isotropic counterpart. For a square plate with the small hole (Table 6.2), the $(C_8)_s$ laminate has 66% the buckling capacity. While this laminate may not be of practical interest, it does demonstrate the influence of geometry.

At this point the tensile and buckling capacities of particular plates can be compared to provide insight into

the overall gains of using the curvilinear fiber format. The tensile and buckling capacities of several laminates and the range of geometries are compared in Table 6.5 and Table 6.6. As before, the buckling capacity of the quasi-isotropic laminate in each case is defined to be unity. From the table it is clear that the curvilinear design has an advantage. While the buckling capacity of both the $(\pm 45/O_6)_s$ laminate and the $(\pm 45/C_6)_s$ laminate are about 5% less than the buckling capacity of the quasi-isotropic laminate as listed in Table 6.5, and even though both laminates carry more in tension than the quasi-isotropic plate, the $(\pm 45/C_6)_s$ laminate is better in tension than the straight-line counterpart as listed and shown in Table 6.6. With the buckling loads being the same, the increased capacity of the curvilinear design makes it superior. Similar comments can be made regarding the $(\pm 45/O_2)_{2s}$ laminate and the $(\pm 45/C_2)_{2s}$ laminate.

In summary, it can be said that the curvilinear fiber format used in the curvilinear designs do not degrade the buckling performance.

Table 6.5

Critical Buckling Load[1]

	L/W = 2 D/W = 1/6	L/W = 1 D/W = 1/6	L/W = 2 D/W = 1/3	L/W = 1 D/W = 1/3
$(\pm 45/0/90)_{2s}$	1.0	1.0	1.0	1.0
$(\pm 45/0_6)_s$	0.95	0.93	0.87	0.84
$(\pm 45/C_6)_s$	0.96	0.94	0.93	0.87
$(\pm 45/0_2)_{2s}$	1.00	0.98	0.94	0.90
$(\pm 45/C_2)_{2s}$	1.00	0.99	0.94	0.93

Table 6.6

Tensile Load Capacity[1]

	L/W = 2 D/W = 1/6	L/W = 1 D/W = 1/6	L/W = 2 D/W = 1/3	L/W = 1 D/W = 1/3
$(\pm 45/0/90)_{2s}$	1.0	1.0	1.0	1.0
$(\pm 45/0_6)_s$	1.43	1.38	1.38	1.27
$(\pm 45/C_6)_s$	1.84	1.79	1.71	1.60
$(\pm 45/0_2)_{2s}$	1.29	1.26	1.28	1.20
$(\pm 45/C_2)_{2s}$	1.47	1.44	1.42	1.33

[1] Designs are normalized by the quasi-isotropic design for each geometry

CHAPTER VII

SUMMARY, CONCLUSIONS AND RECOMMENDATIONS

Summary

This study has addressed and investigated the issue of using a curvilinear fiber format to increase the structural efficiency of layered fiber-reinforced, simply supported, flat plates with centrally located circular holes. The issue of how to determine the orientation and alignment of the fibers from point to point in a laminated plate structure, and how to evaluate the gains and improvement in using the format, have been addressed.

In-plane tensile loading was applied to two opposing plate edges and the fiber directions of the curvilinear layers were determined. Specifically, an iteration scheme and procedure, in conjunction with a finite element discretization of the plate, was formulated and used to determine the fiber orientation and alignment in some or all of the layers such that in those layers computed values of the principal stress directions and the principal material directions coincided. Evidence of the convergence of the scheme was also presented.

In establishing a basis for comparison, a maximum strain failure criterion and the Tsai-Wu failure criterion were both applied and used to predict and determine the maximum in-plane tensile loads which could be carried and the

failure modes of the various designs. The Tsai-Wu failure criterion was applied to support, check and compare the numerical results obtained with the maximum strain failure criterion. The Tsai-Wu failure criterion agreed fully and provided some additional insight on the interactive nature of some failure mechanisms. Increase in capacity was predicted by both failure criteria.

Various geometries were examined and results were compared to a quasi-isotropic laminate with a similar geometry. A quasi-isotropic laminate was chosen as a basis since it represents a rather conventional and often-used design. Several idealistic designs were also considered, e.g., a $(0/C_7)_s$ laminate, and these were found to show about a factor of two increase in tensile load capacity. Due to possible manufacturing difficulties and the inability to resist shear loading, variants of these ideal designs were also considered. This involved replacing the orthogonal layers with $\pm 45^0$ layers. Those laminates have straightline counterparts which are used in current design philosophy. Compared to those straightline counterparts, and the quasi-isotropic basis, the curvilinear designs showed improved tensile load capacity.

It was found that neither the hole size or the aspect ratio of the plate had any correlative effect on increasing the tensile strength of the curvilinear designs over that of the straightline designs. Numerical results obtained on in-

plane tensile strength of the curvilinear designs and straightline designs were highest for the plate parameter case D/W = 1/6 and L/W = 2, followed in descending order by the cases D/W = 1/6 and L/W = 1, D/W = 1/3 and L/W = 2, and D/W = 1/3 and L/W = 1. Contour plots of the force resultant in the x direction indicated that a possible reason for the improved capacity of the curvilinear design is that the load path is directed away from the hole edge, with the curvilinear fibers causing the load to 'flow' around the hole.

Though tensile capacity is important, compression load capacity, particularly in the sense of resisting buckling, is equally important. Thus the designs which evolved for improving tensile loading were checked with regard to their resistance to buckling. Again, buckling resistance was compared to a quasi-isotropic basis. Numerical results for both the curvilinear and straightline designs were obtained by applying a finite element method in the commercial code Engineering Analysis Language to establish a basis for comparing relative resistance to buckling when the designs under simply supported edge conditions were subjected to uniaxial compressive loading on two opposing edges. This portion of the study indicated that the curvilinear designs had little influence on buckling loads compared to their straightline counterparts. Interestingly enough, no design was better than the quasi-isotropic design in resisting buckling, and the presence of $\pm 45^0$ layers improved the buck-

ling resistance for all of the designs.

Conclusions

Of primary importance, it is concluded that use of a curvilinear fiber format improves tensile load capacity and does not degrade buckling capacity.

Of secondary importance, it is concluded that

1. The iteration scheme for finding fiber orientation worked well and should work for other structural elements, e.g., curved panels.

2. In general, the maximum strain and the Tsai-Wu failure criteria predicted identical load capacities in tension. When there were differences it was due to prediction of interaction effects with the Tsai-Wu criterion.

3. The addition of and/or presence of $\pm 45^0$ layers enhances buckling resistance.

Recommendations - Suggestions For Further Study

A natural departure for further study is to consider designs which include nonsymmetrical stacking sequences. The area of interest would be to determine if laminate designs which use a curvilinear fiber format could carry loads more efficiently than similar designs which use a straightline fiber format. Stiffness terms which account for coupling effects resulting in twist due to extension

force (or extension due to moments) would necessarily increase the complexity of the problem.

Another point of departure for further study would be concerned with curved plates (cylindrical sections) and shells subjected to in-plane loads as well as transverse distributed loads. An area of interest to be investigated would involve determining whether and when effects of transverse shear forces should be considered rather than be neglected.

In this study, design of the curvilinear fiber format laminates was based on the application of an in-plane tensile loading. The fiber directions in the curvilinear layers were oriented to provide the most efficient resistance for that type of loading. Buckling resistance of the laminates was shown to be lower than their levels of tensile strength. This establishes response to buckling as a critical design mode and buckling strength as a resistance level which the laminate must support without failure. Thus, further study may be beneficial in generating laminate design criteria by applying in-plane compressive loading to determine whether a basis could be established to justify that fibers should be aligned in a specified direction to increase resistance to buckling and have the design remain capable of satisfying design requirements for tensile loads.

Finally, consideration should be given to fabricating specimens to verify the findings of the study. Baseline designs, curvilinear designs, and their straightline counterparts should be fabricated and tested in tension and in compression.

REFERENCES

1. Jones, Robert M. Mechanics Of Composite Materials. New York: Hemisphere Publishing Corporation, 1975.

2. Shames, Irving H. And Dym, Clive L. Energy and Finite Element Methods in Structural Mechanics. New York: McGraw-Hill Book Company, 1985.

3. Reddy, J. N. An Introduction To The Finite Element Method. New York: McGraw-Hill Book Company, 1984.

4. Tsai, Stephen W. Composites Design 1986. Dayton, Ohio; Paris, Tokyo: By the author, Thierry N. Massard, and Ippei Susuki, 1985.

5. Brush, Don O. And Almroth, Bo O. Buckling Of Bars, Plates, And Shells. New York: McGraw-Hill Book Company, 1975.

6. Whetstone, W. D. EAL Engineering Analysis Language Reference Manual. San Jose, CA.: Engineering Information Systems, Inc., 1983.

7. Pian, Theodore H. H. "Derivation Of Element Stiffness Matrices By Assumed Stress Distributions." AIAA Journal. Vol. 2, No. 7 (July 1964): 1333-1336.

8. Nemeth, Michael P. "Buckling Behavior Of Compression Loaded Symmetrically-Laminated Angle-Ply Plates With Holes." AIAA Journal. Vol. 26, No. 3 (March 1988): 330-336.

BIBLIOGRAPHIC DATA SHEET	1. Report No. Technical Report 90-1	2.	3. Recipient's Accession No.
4. Title and Subtitle Innovative Design of Composite Structures: The Use of Curvilinear Fiber Format in Structural Design of Composites			5. Report Date March 1990 6.
7. Author(s) R. F. Charette and M. W. Hyer			8. Performing Organization Rept. No. Technical Report 90-1
9. Performing Organization Name and Address University of Maryland Mechanical Egnineering Department College Park, MD 20742			10. Project/Task/Work Unit No. 11. Contract/Grant No. NAG-1-665
12. Sponsoring Organization Name and Address NASA Langley Research Center Structural Mechanics Branch Hampton, VA 23665-5225			13. Type of Report & Period Covered FINAL REPORT 5/1/86-10/31/89 14.

15. Supplementary Notes

16. Abstracts

This study investigates the influence of a curvilinear fiber format on load carrying capacity of a layered fiber-reinforced plate with a centrally located hole. A curvilinear fiber format is descriptive of layers in a laminate having fibers which are aligned with the principal stress directions in those layers. Laminates of five curvilinear fiber format designs and four straightline fiber format designs are considered. A quasi-isotropic laminate having a straightline fiber format is used to define a baseline design for comparison with the other laminate designs. Four different plate geometries are considered and differentiated by two values of hole diameter/plate width equal to 1/6 and 1/3, and two values of plate length/plate width equal to 2 and 1. With the plates under uniaxial tensile loading on two opposing edges, alignment of fibers in the curvilinear layers with the principal stress directions is determined analytically by an iteration procedure. In-plane tensile load capacity is computed for all of the laminate designs using a finite element analysis method. A maximum strain failure criterion and the Tsai-Wu failure criterion are applied to determine failure loads and failure modes. Resistance to buckling of the laminate designs to uniaxial compressive loading is analyzed using the commercial code Engineering Analysis Language. Results indicate that the curvilinear fiber format laminates have higher in-plane tensile load capacity and comparable buckling resistance relative to the straightline fiber format laminates.

17. Key Words and Document Analysis. 17a. Descriptors

curved fibers, composite materials, design of composites, failure of composites

17b. Identifiers/Open-Ended Terms

17c. COSATI Field/Group

18. Availability Statement	19. Security Class (This Report) UNCLASSIFIED	21. No. of Pages 157
	20. Security Class (This Page UNCLASSIFIED	22. Price